Diese Dissertation haben begutachtet:

…………………… …………………

**TECHNISCHE
UNIVERSITÄT
WIEN**
Vienna University of Technology

D I S S E R T A T I O N

ICE NUCLEATION ACTIVITY OF

POLLEN AND FUNGAL SPORES

ausgeführt zum Zwecke der Erlangung des akademischen Grades eines Doktors
der Naturwissenschaften unter der Leitung von

Ao. Univ.-Prof. Dr. Hinrich Grothe

E165

Institut für Materialchemie

eingereicht an der Technischen Universität Wien
Fakultät für Technische Chemie

von

Mag. Bernhard G. Pummer

Matr.-Nr.: 0306300

Getreidemarkt 9/BC01A20

A-1060 Wien

Wien, am 02.06.2013

_____

Zusammenfassung (Deutsch):

Wird flüssiges Wasser auf Temperaturen unter 273.15 K (0°C) abgekühlt, ist es thermodynamisch von Vorteil, wenn es zu Eis gefriert. Dafür müssen sich Cluster von Wassermolekülen entsprechend anordnen und wachsen. Da dieser Prozess, genannt Eisnukleation, kinetisch gehemmt ist, kann flüssiges Wasser bis zu 230 K unterkühlt werden. Allerdings gibt es mehrere Arten von kleinen Partikeln, welche die Phasenumwandlung katalysieren und bei viel höheren Temperaturen Eisbildung auslösen. Diese Partikel, sogenannte Eiskeime, fördern die Bildung von Eiswolken in der Atmosphäre. Da Eiswolken von hoher Bedeutung für Klima und Wetter sind (z.B. für den Strahlungshaushalt und die Bildung von Niederschlag), ist es für Modellrechnungen von Bedeutung, die Eiskeimaktivität der verschiedenen atmosphärischen Aerosole zu kennen. Mineralische und bakterielle Eiskeime wurden bereits intensiv untersucht, daher befasst sich diese Arbeit mit Pollen und Pilzsporen, die in der Atmosphäre anzutreffen sind.

Um Information über die Eisnukleation zu gewinnen, wurde das Gefrieren von flüssigen Wolken, die mit Bioaerosolen versetzt wurden, im Labor simuliert. Es zeigte sich, dass einige Arten von Pollen und Pilzsporen signifikante Eisaktivität besitzen, während viele andere kaum bis gar nicht aktiv sind.

Um weitere Informationen über die Eisnukleation von Pollen zu gewinnen, wurden die Proben mit elektronenmikroskopischen, spektroskopischen und nasschemischen Methoden untersucht. Die Messungen zeigten, dass die Eisaktivität von Pollen durch einzelne Makromoleküle ausgelöst wird, und nicht durch die ganzen Pollenkörner. Des Weiteren wurde der Einfluss der Kultivierungsbedingungen auf die Eiskeim-Fähigkeit von Pilzsporen untersucht.

Summary (English):

If water is cooled down below 273.15 K (0°C, 32°F), freezing to ice is thermodynamically favored. For the freezing, clusters of water molecules have to arrange properly and grow. As this process, called ice nucleation (IN*), is kinetically hindered, liquid water can be supercooled down to 230 K. However, there are different types of micro- and nanosized particles which catalyze the phase transition and cause ice formation at far higher temperatures. These particles, so-called ice nuclei (IN), enhance the formation of ice clouds in the atmosphere. As ice clouds are very important for climate and weather (e.g. for the radiation budget and precipitation formation), it is essential for climate modeling to know the IN* potential of different atmospheric aerosols. As mineral and bacterial IN have already been studied intensely, this thesis deals with pollen and fungal spores, which are abundant in the atmosphere.

To gain information about the IN*, the freezing of clouds, which were spiked with bioaerosols, was simulated in the laboratory. It was shown that some pollen and fungal spore species showed high IN* activity, while many others were weakly or not active.

For further information about the pollen IN, the samples were analyzed with electron microscopic, spectroscopic and wet-chemical methods. These measurements showed that the IN* activity of pollen is caused by single macromolecules rather than the whole pollen grains. Furthermore, the impact of cultivation conditions on the IN* potential of fungal spores was investigated.

Table of Contents:

1. Theoretical background

1.1. The troposphere, clouds and aerosols

Earth's atmosphere consists of five different layers. From the planetary surface upwards these are the troposphere, the stratosphere, the mesosphere, the thermosphere and the exosphere. The boundaries of these layers are defined by the change of sign of the temperature gradient.

The troposphere is the lowest layer of the global atmosphere, reaching from the planetary surface to a height of 8 km at the poles and 18 km at the equator. It is mainly warmed by the infrared emission from the ground. So the temperature decreases from bottom to top, causing convection in the troposphere. This fact and the high water content up to 4 wt.% of the tropospheric air are responsible for the weather pattern. Higher atmospheric layers contain much less water, so that clouds are less common than in the troposphere. One example are the Polar Stratospheric Clouds (PSC).

The clouds appearing in the troposphere can be divided in three subcategories: warm clouds, mixed clouds and ice clouds. Warm clouds consist only of liquid droplets, ice clouds only of ice crystals. Mixed clouds contain both liquid and frozen water droplets. Another way of categorizing clouds is their appearance, e.g. there are Cumulus clouds, which are massive and look like sheep, Stratus clouds, which are horizontally stretched and look like fog, and Cirrus clouds, which are flimsy and look like feathers or hair.

Warm clouds consist of water droplets, which are formed by condensing water that has been evaporated from the planetary surface. The Cumulus clouds, which are the most important clouds for our weather, are very thick and contain droplets up to more than 1 mm in size. These are so heavy that they form precipitation. As water is an IR-active molecule, these clouds absorb and reemit

the warmth emitted from the planetary surface and so act like heating blankets for the global atmosphere.

Cirrus clouds are tropospheric ice clouds, which are composed of small ice crystals and are located at heights from 8 km to 12 km. Seen from the planetary surface they look like fine feathers or hairs, what gave them their name. As temperatures in the upper troposphere are as low as 223 K, homogeneous IN* takes place. Like all ice clouds they contribute to the planetary albedo and act as climate cooling units. They appear in many different forms, like Cirrus fibratus, Cirrus intortus and many more [Laube and Höller 1988]. Airplane contrails are anthropogenic Cirrus clouds.
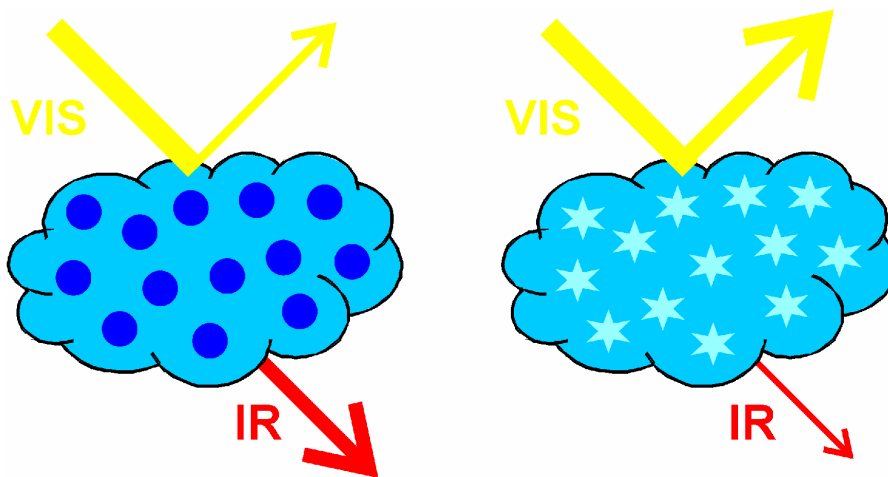
Fig. 1: A schematic showing qualitatively the different radiation effects caused by a liquid cloud (left) and an ice cloud (right).

As warm and mixed clouds are too warm for homogeneous freezing, they can only be turned into ice clouds by heterogeneous nucleation. Ice clouds are of crucial importance for the global radiation budget, as they reflect and scatter more sunlight coming from space than liquid clouds do and so increase the planetary albedo [Mishchenko 1996]. The higher the albedo, the less solar radiation can be converted into heat, the more the atmosphere is cooled. That is why cloud glaciation has become a topic of interest in the debate about climate change.

As Fig. 2[i] demonstrates, clouds play a crucial role in the global energy budget, where flows of heat and radiation, as well as the conversion into each other, are

---

[i]   http://education.gsfc.nasa.gov/experimental/all98invproject.site/pages/trl/inv2-1.abstract.html

quantitatively illustrated. These flows, which are determined by a broad set of parameters, shape Earth's climate. Although these parameters are essential for the living conditions on the planet, they are still poorly understood. The impact of changes in these parameters is even less understood, but essential for every form of life.

EARTH'S ENERGY BUDGET

Reflected by atmosphere 6%

Reflected by clouds 20%

Reflected from earth's surface 4%

64%

6%

Incoming solar energy 100%

Radiated to space from clouds and atmosphere

Absorbed by atmosphere 16%

Radiated directly to space from earth

Absorbed by clouds 3%

Radiation absorbed by atmosphere 15%

Conduction and rising air 7%

Carried to clouds and atmophere by latent heat in water vapor 23%

Absorbed by land and oceans 51%

Fig. 2: Global radiation budget of the terrestrial atmosphere. The picture does not include the latent heat flow between planetary surface and the cloud layer.

Aerosols are small particles or droplets finely suspended in air. Due to their small size, mainly in the range of μm or nm, they are only a little affected by gravitation and can stay in the atmosphere for longer times. Air turbulences help them to be dispersed from the ground, while precipitation washes them out of the atmosphere. As there are many different sources of aerosols, their chemical composition is also widely variable. Sources can be the ground (sand, salt, clay, humus), burning processes (soot, volcanic ash) or the biosphere (microbes, pollen, spores, plankton, fragments of insects and leaves). Aerosols can be divided into two main subgroups: Primary aerosols are directly emitted as

particles from their sources. Secondary aerosols are built up in the atmosphere by gases emitted from the sources. For example, SO_2 and NO_x are oxidized to H_2SO_4 and HNO_3, which condense and attract air humidity to form liquid droplets. Another example is the oxidation-polymerization of terpenes and other organic compounds forming secondary organic aerosols (SOAs) [Saxena and Hildemann 1996]. In most cases aerosols are internally mixed, which means that an aerosol particle is built up by different substances originating from different sources. For example, mineral dust can be coated with organic films or colonized by bacterial cells.

Primary biological aerosol particles (PBAPs), to which the samples analyzed in this thesis belong, make up 25% of the total aerosol mass in Earth's atmosphere [Jaenicke 2005]. The average number concentration of bacteria cells in the atmosphere [Burrows et al. 2009] is about 10^4 m^{-3} over land [Bauer et al. 2002] and about 10-100m^{-3} above the oceans [Prospero et al. 2005, Griffin et al. 2006]. Once in the air, they can react with atmospheric oxidants (O_3, NO_3, OH), making a functionalized, more polar surface [Ariya et al. 2009], what is believed to be advantageous for the attraction of water. In a field study a TOF-MS was used to measure the composition of ice crystal residues in an altitude of 8 km [Pratt et al. 2009]: According to these measurements, 50% of the residues are mineral dust, and 33% are biogenic aerosols.

1.2. Physics of ice and nucleation

Although ice is the thermodynamically most stable water phase at temperatures below 273.15 K at atmospheric pressure, the transition only takes place, if the activation energy barrier is overcome. Therefore, many individual water molecules have to form a structured cluster, which can grow by adsorbing more water molecules. This process is called homogeneous ice nucleation. As the surface energy of the clusters behaves antagonistic against the crystal formation, ultrapure water can be supercooled before nucleation takes place. For example,

water at 268 K can only freeze, when at least 45000 molecules form an ice-like cluster, while at 233 K already 70 molecules are sufficient [Zachariassen and Kristiansen 2000]. Consequently, ultrapure water droplets stay liquid down to temperatures of about 235 K, as the formation of bigger clusters is relatively unlikely. But certain kinds of solid particles, which are insoluble in water, but can bind water molecules by electrostatic interaction and structure them in an ice-like manner [Zachariassen and Kristiansen 2000], catalyze the ice formation at higher temperatures. These particles are called ice nuclei, and the process is called heterogeneous ice nucleation. Both terms are commonly abbreviated as "IN" or "INA". For discrimination, the process of ice nucleation is consistently abbreviated as "IN*" in this thesis, while the ice nuclei are labeled as "IN". Atmospheric IN can trigger cloud glaciations and precipitation, and so have a high impact on the global radiation balance and on the water cycle (see chapter 1.1.). It is still debated, whether IN increase or decrease global albedo, as on the one hand ice clouds reflect more light than liquid water and so cool the climate [Mishchenko 1996], but on the other ice formation is likely to trigger precipitation and so reduce total cloud albedo [Lohmann 2002].

If the microparticle is soluble in water, it condenses humidity to form droplets and causes freezing point depression, like NaCl or monosaccharide particles. According to Raoult's law, any soluble substance at a given concentration lowers the freezing point for the same amount, independent on its chemical formula or structure. The reason is the fact that the vapor pressure over one component of a condensed phase is supposed to be proportional to its fraction (see Eq. 1). Since the presence of another substance decreases the fraction of water in a liquid, its partial vapor pressure decreases in comparison to pure water.

$$p = \Sigma\, p_i = \Sigma\, x_i \cdot p_i{}^{\circ}$$

Eq. 1

with p as the total pressure of the mixture, p_i as the partial vapor pressures of the individual components, x_i as the mole fraction of these components and $p_i{}^{\circ}$ as the vapor pressure of a pure component (x_i=1). In order to decrease the freezing

point of water, the corresponding component has to dissolve in water. Therefore, only water-soluble substances decrease the freezing point, while the insoluble IN increase the freezing point and so encourage ice formation [Ariya et al. 2009]. In contrast to IN, which is a non-colligative effect, freezing point depression is a colligative effect.

Cloud condensation nucleation (CCN*) is the attraction of humidity by soluble particles, so-called cloud condensation nuclei, to form liquid droplets. Common biological cloud condensation nuclei (CCN), like pollen and spores, carry soluble sugar and sugar-alcohols on their surface. These compounds, as well as other polar organic compounds [Gorbunov et al. 1998, Corrigan and Novakov 1999, Giebl et al. 2002, Sun and Ariya 2006] cause CCN* by lowering the surface tension of water and so reducing the water supersaturation threshold. Some particles show both IN* and CCN* activity, with the consequence that they can deposit and freeze air humidity by the detour of forming liquid droplets. The concentration of biological IN in air is about 1-10 particles per litre. Contributions to the total ice nuclei amount originate from bacteria, pollen, spores, fungi, algae [Knopf et al. 2011, Möhler and Hoose 2011, Alpert et al. 2011], plankton [Schnell and Vali 1976] and protozoa, as well as decayed leaf and insect fragments.

IN*, as any other type of nucleation, can only occur, if the atmosphere is sufficiently supersaturated with vapor. The supersaturation degree of ice can be determined with Eq. 2:

$$s^{ice} + 1 = \frac{p_{wat}}{p_{vap}^{ice}(T)}$$

Eq. 2

with s^{ice} as the ice supersaturation, p_{wat} the partial pressure of atmospheric water and $p_{vap}^{ice}(T)$ the temperature-dependent vapor pressure of ice. If $s^{ice}=0$, then the atmosphere is saturated according to ice. At $s^{ice}>0$, the ice phase grows, while at

$s^{ice}<0$ present ice evaporates. When nucleation takes place, vapor is removed from the gas phase, decreasing p_{wat} and s^{ice}.

The same formalism can be employed in regard of liquid supersaturation, with $p_{vap}^{liq}(T)$ as the vapor pressure of liquid water. This way the relative air humidity in meteorology is calculated: $s^{liq}=0$ corresponds to 100% air humidity, which is usually the point, which has to be overcome to allow precipitation. In ultrapure atmosphere with neither condensation nuclei, nor initial droplets, supersaturation with more than 100% humidity occurs. The formation of ice forces s to decrease within time, what is demonstrated by the development of the curves in Fig. 3 [Peter et al. 2006]:
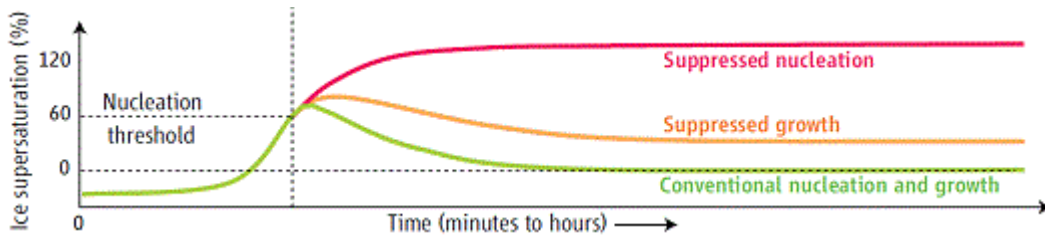
Fig. 3: The time development of supersaturation, depending on the ice formation.

At temperatures below 200 K, a metastable phase, which is called ice Ic or cubic ice, nucleates first and remains steady in the clouds. When calculating the vapor pressure of the ice phase, one has to keep in mind, that cubic ice has a higher vapor pressure than the hexagonal ice Ih, which is the common ice form in our every-day life. Recent research has raised the question, if what we call ice Ic really consists of only cubic crystals: In fact, ice Ic consists of an arrangement of hexagonal and cubic elementary cells, which can be interpreted as "deformed" hexagonal cells, respectively layers with stacking faults [Kuhs and Hansen 2009]. So the properties we nowadays associate with ice Ic could be in fact properties of a mixed-phase system. As the deformation and the phase transition faces make stable packaging less possible, this could explain the experimentally measured higher vapor pressure compared to ice Ih with only hexagonal cells. According to this, pure ice Ic, which has never been observed, does not exist [Sippel et al. 2010].

When ice crystallizes, two antagonistic energy terms have to be considered: The crystallization energy, which is set free, has a negative value and is proportional to the volume ($\sim r^3$), and the surface work, that has to be invested, is positive and proportional to the surface ($\sim r^2$) [Wolde and Frenkel 1999]. For very small radii the surface term is more important, while with increasing r the volume term becomes dominant. In sum, both terms create a sum ΔG-curve with a local maximum that can be interpreted as an activation barrier ΔG^*:

$$\Delta G = 4\pi \cdot \gamma \cdot r^2 + \frac{4}{3} \cdot \pi \cdot \rho \cdot \Delta \mu \cdot r^3$$

Eq. 3

$$\Delta G^* = \frac{16 \pi \gamma^3}{3 \rho^2 \cdot (\Delta \mu)^2}$$

Eq. 4

with r as the droplet radius, γ the surface free energy, ρ the bulk density, $\Delta \mu$ the chemical potential between 2 phases (depending on s). At smaller radii the r^2-term is dominant, at larger radii the r^3-term. The necessity to overcome ΔG^* kinetically hinders the formation of ice, as small water clusters are torn apart by their high surface energy.

The critical cluster size, which has to be outgrown to form a stable crystal, increases with rising temperature. At 233 K clusters with at least 70 water molecules are needed for homogeneous freezing, what is a statistically likely process, while $5 \cdot 10^4$ water molecules are necessary at 268 K, what is statistically impossible[i]. That is why at this temperature only heterogeneous freezing can take place, meaning, that the water has to contain impurities, which ease the formation of clusters.

Following the Ostwald step rule, the phase that crystallizes first is the one with the lowest activation barrier, which is not the same as the most stable one. Consequently, metastable ice Ic is expected to nucleate first, while the thermodynamically stable ice Ih crystallizes with delay.

---

[i]   https://www.uni-hohenheim.de/lehre370/weinbau/praktikm/eisnuk.htm

The working mechanism of most ice nuclei is not known up to now. Two models are suggested, which try to interpret the heterogeneous ice formation on a surface. One model suggests that every droplet on a surface shows a certain surface tension γ, which becomes visible as the contact angle θ at the three-phase point of droplet, surface and surrounding air (see Fig. 4). γ leads to a certain IN* activity [Chen et al. 2008]. The plausibility of this model derives from the presence of γ in the formulation of ΔG (see Eq. 3).

According to another hypothesis, an IN* active particle is covered with functional groups that arrange the water molecules to form an ice embryo, which grows when it reaches the necessary critical size [Liou et al. 2000, Zachariassen and Kristiansen 2000]. No matter, which hypothesis is favored, in all cases it seems that it is not the whole surface that participates in the IN* process, but only relatively small (in comparison to the whole particle) sections called "active sites" [Marcolli et al. 2007]. The surface chemsitry of these sites differs from most of the particle's surface area, either by its geometry or by allocation of certain functional groups. Therefore, a particle can be modeled as soccer ball with distinct fields of different IN* activities [Niedermeier et al. 2011a].

Fig. 4: Visualization of the contact angle of a droplet on a solid surface. The three γ represent the surface tensions of the three phase interfaces.

Ice nuclei can be of different origin and chemical composition. Some types of mineral dust and some biological species (see chapters 1.5. and 1.6.) are known to be IN* active. Also soot particles are debated as possible atmospheric IN. The most efficient known ice nuclei are produced by some plant pathogenic bacteria [Schnell and Vali 1972], which make water freeze at temperatures up to 271 K. These are furthermore the only ice nuclei, where the mechanism has already been investigated and explained up to now.

Although many studies about the IN* activity of mineral dust and soot have been performed [e.g. Möhler et al. 2006, Zimmermann et al. 2008, Pinti et al.

2012, Kärcher et al. 2007, Bingemer et al. 2011], the mechanism is still unknown. Most likely, the IN* activity is caused by active sites, which might be created either by certain structural features of the particle surface, like stacking faults, cavities or edges [Kulkarni and Dobbie 2010], chemical surface functionalizing, like oxidation or nitration, or deposition of contaminants, for example of biological material. In one study, volcanic ash showed IN* activity at approximately 253 K [Shaw et al. 2005]. However, in analogy to soot [Diehl and Mitra 1998], fresh ash seems to be only weakly active, while atmospheric ageing creates active sites on the surface, which significantly increase IN* activity [Kärcher et al. 2007, Bingemer et al. 2011]. In another study [Steinke et al. 2011], the ash of the Icelandic volcano Eyjafjallajökull showed less than 0.1% activity at temperatures higher than 250 K. Thus it was less active than Arizona Test Dust (ATD), which is a commonly applied test substance for laboratory investigation of natural aerosol, but comparable to other types of mineral dust. Furthermore, the IN* activity in the deposition mode was higher than in the immersion mode.

Some low-molecular organic compounds, like phloroglucinol, can form long-range-ordered structures which are able to nucleate ice [Fukuta 1966]. Organic compounds that act as IN have to fulfill several conditions: First, they have to form crystalline structures, second, these crystals shall show low solubility in water, and third, they have to contain polar groups at positions which match the water molecules in the ice lattice. Because of the first point, the preparation of organic samples is crucially important for the IN* activity [Fukuta 1966].

Four different modes of primary nucleation, in nature as well as in experiment, are distinguished [DeMott 1995]:

- Deposition mode: The naked ice nucleus directly adsorbs water vapor from the gas phase to form ice crystals.

- Condensation mode: The naked particle condenses water vapor on its surface to form a liquid droplet, which eventually freezes.
- Immersion mode: The particle is suspended in a water droplet. Then the droplet cools and freezes.
- Contact mode: The naked particle co-exists with a super-cooled water droplet. When the droplet collides with the IN, it freezes.

Fig. 5: Difference between immersion freezing (A) and contact freezing (B).

Apart from the primary modes, there are also secondary ice nucleation processes, which are mechanisms of ice multiplication:

- Hallet-Mossop effect (riming-splintering): An ice crystal is shattered. The fragments then collide with liquid droplets and so initiate contact freezing.
- Bergeron-Findeisen process (seeder-feeder): Ice has a lower vapor pressure than water. In a humid atmosphere, the ice crystals will deposit vapor on their surface and so grow, while liquid droplets will evaporate. So the ice crystals feed on the liquid droplets via the vapor phase.

Since the different modes of IN* are model conceptions, and as the assignment of a real IN* event to one mode is not always distinct, the given classification is a continuous subject of debate. For example, the condensation mode could be interpreted as consisting of two steps: As first step, the particle acts as CCN to form a droplet, and then it acts as ice nuclei in the immersion freezing mode [Pruppacher and Klett 1997]. Furthermore, the necessary vapor supersaturation for the condensation mode is higher than for the deposition mode. Therefore, a particle is expected to initiate deposition freezing sooner than condensation freezing, unless it is IN* inactive in this mode.

The deposition mode is fundamentally different from the other three, since it catalyzes vapor-to-ice transition instead of liquid-to-ice transition. Therefore, the

capability of particles to initiate IN* can be dependent on the mode. For example, pollen are IN* negative in deposition freezing, while they show appreciable IN* activity in the other three modes [Diehl et al. 2001, Diehl et al. 2002]. The median freezing temperatures for birch pollen, which were the most effective sample in Diehl's study, were 261 K in the condensation, 258 K in the immersion and 260 K in the contact mode. The difference between contact mode and immersion mode could be explained by the fact that the collision between an aerosol and a droplet causes density fluctuations within the droplet. If the density in a droplet locally matches the density of ice, the droplet starts freezing [Cheftel et al. 2000].

The IN* temperature is measured in a thermoregulated system, either at different constant temperatures, or with a certain cooling rate. The result is a diagram temperature versus percentage of frozen particles. The curve is sigmoid with a steep slope around the nucleation temperature. At lower temperatures, the curve forms a saturation plateau, at higher ones a basin at about 0% (see Fig. 31).

As deposition mode is the only one that catalyzes direct phase transition from gas to solid state, while the others only freeze liquid water, it only takes place, if the IN* simulates the structure of hexagonal ice crystals. For being active in the immersion mode, an IN has to be also a CCN. The immersion mode can be either realized with droplets floating in a chamber or flow tube, or by preparing a water-in-oil emulsion [Clausse et al. 1991, Shaw et al. 2005, Marcolli et al. 2007, Koop and Zobrist 2009]. The latter approach allows to model a cloud in handy dimensions and observe it with simpler methods, like a microscope. In a simplified way, a cloud is an ensemble of liquid droplets or ice crystals with diameters in the micrometer range. In the oil immersion mode, the merging of individual droplets to a continuous aqueous phase is prevented by a hydrophobic oil blended with an emulsifier.

As the nucleation event is a statistical process, it cannot be predicted exactly. One can only calculate the probability of an event to take place. Principally three terms determine, if a nucleation event occurs:

- observation time: the longer the system is observed, the more nucleation events can take place
- droplet size: the more water molecules are available for cluster formation, the easier it becomes
- system temperature: at lower temperatures smaller molecule clusters are needed for forming a nucleus

For homogeneous nucleation, all terms are accounted for in one equation [Murray et al. 2010]:

$$\ln \frac{n_{tot} - n_{ice}}{n_{tot}} = \ln\left(1 - f_{ice}\right) = -J_{hom} \cdot V \cdot t$$

Eq. 5

with n_{tot} as the total number of droplets, n_{nuc} as the number of frozen droplets, $V[\text{cm}^3]$ as the droplet volume and $t[\text{s}]$ as observation time. $J_{hom}[\text{cm}^{-3}\text{s}^{-1}]$ is the nucleation rate coefficient, which is temperature-dependent. Formally the nucleation process can be seen as a first order reaction with J_{hom} as reaction rate constant. For intervals of a few K it shows a more or less common logarithm relationship. The slope of this curve is very steep, so that J_{hom} increases for about 4 orders of magnitude in an interval of 3 K. Thought the other way, the time demanded for nucleation to occur will decrease in the same way at falling temperatures. That is why nucleation rates can only be measured in a small temperature interval. For pure water this is about 238 K. At 233 K all droplets will be frozen within a fraction of a millisecond, while at 243 K it may need more than a year for a nucleation event to occur. So it is legitimate to measure nucleation spectra, where the fraction of frozen droplets is plotted against temperature, without accounting for the time.

For heterogeneous nucleation the dependence on V is replaced by the contact area between the nucleus an the droplet $\sigma[\text{cm}^2]$ [Iannone et al. 2011, Murray et

al. 2011]. That is why J_{hom} has to be replaced by $J_{het}[\text{cm}^{-2}\text{s}^{-1}]$. A demonstrative example: In a homogeneous nucleation experiment a small droplet nucleates at a lower temperature than a big droplet. In a heterogeneous IN* experiment a small droplet with one ice nucleus and a large one with one ice nucleus are expected to nucleate at approximately the same temperature, while a droplet containing more ice nuclei will nucleate sooner (see Fig. 6). Of course, if the ice nuclei are homogeneously distributed
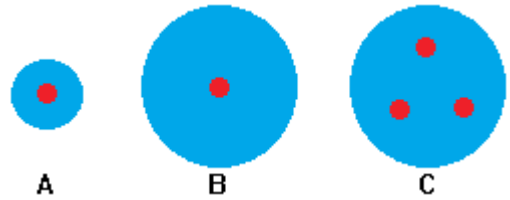

Fig. 6: A graphic showing IN (red) in water droplets (blue). Despite the different size, droplets A and B will freeze at the same temperature, while droplet C will freeze before due to its higher number of IN.

among the liquid phase, a larger droplet is expected to contain more ice nuclei than a small one. In this case, as an approximation, one can simply use V for calculation of J_{het} and avoid the measurement of the contact surface. Furthermore, it allows a direct comparison between J_{hom} and J_{het}, which then are in the same units.

1.3. Properties of pollen and fungal spores

Both pollen and spores are living reproduction units that are distributed via the atmosphere. To protect the sensitive genetic material they transport they have a sturdy shell built up by a biopolymer. Additionally, they are filled and covered with numerous molecules of certain functions, for example in metabolism.

Pollen are the male gametes (= sexual reproduction cells) of spermatophytes (= flowering plants), which are plants that originate from a seed. A seed is a plant embryo capsule formed by sexual reproduction. Therefore, the plants form florescence, which produces male and female gametes. In contrast, other multicellular plants, namely mosses and ferns, reproduce by forming asexual spores. Pollen are produced to transport the male germ cells between different individuals, either by wind for anemophilic plants, by animals for zoophilic plants, or by water for hydrophilic plants. Most plant species are monoicous –

meaning, that one individual produces both male and female germ cells. But some, like yew, juniper and willow, are dioecious – meaning, that there are male and female individuals, of which only the male ones produce pollen, and only the female ones carry fruits.
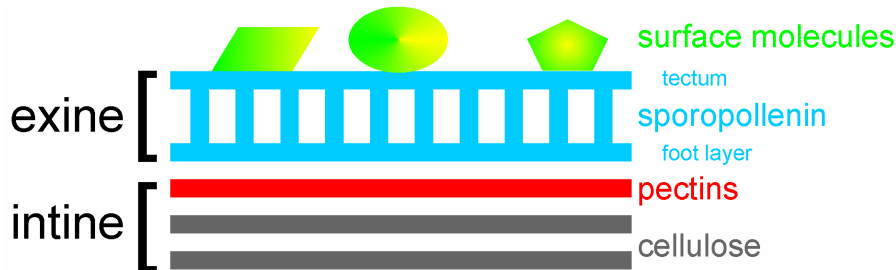

Fig. 7: A schematic presentation of the pollen wall.

Pollen have a diameter of 5-200 μm with *Myosotis* (forget-me-not) pollen as one of the smallest and *Abies alba* (European silver fir) pollen as the largest. The pollen wall consists of two layers: The inner layer, the intine, continuously coats the whole pollen and is built up by 2-3 flimsy sheets. While the outermost is mainly made of pectins (poly-galacturonic acid), the others are mainly cellulose fibres. The exine consists of sporopollenin, which is a polymer built up by aromatic carboxylic acids, phenylpropanoids and unbranched aliphatic chains, and has a mainly granular structure with a particle size of a few nanometers. This layer is very rigid and gives the pollen a high stability and water keeping ability. Furthermore, it is penetrated by many nano-capillaries with a diameter of about 25 nm [Kovacik et al. 2009]. On the exine, surface molecules are located. Apart from low-molecular species, like sugars, lipids and carotenoids [Schulte et al. 2009], also large biomolecules, like proteins [Breiteneder et al. 1989] and polysaccharides [Clarke et al. 1979] can be found on the pollen surface. Many of them are hydrophilic, like the pollen allergene proteins. This is the reason for their ability to diffuse into human mucous membranes and consequently cause allergic reactions[i]. Zoophilic pollen are additionally coated with an extracellular lipid matrix that emits insect-attracting odours. Pollen can adsorb high amounts

---

[i]   http://www.polleninfo.org

of water, which is either deposited on their surface, or sucked into their capillaries.

Fungal spores are 1-100 μm in diameter, but those of most species are smaller than 20 μm. Their cell wall consists of an intine which is made of chitin (poly-N-acetylglucosamine) and glucans (mainly cellulose), while the holey outer wall consists of glycoproteins, which make more than half of the total cell wall mass [Schoffelmeer et al. 1999].

Most fungal species exist in an anamorphic (asexual) and a teleomorphic (sexual) form [Jaeger et al. 2003], both together are called the holomorphic. As the two forms can have totally different appearance and properties, they often could not be assigned in former times. Another problem is, that many fungi reproduce themselves mainly asexually, especially under laboratory conditions, so that many teleomorphic forms are unknown. Fungi without a known teleomorphic form used to be called "Fungi imperfecti" – a denotation that is nowadays obsolete. Strictly speaking, the name of a species (holomorphic) should be the same as the teleomorphic, unless just the anamorphic is meant, but many species are traditionally called by their anamorphic name, because they are far better known in their asexual form (e.g. *Fusarium*, *Aspergillus*, *Penicillium* species). As more and more teleomorphic fungi are discovered within time, the taxonomy is continuously reorganized.

The anamorphic forms reproduce themselves by conidia, which are mitotic spores consisting of converted hyphae cells. The teleomorphic forms build up an imposing fruiting body (what we call mushrooms are in fact the fruiting bodies of some fungal species), which produce meiotic spores. Those spores can just form a primary mycel, which readily fusions with another primary mycel to form a secondary mycel. This way, fungi can reproduce in both ways: the asexual one, making an individual independent of a partner, and the sexual one, which increases genetic turbation.

Most sample fungi in this thesis belong to the *Ascomycota* division, also called sac fungi. Their reproduction organs are called asci – tubular bags, in which the spores are lined up. Some genera, like *Aspergillus* and *Penicillium*, form characteristic asci-carrying stands, which grow on the mycelium. The Sordariomycetes (e.g. *Fusarium*) grow their asci in cavities in the mycelium.

Many molds belong to the *Ascomycota* division, but also most lichen fungi and yeasts, as well as truffles and morels. The second big branch of fungal species belong to the *Basidiomycota* division, also called club fungi. A basidium is a microscopic pedestial- or club-like structure consisting of one or few cells which carry the spores on their ending.

1.4. Biological macromolecules

Macromolecular structures are essential for every form of life. The two most important ones of them are proteins and saccharides, sicne they play a vital role in the biochemistry of all types of living cells [Elliot and Elliot 2005].

Proteins are polymer sequences built up by amino acids as monomers.The centre of an amino acid is a chiral C atom, to which four functional groups are bound: a carboxyle (-COOH), an amine ($-NH_2$), a hydrogen (-H) and another organic functional group (-R), which is specific for every amino acid [Baltes 2007]. Out of the 20 naturally common amino acids, two are a bit different: For glycin, R is only H, and thus it is the only achiral amino acid. In prolin, R forms a ring with the amino group, which carries only one H. For the chiral amino acids, two enantiomers, in terms of the Fischer projection a D- and a L-form, exist. In nature, the L-form is far more common than the D-form.

Amino acids are bound to each other via a peptide bond. Therefore, the carboxyle of one amino acid esterifies with the amine of another one under release of H_2O. The peptide is a planar C_1-CO-NH-C_2 structure with C_i as the

chiral centres of two amino acids. A protein is a long sequence of peptide bonds. A specific protein has a defined sequence of amino acids, which is coded in the genes of the lifeform expressing it. While the peptide backbone is alike in all proteins, the sidechains R determine the specific properties of a specific protein. The sequence of amino acids is known as primary structure of the protein.

Due to intramolecular interactions, a peptide chain will not stay linearily, but fold in a certain way. Hydrogen bonds between backbone functional groups lead to formation of helical, sheet-like or other defined geometries, which are called secondary structures. Although the R do not participate directly, they can favor particular structures by their steric and functional properties. Direct interactions of the R lead to a further arrangement of the secondary structure elements into a total protein geometry, which is called the tertiary structure. It is mainly driven by non-covalent forces, for example hydrophobicity, with the exception of disulfide bridges that are generated by linkage of the thiogroups (-SH) of two cysteine units. In contrast to the secondary structure, which is equivalent to the short-range local conformation of the peptide chain, the tertiary structure is the holistic, long-range folding of the protein. Folding is essential for the functioning of a protein, since interactions with both the surrounding and potential substrates are determined by the geometry and the location of characteristic groups. Therefore, changes in secondary and tertiary structure, which are far less stable than the covalently fixated primary structure, can adulterate or inactivate the function of the protein. Therefore, even moderate stresses lead to unfolding and therefore fundamental change of the properties, although the primary sequence is not harmed. A full protein can consist of one polypeptide chain, but also of several covalently linked chains. For example, antibodies are built up by four chains that are linked by disulfide bridges. In some cases, several proteins form loose homoaggregates. Although an individual unit would show the demanded activity, the aggregation, which is called

quaternary structure, leads to a higher efficiency. An overview over protein structures is shown in Fig. 8.

A lot of proteins do not consist only of peptide chains, but are posttranslationally modified. For example, the active center of Hemoglobin, myoglobin, chlorophyll and vitamine B_{12} is a metallo-tetrapyrrol system. Furthermore, the R of some amino acids are capable of covalently binding to sugar or fat molecules. Therefore, one can discriminate between pure proteins, glycoproteins, lipoproteins and lipoglycoproteins. Also loose aggregates between proteins, lipids and saccharides are known to exist.
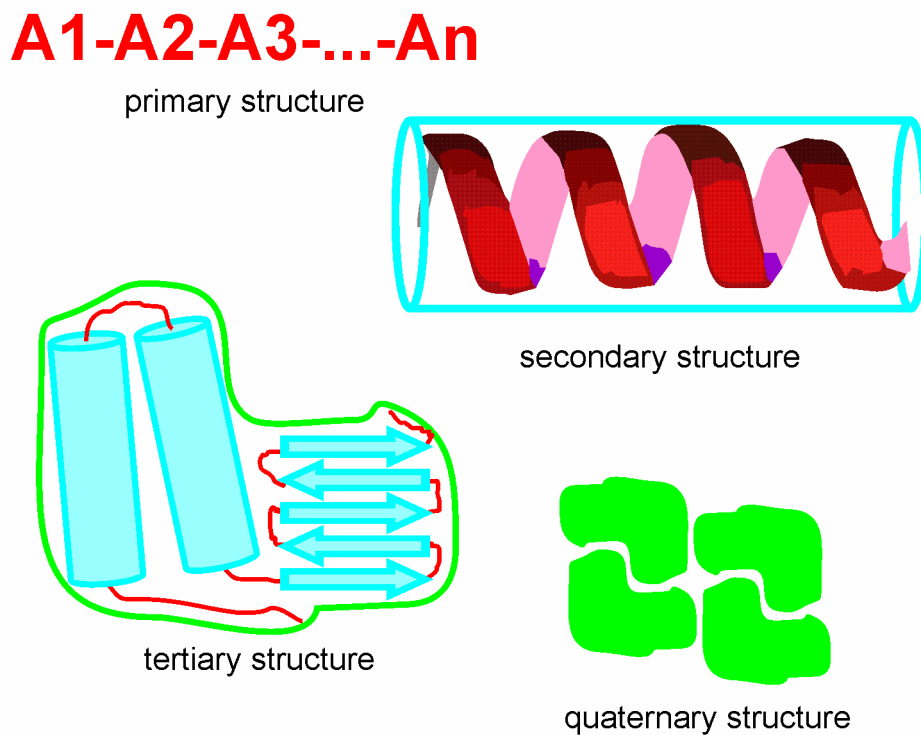
Fig. 8: Overview over the different levels of protein structure. "A" in the sequence represents an individual amino acid.

Proteases are enzymes that split the peptide bond and so break down proteins. Although all linkages in the primary structure should be prone to hydrolyzation, many proteases attack only, respectively favoredly, certain positions or amino acids. However, since typical proteins contain most or all of the 20 naturally common amino acids, proteases are rather universal.

Saccharides are built up of monosaccharide molecules. A monosachharide is a polyol with a carbonyl function. The sum formula of a single sugar monomer is $(CH_2O)_n$. The carbonyl can either be an aldehyde or a ketone, n can be a number from 3 to 7. Under physiological conditions, the sugars form a hemiacetal ring by an intramolecular nucleophilic addition of a hydroxy-O on the carbonyl-C [Vollhardt and Schore 2003]. The carbonyl-C becomes a chiral centre in the process, which can be either a R-form or a S-form. Therefore, this C is called the anomeric C-atom, the two possible product molecules are a pair of anomeres.

The monosaccharide family tree contains more than 40 different compounds [Baltes 2007], and every one of them exists in the naturally more common D-form and the less common S-form (in the Fischer projection, the OH group of the chiral C that is furthest away from the carbonyl, is either on the right or on the left side of the chain; the D- and the L-form are enantiomers; different monosaccharides differ by the positioning of the OH groups relative to each other).

Monosaccharide molecules can bind to each other by esterification of two hydroxy groups. Depending on the number of linked monosaccharide units, one can discriminate between di-, oligo- and polysaccharides. Low-molecular saccharides are commonly called sugars. Although a set of more than 40 different building blocks is available, most polysaccharides are built up by only one or a low number of different monomers. This is in contrast to proteins, where usually most or all of the 20 building blocks are present.

In contrast to the peptide bond, different connections are possible due to the presence of several OH groups at different positions, which are additionally chiral centres. For example, glucose, the most common monosaccharide, typically binds on C-position number 1, 4 or 6 to another sugar molecule, where 1 is the anomeric position, which can be either in α- or in β-orientation. For example, amylose (=starch) and cellulose are both polysaccharides consisting only of 1,4-linked glucose units, however, the difference is the orientation of the

glycosidic oxygen relative to the antecendent sugar molecule, which is in α-conformation in amylose, but in β-conformation in cellulose.

Since monosaccharides can bind on more than 2 positions to other molecules, sequences can be either linear or branched, what multiplies the number of possible products. For example, amylose consists of a sequence of α-1,4-linked glucose molecules, while glycogen also features some α-1,6-linkages, what leads to branching of the molecule.

In some cases, functional groups of the monomers are substituted. For example, a -CH_2OH group can be oxidized to a -COOH group. Such monosaccharides are called uronic acids, a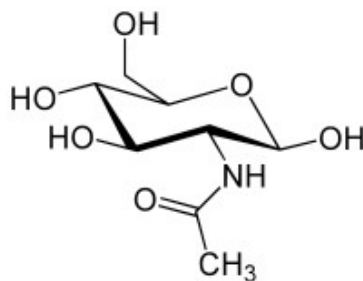nd the corresponding polysaccharides are pectins. If an -OH is substituted with -NH_2, the product is called an aminosaccharide. Some of the most common polysaccharides in nature are such compounds: Chitin is a polymer built up by N-acetylglucosamin units (see Fig. 9). It is present in the exoskeleton of arthropods and the cell wall of fungi. Murein is a copolymer that stabilizes the cell wall of bacteria.

Fig. 9: N-acetylglucosamin

Because of all these facts together, many different types of polysaccharide backbones exist, in contrast to the rather universal backbone in proteins. Therefore, saccharases – enzymes that split the ester bonds between the building units – are very substrate-specific. For example, cellulase only breaks down cellulose, amylase only amylose, because they can only attack one conformation of the 1,4-gylcosidic-link between two glucose molecules. Although this is advatageous for specific substrate-breakdown, it makes a collective enzymatic breakdown of all saccharides impossible.

1.5.   Biogenic ice nucleation and antifreezing

More than 80% by mass of all lifeforms are exposed to temperatures below 278 K, either living in the oceans or in the polar regions [Christner 2010]. As a

consequence cold environment adaptation is essential for a lot of species to survive. One strategy is the expression of either IN or Antifreezing Proteins (AFP). Most, but not all, of the high-efficient biological IN, which are able to nucleate at temperatures above 263 K, are ice nucleation proteins (INP) [Christner et al. 2008]. Among those are the IN expressed by bacterial and fungal species. The AFP inhibit the formation of ice by decreasing the freezing point, but they do not have an effect on the melting point. So they cannot melt already formed ice.

Although ice nucleation and antifreezing seem to be fundamental opposites, they are caused by similar mechanisms. Bacterial INP (BINP) and some AFP simulate an ice-like structure with their trigonal symmetry (see Fig. 10[i]) and by presenting OH groups at proper distances on their surface (e.g. Threonine, Aspartic acid, Serine, sugars). By adsorption and structuring of water molecules non-covalently INP form ice clusters large enough to cause further crystal growth. For AFP two mechanisms for antifreezing are suggested:

Fig. 10: The beta-helical AFP of *Choristoneura fumiferana*

- Since they are smaller and do not form aggregates, the water-adsorbing site is much smaller than in IN. So the formed water clusters are smaller than the critical size for crystal growth. [Graether and Jia 2001].
- They contact the ice crystals on their growth faces and so block further crystal growth [Hoshino 1999, Zachariassen and Kristiansen 2000].

AFP are expressed by some bacteria, insects, Arctic bony-fish and plants. The animal AFP all are very effective and expressed in extracellular fluids, like the insect hemolymph or vertebrate blood [Duman and Horwath 1983, Zachariassen and Kristiansen 2000]. Most of their properties, as well as sequence and structure, are already known, for example that they have a mass of 2-34 kDa

---

[i] http://en.wikipedia.org/wiki/Beta_helix

[Zachariassen and Kristiansen 2000]. The insect AFP are mostly 9-14 kDa beta-helical lipoproteins [Gronwald et al. 1998, Liou et al. 1999], which simulate the structure of ice and are most efficient.

As AFP consist of an above-average amount of hydrophilic amino acids [Liou et al. 1999, Graether and Jia 2001], most of them lack intramolecular hydrophobic interaction [Liou et al. 2000]. As a consequence their tertiary structure has to be stabilized by a lot of disulfide and hydrogen bridges, what makes them very sensitive towards disulfide-splitting chemicals [Yeh and Feeney 1996]. A lot of TxT-units in the sequence (T stand for Threonine, which has a chiral OH group, x is any rather unpolar amino acid) are the initiation points for ice cluster formation [Graether and Jia 2000]. The distances in the oxygen positions of the Threonine-OH match the distances in an ice crystal [Liou et al. 2000]. Insects producing this kind of AFP are *Choristoneura fumiferana* (spruce budworm) [Graether and Jia 2000, Jia et al. 2002, Doucet et al. 2002], *Tenebrio molitor* (mealworm beetle) [Liou et al. 1999, Liou et al. 2000], *Rhagium inquisitor* (a longhorn beetle) [Kristiansen et al. 1999] and larvae of *Dendroides Canadensis* (a fire-colored beetle) [Olsen and Duman 1997].

Fig. 11: L-Threonine

beetle) [Olsen and Duman 1997]. One side of the *Tenebrio molitor* AFP is a flat, perfectly structured beta sheet, which is the nucleation site, while the *Choristoneura fumiferana* AFP consists of three beta sheets. Fish AFP are either pure proteins, but more often glycoproteins. The latter ones contain a lot of AAT-sequences, with A standing for alanine and T for threonine. The OH-groups in the sidechains of Threonine are esterified with disaccharide units, which are all located on one side of the molecule [Heggemann et al. 2010, Yeh and Feeney 1996]. Some purely proteinaceous fish AFP are very alanine-rich (~65%) alpha-helices, where most of the alanine is on one side, while on the other there are hydrophiloc amino acids, which interact with ice. Others are beta-sheets with about 15% alanine, which are stabilized by disulfide bridges. AFP of the third group are only 62-66 residues long and have a globular structure.
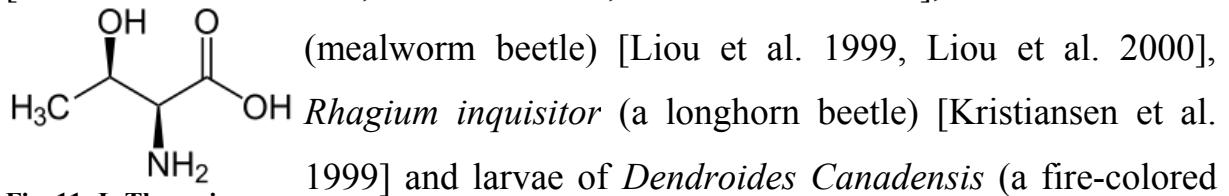
Plants like clubmoss, winter wheat and ginkgo [Duman and Olsen 1993], as well as winter rye [Hon et al. 1994, Hon et al. 1995], carrot [Meyer et al. 1999], bittersweet nightshade [Huang and Duman 2002] and more, also contain AFP with a size of 11-82 kDa, but they are different from their animal counterparts: The winter rye AFP is similar to pathogenesis-related proteins, which are produced by the plant under stress situations.

Another way of freeze protection are INP. As they are located in extracellular fluids, they draw away the ice from more sensitive compartments, like the cell membranes [Zachariassen and Kristiansen 2000]. INP that have the purpose of freeze protection nucleate at lower temperatures (263-267 K) than BINP (268-271 K), what can be explained by their different functions: The higher the nucleation temperature is, the larger – and so more damaging – are the ice crystals, but efficiency decreases at lower temperatures. So a moderate nucleation temperature, which is realized in animal INP, causes a smooth, gentle freezing process [Somero et al. 1992]. At higher IN* temperatures, the growing ice crystals are like growing knives, while at too low temperatures other sites may compete with the INP for nucleation.

As IN have also been detected in non-psychrophilous species not exposed to freezing temperatures, these are suspected to be incidental IN, which are ice nuclei in the experiment, but of no biological function in the living creature [Lundheim 2002]. For example, the human low-density-lipoprotein is a good ice nucleus in experiments, but it fulfills a totally different purpose in metabolims. The IN expressed in psychrophilous species, however, are most certainly adaptive, meaning that they fulfill a certain purpose in cold environments, like freeze protection.

Some species protect themselves by expressing IN, like the larvae of *Tipula trivittata* (a crane fly) expressing a 800-kDa-lipoprotein, which contains two protein elements with 265 and 80 kDa [Duman et al. 1985, Neven et al. 1989,

Duman et al. 1991]. It is a hypothesis that the *Tipula*-INP originally served as a lipid shuttle, but was later optimized by evolution to serve as a cryoprotective mechanism [Duman et al. 1985].

Other animals producing IN are the larvae of *Dendroides Canadensis*, which also express AFP [Olsen and Duman 1997], *Eurosta solidaginis* (goldenrod gallfly) expressing inorganic calcium phosphate spherules [Mugnano et al. 1996], queens of *Vespula maculata* (a hornet), which produce a rather hydrophilic 74-kDa-INP [Duman et al. 1984], the frog *Rana sylvatica* [Wolanczyk et al. 1990], the turtle *Terrapene carolina* [Costanzo and Claussen 1990], the snail *Melampus bidentatus* [Hayes and Loomis 1985, Madison et al. 1991] and the mussel *Mytilus edulis* [Aunaas 1982, Lundheim 1997a].

The extracellular INP in *Secale cereale* (winter rye) also depend on phospholipides and saccharides, which become the more important, the higher the cultivation temperature is [Brush et al. 1994]. Five different INP found in *Lolium perenne* (ryegrass) form hexagonal ice crystals [Kumble et al. 2008].

The succulent plant *Lobelia telekii* contains IN which cause slow freezing of its internal water reservoir. The released crystallization heat prevents the dropping of temperatures within the plant. As the fluid mainly contains carbohydrates, they are the most probable candidates for being the responsible IN [Krog et al., 1979]. The IN in the wood of some *Prunus* species (fruit trees, e.g. peach) are non-protein compounds, since they are insensitive towards pronase and other protein-damaging substances [Gross et al. 1988]. Other plant IN have been found in citrus fruits [Constantinidou and Menkissoglu 1991], sea buckthorn berries [Jann et al. 1997], seaweed [Lundheim 1997b] and beans [Zachariassen and Kristiansen 2000]. It was also suggested that lignin, a firm polymer built up by aromatic alcohols, which is the structural substance of wood, shows high IN* activity [Gao et al. 1999].

1.6.   IN of bacteria, fungi and pollen

The ice nucleation ability of certain gram-negative plant pathogenic bacteria, like the *Pseudomonas* species *syringae*, *viridiflava* and *fluorsecens*, as well as *Erwinia ananas*, *herbicola* and *uredovora*, *Pantoea agglomerans* and *Xanthomonas campestris* [Kawahara 2002, Christner 2010], is caused by a special type of INP, which is coded by very similar genes in all species [Green and Warren 1985, Wolber et al. 1986, Abe et al. 1989, Warren and Wolber 1991]. The postulated biological function of these proteins is to grow crystals cutting into the plant tissue and so make its nutrition-rich inwards more accessible for the bacteria. They form ice in the affected plant tissue to cause cell rupture, cell dehydration and concentration of cytosol salts to toxic levels in order to make nutrients better available for the bacteria [Lindow et al. 1982a+b, Zachariassen and Kristiansen 2000]. Another advantage of IN* activity is that cells which are lifted into the atmosphere and distributed can cause their precipitation by cloud seeding, and so return to the surface [Morris et al. 2004]. The presence of thriving bacterial communities in the clouds [Sattler et al. 2001] impressively demonstrates the adaptability of these species to very cold environments. Since the production of these INP is energetically costly for the bacteria [Schnell 2009], only a selective advantage can be the reason for their expression. Therefore, the BINP are typical examples of adaptive IN.

All BINP are quite similar to each other, with a genetic sameness of 75% [Lindow 1995]. They share a lot of properties with insect AFP, like being very efficient, bearing non-proteinaceous residues, containing many beta-sheets [Schmid et al. 1997], lacking a hydrophobic core and containing TxT-sequences [Graether and Jia 2001]. The naked protein sequence has a mass of circa 120 kDa [Kozloff et al. 1991, Turner et al. 1991], is located in the outer cell membrane [Kawahara 2002] and mainly consist of one so-called R-domain, which makes up about 80% of the sequence, is highly repetitive and hydrophilic [Abe et al. 1989, Kawahara 2002]. The other domains are the hydrophilic C-

terminus and the hydrophobic N-terminus, which is responsible for anchoring the protein in the cell membrane. The R-domain forms a beta-helical structure similar to that of many insect AFP [Graether and Jia 2001].

Of highest importance are again the TxT sequences of the R-domain, which simulate the structure of ice and act as the first fixation point for water molecules. But BINP contain much more TxT sequences than their AFP counterparts, making them advance ice growth instead of suppress it [Graether and Jia 2001]. The importance of the TxT sequences has been proven by genetically engineering the DNA of bacterial cultures. The change of the TxT sequence leads to a 70% loss of ice nucleating ability, while other genetic modifications show just little change [Graether and Jia 2001]. For stabilizing the structure intramolecular disulfide bridges are necessary, what makes it possible for disulfide splitting reagents to destroy the IN* activity [Pouleur et al. 1992].

The apparent mass of the INP in gel electrophoresis is 150-180 kDa, what is caused by posttranslational modification of the protein sequence [Kozloff et al. 1991, Turner et al. 1991]. The discrepancy between the protein sequence mass of 120 kDa and the full mass of 150-180 kDa has led to confusions in the past [Warren and Wolber 1991].

The side chains are both sugars, especially mannose [Humphreys et al. 2001, Turner et al. 1991], which also provide OH-groups, and phospolipids, especially phosphatidylinositol [Kozloff et al. 1984, Humphreys et al. 2001], which is responsible for the linkage of the INP to the cell wall [Kozloff et al. 1991]. The presence and nature of these side chains can increase the nucleation temperature for some Kelvin in comparison to a naked INP.

Furthermore, INP units tend to form homoaggregates with total masses of several MDa. These molecular clusters perfectly match the active sites model (see chapter 1.2.). According to theoretical considerations the IN* activity of a certain class of ice nuclei increases with the molecular size. Nucleation at 261 K is associated with INP-masses of at least 150 kDa (about 1 INP unit), at 263 K

with more than 360 kDa (about 2-3 INP units) and at 270 K with 8-20 MDa (50-125 INP units) [Warren and Wolber 1991]. In contrast AFP do not agglomerate and so do not reach the critical size to cause ice nucleation [Graether and Jia 2001]. The IN clusters are held together by the lipidic components, which anchor the single INP units [Kozloff et al. 1991]. That is why lipase and delipidating agents can reduce the bacterial IN* activity by breaking up these aggregates [Govindarajan and Lindow 1988]. The sugars are connected to the protein core as N- or O-glycans [Kozloff et al. 1991]. Mannose molecules form a glycosidic link between nitrogen atoms of the peptide backbone and phosphatidylinositol, which is incorporated in the lipidic outer cell mebrane. These large lipoglycoprotein-complexes consist of hydrophobic and hydrophilic sections, which are both necessary to cause efficient ice nucleation [Kawahara 2002]. Hydrophilic sequences are necessary to bind water molecules [Graether and Jia 2001], but purely hydrophilic molecules dissolve in water and do not keep structures large enough for ice nucleation. A study on alcohols has shown, that monolayers of aliphatic long-chained alcohols are ice-nucleating, while short-chained water-soluble alcohols are freeze-depressing [Gavish et al. 1990].

The high similarity between BINP and *Tipula* INP is proven by the fact, that antibodies against the *Tipula* INP show cross reactivity towards BINP [Warren and Wolber 1991]. The main difference between these INP and AFPs like those in *Tenebrio molitor* is the size and so the number of TxT sequences. For example, while an AFP of this kind has only about 6 such sequences, an average INP of this kind has about 60 [Graether and Jia 2001].

In some cases one protein can act as both an INP and an AFP. *Pseudomonas putida* is the first species, in which such a protein has been detected [Xu et al. 1998]. It is a lipoglycoprotein, 164 kDa in size, which is rich in glycine and alanine. The removal of the carbohydrates destroys the IN*, but not the antifreezing properties.

The amount of expressed INP and along with it the efficiency of a bacterial culture strongly depend on the conditions at which it has been grown. For example, low temperatures and low nutrition concentrations lead to a higher expression of IN in the bacteria [Rogers et al. 1987, Nemecek-Marshall et al. 1993, Gurian-Sherman and Lindow 1995, Fall and Fall 1998]. It was also found that by insertion of the BINP-gene into the DNA of IN-negative bacteria, like *Escherichia coli*, these species can be made IN* positive [Orser et al. 1985].

Furthermore, the IN* activity of decaying leaves dust was tracked down to bacteria participating in the decaying process and their metabolic products [Vali et al. 1976]. However, decaying leaf contain also other IN apart from the BINP, which are less efficient, but more stable [Schnell 2009].

Because of their high IN* efficiency, IN* positive cultures of *Pseudomonas syringae* are grown, shred and dried. This commercially available substrate is known as "Snomax" and is applied as additive in snowguns.

The mycelium of some lichen [Kieft 1988, Kieft and Ahmadjian 1989, Kieft and Ruscetti 1990, Kieft 1992] and mold [Pouleur et al. 1992, Richard et al. 1996, Hasegawa et al. 1994] fungal species was IN* positive in the droplet freezing mode. For the lichen fungi it was proven, that the IN* activity is contributed by the fungal and not the photobiotic partner. Thermal, chemical and enzymatic investigation showed furthermore that fungal ice nuclei are proteinaceous [Kieft and Ruscetti 1990, Pouleur et al. 1992, Tsumuki and Konno 1994].

The non-lichen fungal species already known to possess IN* ability are the *Fusarium* species *acuminatum*, *avenaceum*, *moniliforme*, *oxysporum* and *tricinctum* [Pouleur et al. 1992, Richard et al. 1996, Tsumuki et al. 1995, Humphreys et al. 2001], which nucleate at about 268 K. These species produce also IN* positive conidia (asexual spores), what is understandable, as they originate from hyphae. Additionally, two ice nucleating yeast species were found, but not specified or analyzed further [Maki and Willoughby 1978]. There

have been reports of other ice nucleating species, like *Cladosporium herbarum* and *Penicillium digitatum*, but as the homogeneous freezing temperature in that study was about 248 K, these results have to be taken with care [Jayaweera and Flanagan 1982]. Generally, in the older studies comparatively giant droplets (0.5-10 µl) were placed on a substrate with immense particle concentrations, so these results are not applicable for conditions in the upper troposphere. According to a more recent study *Cladosporium* spores are IN* negative [Iannone et al. 2011]. Very recently, IN* activity was found in *Isaria farinosa* and *Acremonium implicatum* [Huffman et al. 2013]. The total impact of fungal IN in the atmosphere is still debated, since their total number is far lower than that of mineral dust [Hoose et al. 2010, Sesartic et al. 2013], their total number can be boosted by certain processes, for example by rainfall [Huffman et al. 2013].

Fungal INP (FINP) have some properties in common with BINP: They are proteins, what can be derived from their deactivation by proteases [Kieft and Ruscetti 1990, Tsumuki and Konno 1994], they contain beta-sheets, and they often have a similarly strong ice nucleating effect, but there are also some grave differences: FINP show higher stability and are therefore active even after having been exposed to temperatures up to 333 K. Furthermore, the pH-range in which they are stable reaches from 1 to 13 for *Fusarium* and from 1.5 to 12 for lichen fungi. They are not anchored to the cell surface, as they can be separated from the cell and match through a 0.22-µm-filter. They contain fewer charged amino acids, what explains their increased pH stability [Kieft 1995], and their structure is not held together by disulfide bridges. Furthermore, they are pure proteins, not depending on lipid or saccharid components, as their activity is not decreased by treatment with chloroform, cellulase, chitinase or phenylboric acid [Kieft and Ruscetti 1990, Hasegawa et al. 1994, Tsumuki and Konno 1994]. At last, their expression seems to be independent of the cultivation temperature

[Humphreys et al. 2001], while bacteria tend to express more ice nuclei when cultivated at low temperatures and on nutrient-poor media [Rogers et al. 1987, Nemecek-Marshall et al. 1993, Gurian-Sherman and Lindow 1995, Fall and Fall 1998]. As there is no detailed sequence or structure information available, it is not surely known, how much FINP and BINP are really alike. Their genetic codes do not match each other, but as in many cases the same amino acid can be coded by several nucleic acid triplets, this fact is not significant [Hasegawa et al. 1994].

It is furthermore known, that diverse subspecies of one fungus can show different nucleation behavior, and that even initially IN* positive fungal strains can lose their activity during cultivation in the laboratory [Tsumuki et al. 1995]. The reason is most probably the lack of stress under laboratory conditions, which makes the expression of costly stress adaptative proteins obsolete for survival. This process has been already observed in IN* positive bacteria cultures [Rogers et al. 1987, Nemecek-Marshall et al. 1993, Gurian-Sherman and Lindow 1995, Fall and Fall 1998].

Pollen have the ability to initiate both cloud condensation [Dingle 1966] and ice nucleation [Diehl et al. 2001, Diehl et al. 2002, von Blohn et al. 2005]. Although there are only few data about pollen ice nuclei (PIN), it has been shown, that some pollen are ice nucleating up to 265 K in three of the freezing modes, but definitely inactive in the deposition freezing mode. Negative results in the deposition mode means, pollen lack of those special water-simulating proteins discovered in bacteria and fungi. Up to now, the nature of the PIN is unknown. Once their IN* activity was derived from the roughness, edges, pores and grooves of the pollen surface [Diehl et al. 2001], but very recently it has turned out, that the IN of pollen are in fact extractable surface components [Pummer et al. 2012].

Pollen of the following plant species have been tested in the past [Diehl et al. 2001, Diehl et al. 2002, von Blohn et al. 2005]: *Alnus incana* (alder), *Populus nigra* (poplar), *Betula alba* (birch), *Quercus rubra* (oak), *Picea alba* (spruce), *Pinus sylvestris* (pine), *Secale cerale* (rye), *Agrostis alba* (bentgrass), *Agrostis gigantea* (redtop grass), *Poa pratensis* (Kentucky bluegrass), *Dactylis glomerata*.

1.7.   Chosen pollen plants

Agrostis gigantea	redtop grass (3)	light yellow	20 μm
Ambrosia artemisiifolia	ragweed (4)	light yellow	20 μm
Artemisia absinthium	wormwood (4)	beige	20 μm
Betula alba/pendula	silver birch (1)	strong yellow	20 μm
Betula occidentalis	Water birch (1)	Strong yellow	20 μm
Carpinus betulus	European hornbeam (1)	yellow	35 μm
Corylus avellana	common hazel (1)	strong yellow	25 μm
Juniperus chinensis pfitzeriana	Pfitzer juniper (2)	yellow	20 μm
Juniperus communis	common juniper (2)	orange-yellow	20 μm
Lolium perenne	perennial ryegrass (3)	beige	35 μm
Pinus sylvestris	Scots/Scotch pine (2)	light yellow	40 μm
Plantago lanceolata	English plantain (4)	beige	20 μm
Platanus orientalis	plane tree (1)	yellow	20 μm
Rumex acetosa	sorrel (4)	yellow	20 μm
Salix caprea	goat willow (1)	strong yellow	20 μm
Taxus baccata	Irish yew (2)	orange-yellow	20 μm
Thuja occidentalis	Northern whitecedar (2)	orange-yellow	20 μm
Thuja orientalis	arborvitae (2)	yellow	20 μm
Triticum aestivum	wheat (3)	orange-yellow	45 μm
Ulmus americana	American elm (1)	light yellow	25 μm
Urtica dioica	big nettle (4)	beige	13 μm
Zea mays	corn (3)	strong yellow	65 μm

Tab. 1: Latin and English names of species investigated, plus the pollen color and the average diameter.

The pollen-producing plants chosen for research can be divided into four trivial subgroups: broadleaf trees (1), conifers (2), grasses (3) and weeds (4). Among

every group several samples were chosen. Tab. 1 presents the Latin and English names of the species, their classification number defined above, as well as color and diameter of their pollen. A more scientific classification is given in the table of green plants systematics at the end of this chapter.

Plants only produce pollen during a certain time of the year, the so-called pollen season (see Tab. 2). The exact pollination period, which usually peaks over a few weeks, depends on temperature and humidity and can therefore vary annually due to variable ambient conditions.

	Jan	Feb	Mar	Apr	May	Jun	Jul	Aug	Sep	Oct
Hazel	red	red	red	red						
Willow		red	red	red	red					
Birch		red	red	red	red	red				
Elm			red	red	red					
Hornbeam				red	red					
Plane Tree					red	red				
Yew			blue	blue	blue					
Juniper				blue	blue					
Thuja				blue	blue					
Pine					blue	blue	blue			
Grasses				green	green	green	green	green	green	green
Nettle					green	green	green	green	green	
Ragweed					green	green	green	green	green	green
Wormwood						green	green	green	green	green

Tab. 2: Pollen Calendar

Not only the pollen season, but also the regional distribution strongly differ between the given species, thus exposing them to different climatic conditions. Birch and pine species, as well as common juniper, are distributed across the whole Northern temperate climate zone, from 35°N up to 70°N. The maximum population density of pine species is among the boreal forests at latitudes above 60°N (Canada, Siberia, Scandinavia), so these species are exposed to a very frosty climate. Most other species are typically present South of the boreal

region, namely at 25°N to 60°N. Corn was originally cultivated in Central America (10-30°N), which is dominated by a Tropical climate.

The following list presents an (incomplete) overview over green plant systematics to demonstrate the relations between the investigated species:

Regnum *Viridiplantae*
- Subregnum *Chlorophytes* (green algae)
- Subregnum *Bryophytes* (mosses)
- Subregnum *Pteridophytes* (ferns)
- Subregnum *Spermatophytes* (flowering plants)
  - Div. *Ginkgophyta* (1 species)
  - Div. *Cycadophyta* (100-300 species in 1 order)
  - Div. *Gnetophyta* (50-150 species in 1 order)
  - Div. *Coniferophyta* (500-700 species in 1 order)
    - Cl. *Coniferopsida*
      - Ord. *Coniferales*
        - Fam. *Cupressaceae*
          - Gen. *Juniperus*
            - *communis* (common juniper)
            - *chinensis pfitzeriana* (Pfitzer juniper)
          - Gen. *Thuja*
            - *orientalis* (Chinese arborvitae)
            - *occidentalis* (Northern whitecedar)
        - Fam. *Pinaceae*
          - Gen. *Pinus*
            - *sylvestris* (scotch pine)
            - *nigra* (black pine)
        - Fam. *Taxaceae*
          - Gen. *Taxus*
            - *baccata* (Irish yew)
  - Div. *Magnoliophyta*
    - Cl. *Magnoliopsida* (~10.000 species)
    - Cl. *Liliopsida* (~60.000 species)
      - Ord. *Poales*
        - Fam. *Poaceae*
          - Gen. *Agrostis*
            - *gigantea* (redtop, giant bentgrass)
            - *alba/stolonifera* (creeping bentgrass)
          - Gen. *Lolium*
            - *perenne* (perennial ryegrass)
          - Gen. *Triticum*

- ▪ *aestivum* (wheat)
  - ◦ Gen. *Zea*
    - ▪ *mays* (maize, corn)
  - ◦ Gen. *Secale*
    - ▪ *cereale* (rye)
- ◦ Cl. *Rosopsida* (~170.000 species)
  - ▪ Ord. *Rosales*
    - • Fam. *Ulmaceae*
      - ◦ Gen. *Ulmus*
        - ▪ *americana* (American elm)
    - • Fam. *Urticaceae*
      - ◦ Gen. *Urtica*
        - ▪ *dioica* (stinging nettle)
  - ▪ Ord. *Fagales*
    - • Fam. *Betulaceae*
      - ◦ Gen. *Betula*
        - ▪ *alba/pendula* (silver birch)
      - ◦ Gen. *Corylus*
        - ▪ *avellana* (common hazel)
      - ◦ Gen. *Carpinus*
        - ▪ *betulus* (European hornbeam)
  - ▪ Ord. *Asterales*
    - • Fam. *Asteraceae*
      - ◦ Gen. *Ambrosia*
        - ▪ *artemisiifolia* (ragweed)
      - ◦ Gen. *Artemisia*
        - ▪ *absinthium* (wormwood)
  - ▪ Ord. *Proteales*
    - • Fam. *Platanaceae*
      - ◦ Gen. *Platanus*
        - ▪ *orientalis* (Oriental plane tree)
  - ▪ Ord. *Malphigiales*
    - • Fam. *Salicaceae*
      - ◦ Gen. *Salix*
        - ▪ *caprea* (goat willow)
  - ▪ Ord. *Caryophyllales*
    - • Fam. *Polygonaceae*
      - ◦ Gen. *Rumex*
        - ▪ *acetosa* (common sorrel)
  - ▪ Ord. *Lamiales*
    - • *Plantaginaceae*
      - ◦ Gen. *Plantago*
        - ▪ *lanceolata* (English plantain)

While the *Magnoliophyta* are genetically and morphologically a quite heterogeneous group, all the conifers are very similar. In fact, all recent *Coniferophyta* belong to the order *Coniferales*, as the other three orders, namely *Cordaitales*, *Voltziales* and *Vojnovskyales*, died out in the End-Permian mass extinction 251 million years ago, which wiped out more than 90% of all species living then [Benton 2003].

The *Liliopsida* are monocot plants – meaning, that they form one primary leaf after germination. Most of them lack secondary growth and so are herbaceous plants – like grasses (including cereals), lilies, asparagus and onion. The palm trees are an exception in this group. The *Magnoliopsida* are the basal group of the angiosperms. Magnolia, laurel, pepper, avocado and sea lilies are part of this group. They form two primary leafs after germination – so they are dicots. Also the *Rosopsida* are dicots. Most flowers, weeds and broadleaf trees belong to this group. The majority of edible fruits and vegetables is produced by plants of this class.

1.8. Chosen fungal species

Fungal species were chosen depending on three criteria:

First, frequently appearing species were chosen, for they might contribute massively to cloud formation, if they are positive. According to earlier studies, the relatively most common fungi in Viennese atmosphere are *Nectria* and *Cladosporium* species [Schüller 2008]. A recent study gave an overview over the presence of fungal spore species at different sites across the globe [Fröhlich-Nowoisky et al. 2012].

Second, fungi, which are known to rise to higher atmospheric levels, were chosen. *Engyodontium album* was the only fungus detectable in the Antarctic stratosphere [Pearce et al. 2009], while following species were found alive in the mesosphere: *Aspergillus niger*, *Penicillium chrysogenum*, *Circinella muscae* and *Papulaspora anomala* [Imshenetsky et al. 1978]. All of them are richly

pigmented, which is advantageous to survive the intense ultraviolet radiation in high atmospheric levels.

Third, a mixture of IN* positive, negative and untested fungi was aimed for – in respect to literature data: *A. niger*, *P. chrysogenum*, *P. citrinum* and *T. virens* were IN-negative in former studies, while *F. avenaceum* was positive [Pouleur et al. 1992]. For *C. herbarum*, *F. oxysporum* and *P. digitatum* the results were not distinct [Jayaweera and Flanagan 1982, Tsumuki et al. 1995]. However, many common fungal species, which are additionally of ecological, economical or sanitary importance, have been investigated in this thesis for the first time.

Spores of following species were investigated in this thesis: *Agaricus bisporus*; *Aspergilluis fumigatus*, *flavus oryzae* and *niger*; *Cladosporium cladosporioides* and *herbarum*; *Engyodontium album*; *Fusarium avenaceum* and *oxysporum*; *Lentinula edodes*; *Penicillium chrysogenum*, *citrinum*, *digitatum* and *glabrum*; *Pleurotus ostreatus*; *Psilocybe cubensis*; *Trichoderma atroviride*, *reesei* and *virens*.

The *Ascomycota* make up about 34% of the fungal spore amount in the continental, and about 72% in the marine atmosphere [Fröhlich-Nowoisky et al. 2012]. The most common classes are the *Sordariomycetes* (e.g. *Fusarium* and *Trichoderma*), the *Eurotiomycetes* (e.g. *Aspergillus* and *Penicillium*) and the *Dothideomycetes* (e.g. *Cladosporium*).

The *Fusarium* species are the anamorphs of a quite polymorphic group of plant parasitic fungi, which mainly affect corn, wheat and oat. Their spores reach altitudes of 6 km, and they are closely related to many lichen fungal species [Pouleur et al. 1992]. Frost-damaged plants are affected in favor, but as INP-induced ice growth causes further damage to the plant, it is most likely a mutual amplification process. *Fusarium* fungi produce toxins (e.g. Deoxy-Nivalenol) and even kill their host. They are usually colored pink or purple. The most common exponents are *F. solani* and *F. oxysporum*. Many species have a known

teleomorphic counterpart, which can be *Gibberella*, *Nectria* [Guadet et al. 1989] or others – sometimes the *Nectria* genus is further divided into e.g. *Albonectria*, *Calonectria*, *Haemonectria*, and more. The teleomorphs are orange parasitic or saprophytic xylobiontic fungi that are feared as pathogens in fruit tree cultures.

Aspergillus species are a very important group of fungi, which express their asci on a stand, that look like an aspergil (see Fig. 12) or a watering can rose. They are related to at least ten teleomorphic genera of the *Trichocomaceae* family, namely *Eurotium* (*glauci* and *restricti* section), *Emericella* (*nidulantes* and *usti* section), *Fennellia* (*terrei* and *flavipedes* section), *Petromyces* (*flavi* section), *Neopetromyces* (*circumdati* section), *Chaetosartorya* (*cremei* section), *Neo-/Hemisartorya* (*fumigati* section [O'Gorman et al. 2009]), *Neocarpenteles* (*clavati* section), *Warcupiella* (*warcupi* section) and *Hemicarpenteles* (*ornati* section, former *Sclerocleista*). There are several other sections (like *nigri* and *candidi* section), which have not been assigned to a teleomorph up to now. *A. flavus* has become popular as "curse of the Pharaohs", as it grows in ancient tombs and emits highly toxic, carcinogenic substances. A non-toxic mutant called *A. flavus oryzae*, also known als Koji, is commonly used in East-Asian cuisine as a fermenter for soy products. *A. niger* is a very common black fungus growing in soils and affecting food (esp. fruits, nuts and vegetables), whose spores can cause lung diseases. It produces ochratoxin and kojic acid, and it adsorbs heavy metals. A genetically modified strain is industrially used for biological synthesis of citric acid. No species of the *nigri* section has ever been assigned to a teleomorph. *A. fumigatus* spores can even be detected in the Saharan desert and Antarctica. It is highly toxic, causes allergies, aspergillosis and farmer's disease. Because of its spreading and its toxicity it is the most frequent airborne fungal pathogen in developed countries [Latge 2001].

Penicillium species are another common group of anamorphic fungi, which are closely related to *Aspergillus*, but form brush-like asci stands (penicillus is the Latin word for brush, see Fig. 12). Like *Aspergillus*, they can be either spoilage

flora, or usefully applicable for humans. *P. citrinum* affects citrus fruit, *P. expansum* is toxic and causes formation of brown areas on fruit. *P. chrysogenum* grows in green punctiform cultures on bread, but is also applied as antibiotics producer. *P. roqueforti* and *camemberti* are of importance in cheese processing. Most teleomorphics of *Penicillium* species belong to the *Eupenicilliu*m or the *Talaromyces* genus.
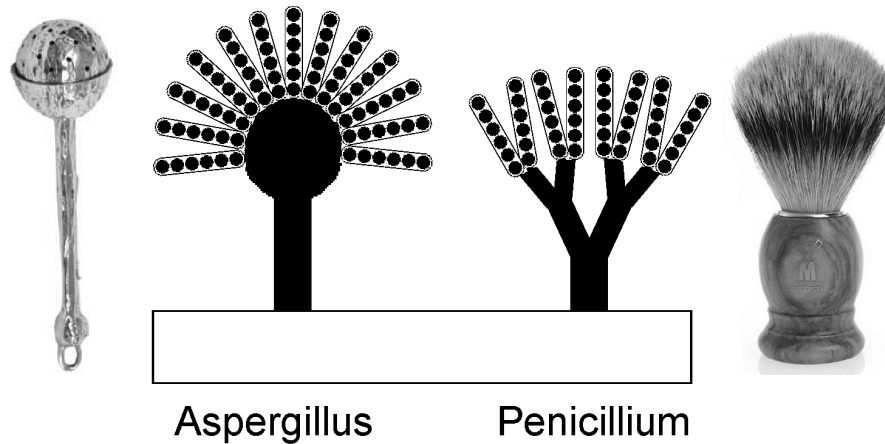

Aspergillus   Penicillium

Fig. 12: Schematics of Trichocomaceae asci stands, plus the tools after which they are named.

Cladosporium species are mold fungi causing lung infections, allergies and toenail fungus. They are usually colored from olive to dark brown, and possibly the most common fungi at all [Ariya et al. 2009]. Although their toxins are not that dangerous, they often cause an intense stench. Today the genus is equalized with the teleomorphic genus *Davidiella*, while all species correlating with other teleomorphs have been excluded from the *Cladosporium* genus. *Cladosporium cladosporioides* and *herbarum* are most likely the most common *Ascomycota* in the atmosphere.

The *Trichoderma* genus is the anamorphic counterpart of the *Hypocrea* genus. They are filamentous fungi that grow on plant tissues and in soils. As many of them show mycoparasitic behavior, they can be used as biological fungicides in agriculture and forestry to kill off pathogens [Kubicek et al. 2011]. Since they have been intensely studied in the past, their genomes are well-known [Atanasova and Druzhinina 2010]. The *Trichoderma* species of this study have profound expansion of hydrophobin genes in comparison to other fungi

[Kubicek et al. 2011]. Hydrophobins are hydrophobic, cysteine-rich fungal proteins with a mass of only about 10 kDa, which are expressed on the surface of the cell wall [Wösten et al. 1995, Frischmann et al. 2013]. Due to their hydrophobicity they repel water from the cell surface.

Engyodontium album, which is also known as *Tritirachium album* and as *Beauveria alba*, is famous for its production of the enzyme Proteinase K, which digests keratin [Ebeling et al. 1974] and so human hair [Simonovicova et al. 2004]. Although three different anamorphic forms of this species are known, the teleomorph is still unknown. However, all teleomorphs of *Beauveria* species that are known up to now belong to the *Cordyceps* genus.

As 64% of the fungal spores in the continental atmosphere are emitted by *Basidiomycota*, also known as club fungi [Fröhlich-Nowoisky et al. 2009, Fröhlich-Nowoisky et al. 2012], they were also of interest. Most of the typical mushrooms belong to the class of *Agaricomycetes*, whose spores make up about 87% of the whole atmospheric *Basidiomycota* spore amount [Fröhlich-Nowoisky et al. 2009]. The most important orders among the *Agaricomycetes* are the *Agaricales* (white mushroom, shiitake, fly agaric, inky caps, death caps, oyster fungi), the *Boletales* (earthballs, boletes), the *Cantharellales* (chanterelles) and the *Polyporales* (polypores). Only a few mushrooms belong to the *Pezizales* order among the *Ascomycota*, like truffles, morels and scarlet cups. *Agaricus bisporus* (button mushroom) is common and easily available, as it is the most important edible mushroom. *Lentinula edodes* (shiitake) and *Pleurotus ostreatus* (oyster mushroom) were chosen as commerically available representatives for xylobiontic fungi, which are very common in woodlands and parks [Schüller 2008]. *Psilocybe cubenis* (magic mushroom) produces alkaloids with psychoactive effects. Because of this, it is commonly cultivated for acquisition of hallucinogenic drugs – what is the reason for the trivial denotation as "magic mushroom". *Coprinus* species (inky caps), which typically grow on

animal excreta, are the most common *Basidiomycota*, contributing massively to the total fungal spore amount in the atmosphere [Calderon et al. 1995].

Fig. 13: A collage of fungi pictures which demonstrates the diversity of species. In a row from left to right and from top to bottom: A xylobiotic mushroom, *Agaricus bisporus*, *Scleroderma citrinum* (all Basidiomycota), *Aspergillus niger*, *Morchella esculenta*, *Fusarium avenaceum*, *Penicillium citrinum*, *Penicillium roqueforti*, a lichen, *Saccharomyces cerevisiae* (all Ascomycota). Source: www.google.com

The list below shows an (incomplete) overview of fungal systematics:

Regnum *Fungi*
- Subregnum *Dikarya*
- Div. *Ascomycota* (sac fungi)
  - Subdiv. *Taphriniomycotina* (basal taxon)
  - Subdiv. *Saccharomycotina* (true yeasts)
  - Subdiv. *Pezizomycotina* (true sac fungi)
    - Cl. *Pezizomycetes*
      - Ord. *Pezizales*
    - Cl. *Lecanoromycetes* (many lichen fungi)
      - Ord. *Lecanorales*
        - Fam. *Lecanoraceae*
          - Gen. *Rhizoplaca*
            - *chrysoleuca*
    - Cl. *Lichinomycetes* (many lichen fungi)
    - Cl. *Eurotiomycetes*
      - Ord. *Eurotiales*
        - Fam. *Trichocomaceae*
          - Gen. *Trichocoma*
            - *paradoxa* (=*P. trichocomae*)
          - Gen. *Eurotium*
            - *herbariorum* (=*A. glaucus*)
          - Gen. *Neosartorya*
            - *fumigata* (=*A. fumigatus*)
          - Gen. *Petromyces*
            - **unknown** (=*A. flavus, P. rubrum*)
          - Gen. *Aspergillus*
            - *niger*
          - Gen. *Eupenicillium*
            - **unknown** (=*P. chrysogenum*)
            - **unknown** (=*P. citrinum*)
            - **unknown** (=*P. digitatum*)
            - **unknown** (=*P. glabrum*)
    - Cl. *Dothideomycetes*
      - Ord. *Capnodiales*
        - Fam. *Davidiellaceae*
          - Gen. *Davidiella*
            - *tassiana* (=*C. herbarum*)
            - **unknown** (=*C. cladosporioides*)
      - Ord. *Pleosporales*
        - Fam. *Pleosporaceae*
          - Gen. *Lewia*

- **unknown** (=*Alt. alternata*)
  - Cl. *Sordariomycetes*
    - Ord. *Hypocreales*
      - Fam. *Hypocreaceae*
        - Gen. *Hypocrea*
          - *atroviridis* (=*T. atroviride*)
          - *jecorina* (=*T. reesei*)
          - *virens* (=*T. virens*)
      - Fam. *Nectriaceae*
        - Gen. *Nectria*
          - *galligena* (=*F. mali/heteronemum*)
          - *rigidiuscula* (=*F. decemcellulare*)
          - *haematococca* (=*F. solani*)
          - *stilbosporae* (=*F. expansum*)
          - *cinnabarina* (=*Tubercularia vulgaris*)
        - Gen. *Gibberella*
          - *acuminata* (=*F. acuminatum*)
          - *avenacea* (=*F. avenaceum*)
          - *intricans* (=*F. equiseti*)
          - *pulicaris* (=*F. sambucinum*)
          - *tricinicta* (=*F. tricinictum*)
          - *moniliformis* (=*F. moniliforme*)
          - *xylarioides* (=*F. xylarioides*)
          - *zeae* (=*F. graminerarum/roseum*)
        - Gen. *Fusarium*
          - *culmorum*
          - *javanicum*
          - *oxysporum*
          - *poae*
          - *sporotrichoides*
      - Fam. *Clavicipitaceae*
        - Gen. *Beauveria*
          - *alba* (=*E. album*)
    - Ord. *Xylariales*
      - Fam. *Amphisphaeriaceae*
        - Gen. *Monographella*
          - *nivalis* (=*F. nivale*)
          - *cucumerina* (=*F. tabacinum*)
- Div. *Basidiomycota* (club fungi)
  - Subdiv. *Puccinomycotina* (rust fungi)
  - Subdiv. *Ustaligomycotina* (smut fungi)
  - Subdiv. *Agaricomycotina* (stand fungi)
    - Cl. *Tremellomycetes*
    - Cl. *Dacrymycetes*

- Cl. *Agaricomycetes*
  - Ord. *Agaricales*
    - Fam. *Agaricaceae*
      - Gen. *Agaricus*
        - bisporus
    - Fam. *Marasmiaceae*
      - Gen. *Lentinula*
        - edodes
    - Fam. *Pleurotaceae*
      - Gen. *Pleurotus*
        - ostreatus
    - Fam. *Strophariaceae*
      - Gen. *Psilocybe*
        - cubensis
  - Ord. *Boletales*
  - Ord. *Cantharellales*
  - Ord. *Polyporales*

2. Ice nucleation measurements

2.1. Sample acquisition

Pollen were either bought or collected. In second case, the pollen, which were set free by shaking the twigs of the plant, were collected in a petri dish and then dried in an exsiccator over silica gel. Humid samples had to be carefully dried additionally in the oven at 318 K over night to prevent mold formation.

- Pollen of *Juniperus chinensis pfitzeriana*, *Pinus nigra* and *Taxus baccata* were collected.

- Pollen of *Betula alba*, *Corylus avellana* and *Zea mays* were purchased from two companies, namely Pharmallerga© and AllergonAB©.

- All conifer pollen except for *Juniperus chinensis pfitzeriana* and *Pinus nigra* were purchased only from Pharmallerga©.

- All other pollen were purchased only from AllergonAB©.

Fungal spores were obtained from five different sources:

- Spores of *Ag. bisporus albidus* and *avellaneous*, *L. edodes*, *Pl. ostreatus* and *Ps. cubensis* were purchased from the Mushroom Research Center of Austria.

- *L. edodes* spores were obtained from growing mushroom cultivation sets by the Mushroom Research Center of Austria.

- *Ascomycota* cultures (*A. fumigatus*, *A. niger*, *A. oryzae*, *E. album*, *C. herbarum*, *C. cladosporioides*, *P. chrysogenum*, *P. digitatum*, *F. avenaceum* and *F. oxysporum*) were bought from the fungi bank at the University of Natural Resources and Life Sciences (BOKU) Vienna and cultivated in the lab for spore production.

- *Ascomycota* cultures *(A. niger, P. glabrum, T. atroviride, T. reesei, T. virens)* were acquired from the fungi bank of Vienna University of Technology and cultivated on agar to generate spores.

- Pieces of food (bread, lemon, carrot, tomato) were left for decomposition. When they were covered in mold, the spores were harvested. This way we collected spores of *A. niger*, *P. chrysogenum* and *P. citrinum*.

The *Ascomycota* were taken from the stock (stored at 193 K) and cultivated on plates filled with potato dextrose agar as a nutrient medium. After the inoculation of the plates, they were stored at 298 K for some weeks, until they were covered with conidia. Then each plate was harvested by covering it with 5-7 ml of 96% ethanol and scratching off the fungi with a flame-sterilized Drigalski speedle. To get rid of the mycelium, the suspension was then filtered through a funnel filled with mineral wool. The filtrate then contained only small particles, like the spores. The suspension was then centrifuged at 4000 rpm, and the ethanol was decanted and discarded. Finally, the pellet was air-dried and then stored at 255 K.

Bread and carrot were each infected with much *P. chrysogenum* and a few *A. niger* colonies. Lemon was mainly infected with *P. citrinum*. Tomato was infected mainly with *A. niger*, but also with *P. chrysogenum*. On carrot only non-pigmented fibrous mycelium grew (mainly from *P. chrysogenum*), so no spores were collected. The spores from tomato were not harvested, as the high water content of the fruit wetted and contaminated the mold cultures. Since these species were naturally grown, they were impure. This would be problematic, only if a culture turned out to be IN* positive.

2.2. Cryo-microscopy

The intention of this experimental setup was to gather nucleation spectra. Therefore, a closeable can with a Peltier element was placed under an impinging light microscope (see Fig. 15). Then a water-in-oil emulsion was dripped on a glass slide and inserted into the can, which was then cooled, starting from temperatures above 273 K. The freezing of droplets was observed and

documented with a camera. Then the number of frozen droplets in each picture is counted and plotted against temperature (see Fig. 31) [Pummer et al. 2012].

A warm cloud is in fact an ensemble of micrometer-sized water droplets. Thus an emulsion of water in oil is a suitable model of a cloud. The purpose of the emulsion is to stabilize small water droplets and isolate them from each other, the sample holder and air contaminants. This way the droplet density can be higher than if they were airborne, where they would collide and form larger droplets. Because of this an emulsion is like a cloud model miniaturized to the microlitre scale, which is small enough to be placed under a simple light microscope. Following reagents were taken for the preparation:

- paraffin oil, light, pure grade; by AppliChem GmbH
- lanolin, anhydrous; by VWR International Ltd.
- MilliQ water

80-90 wt.% of paraffin were mixed with 10-20 wt.% lanolin to a homogeneous oil phase. Therefore, the lanolin, which is highly viscous at room temperature, was tempered to 330 K in a water bath, so that the lanolin became liquid, and then mixed with paraffin. As lanolin tends to sediment when mixed with a cold liquid, the mixture was sealed, also warmed to 330 K and occasionally shaken up, until it is homogeneous. A few millilitres of the so-prepared oil phase were then mixed with MilliQ water in a test tube, so that the water fraction was 40-45 wt.%. The water content must not exceed 50 wt.%, or else the emulsion will be unstable. MilliQ water was applied in all cases – also for the chemical tests in Chapter 3.3. and for washing the glassware. The test tube was sealed and shaken for 10-30 seconds, then left to rest for some time, and shaken again. This cycle is repeated, until the whole emulsion is homogeneous. Every time before retaining an aliquot of it for a measurement, the emulsion had to be shaken up again, since a slow segregation of the water droplets in the sample takes place over time. A perfect emulsion is white and opaque due to intense Mie scattering caused by the

micrometer sized water droplets. The same phenomenon is responsible for the whiteness of natural droplet ensembles, like clouds and fog.
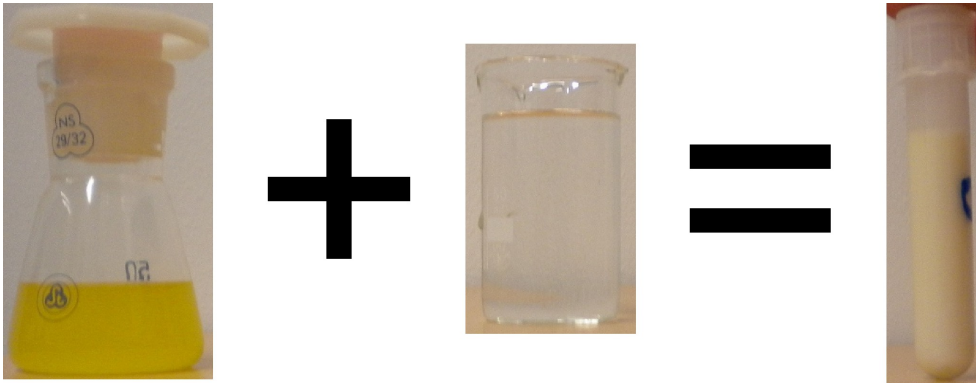
Fig. 14: Preparation of the emulsion by mixing Paraffin-Lanolin and MilliQ water.

Different parameters of the preparation allow a tuning of the emulsion properties:

- Lanolin content: Lanolin is the mediator stabilizing the emulsion of two unmiscible phases. Without any of it, the sample would segregate within seconds. The stability of the mixture increases with the lanolin content. A too high amount, however, would deposit in the oil after the preparation of the oil phase, when the temperature of the oil falls below the melting point of lanolin. The optimum lanolin content is 15-20 wt.%. Emulsion with 10 wt.% are stable enough to be applied, although slow segregation already takes place, as droplets are likely to fusion and form bigger droplets.

- Water-to-oil ratio: A higher water content causes formation of more and bigger droplets. However, if the water content reaches a critical value, phase separation takes place. This value is the higher, the higher the lanolin content is. For example, an emulsion containing 50 wt.% water is not stable if the lanolin content in the oil is only 10 wt.%, but is stable, if the content is 20 wt.%. A high water content improves statistics because of the higher droplet number, however, droplets might become too large to be of interest.

- Mixing time and strength: The mixing process increases the number of droplets and decreases their average diameter. The more often a sample is shaken, the more of the small droplets are generated. Intense mixing in an

ultrasonic bath will create an emulsion with a high amount of droplets with less than 10 µm diameter within 30 seconds. After ultrasonic mixing for several minutes, the number of larger droplets is negligible, however, many droplets become too small.
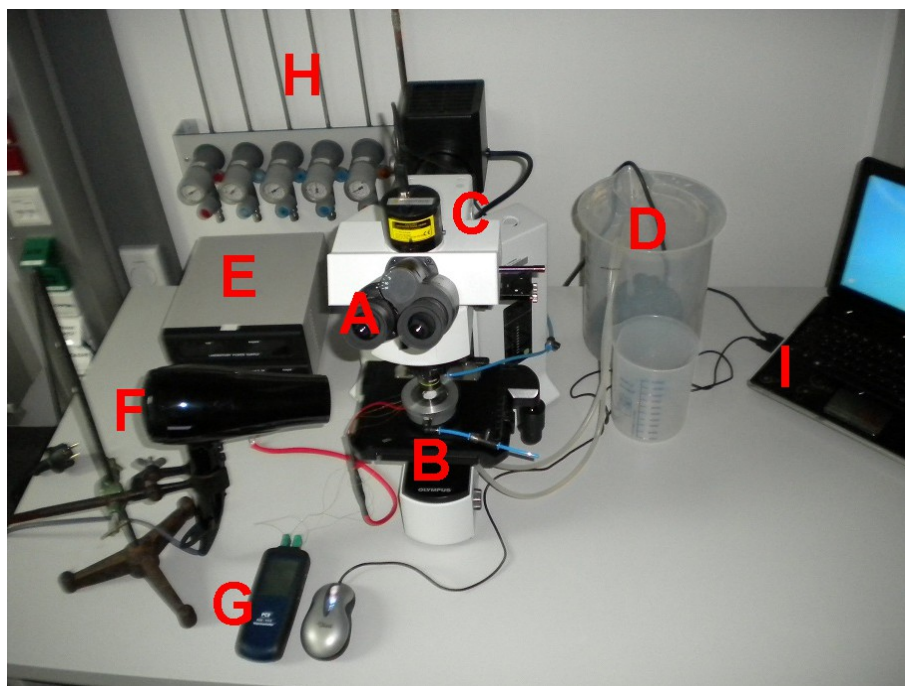
Fig. 15: The complete cryo-microscopic setup. The components are: microscope (A), cryo cell (B), camera (C), water bath (D), power supply (E), blow dryer (F), temperature sensor (G), gas supply (H) and computer (I).

The measurements were mainly performed on an Olympus BX51 microscope, but temporary also on a Zeiss Axio ScopeA1 microscope. To keep the cell dry, it was flushed with nitrogen every time a new sample was inserted. A non-heating blow dryer prevented the fogging of the glass window of the cell. Cooling was achieved by a three-stage Peltier element. Such a device consists of a series of p- and n-doped semiconductors and a ceramic plate on both sides. By applying direct current, heat is pumped from one side to the other by a thermoelectrical effect, so that one side cools down, while the other heats up. The Peltier element was fixed on a copper cooling element filled with distilled water. The water of a cooling bath, which was tempered to about 300 K, was pumped through the cooling element for conducting the heat from the warm side of the Peltier stage. Photos were taken mainly by a Hengtech MDC320 Microscope CCD Camera.

Temporarily, a Tucsen TCA-3.0C Color CMOS Digital Microscope Camera was applied. The full setup with the Olympus microscope is shown in Fig. 15.

In a sample at room temperature, the droplets are liquid, so they are transparent. When droplets freeze, they turn darker and often form internal structures due to the scattering of the microscope light. Fig. 16 shows on the right a pure water sample at 237.1 K, which contains both liquid and frozen droplets.
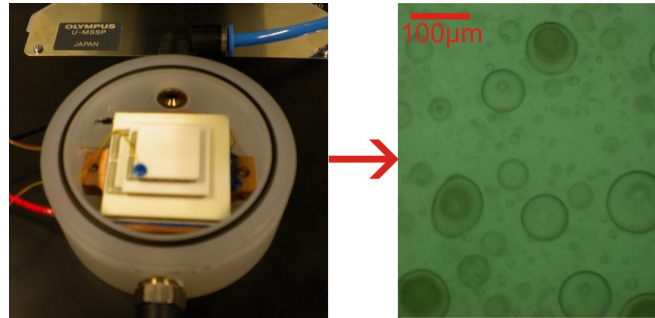
Fig. 16: The open Teflon cell with the Peltier stage inside (left). By microscoping a sample, pictures of emulsions (right) can be taken [Pummer et al. 2012].

As a very light-sensitive photo camera was applied, the intensity of the microscope beam could be reduced to a level, which is too dark for the naked human eye to see. This way, a potential temperature error in the measurements due to light-induced heating of the sample was prevented. The automatic data processing of the camera software then lightens up the pictures. Depending on the applied camera, this process stains the image in a certain color, in the case of the MDC320 it is green. In comparison, the pictures taken with the TCA-3.0C were stained dusky pink. Fig. 17 to 30 show a model photo series of a typical pure water-in-oil emulsion.
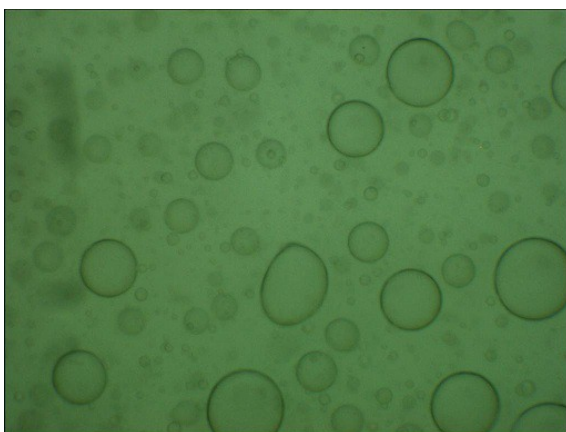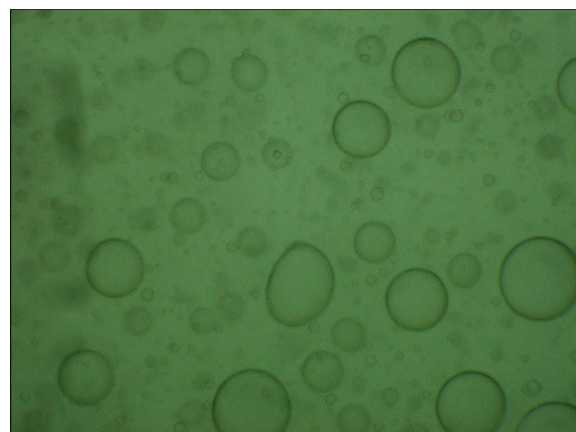
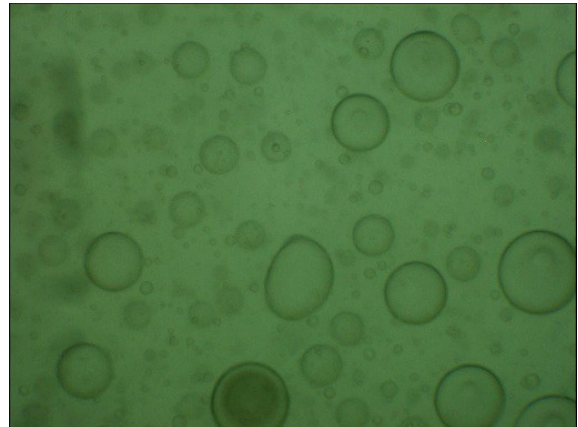| **Fig. 17: 273.5 K** | **Fig. 18: 247.9 K** |
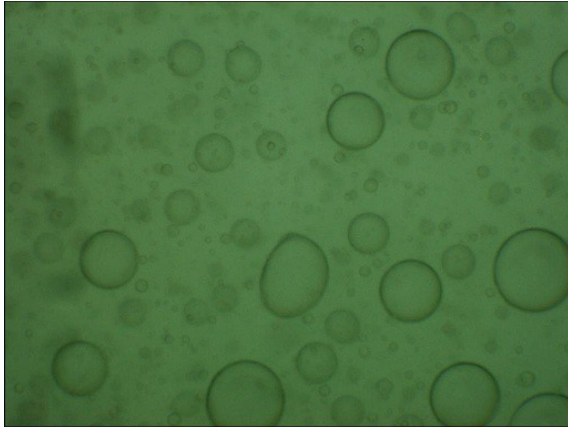
Fig. 19: 246.0 K
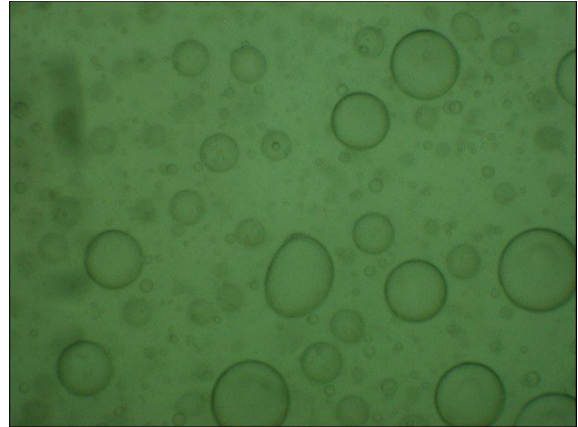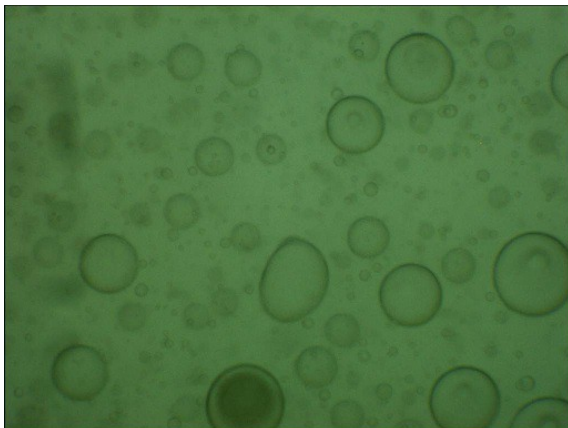

Fig. 20: 243.8 K
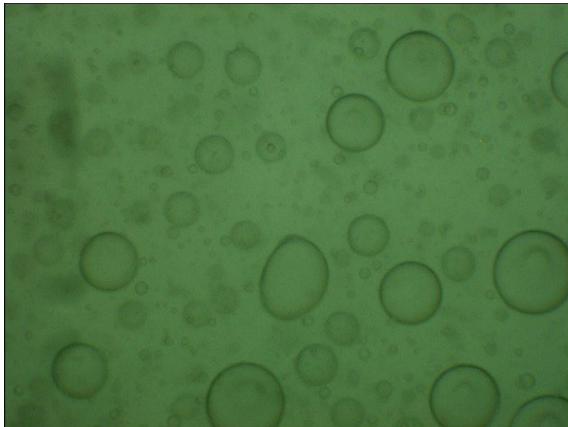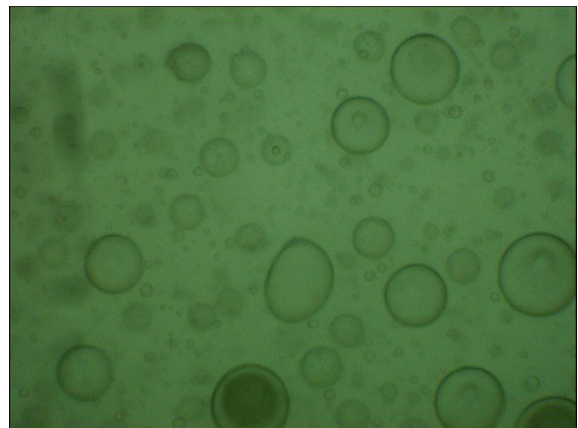

Fig. 21: 241.9 K

Fig. 22: 241.6 K

Fig. 23: 240.1 K
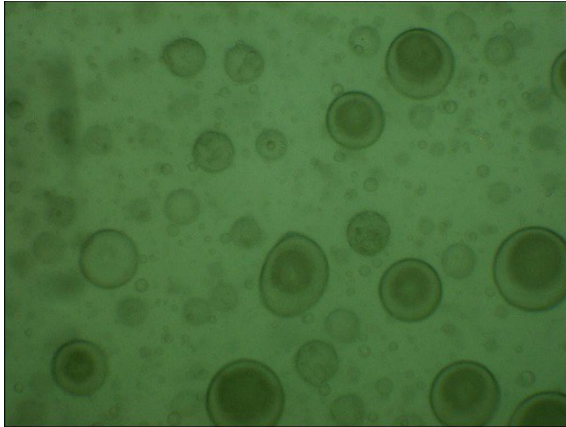

Fig. 24: 238.8 K
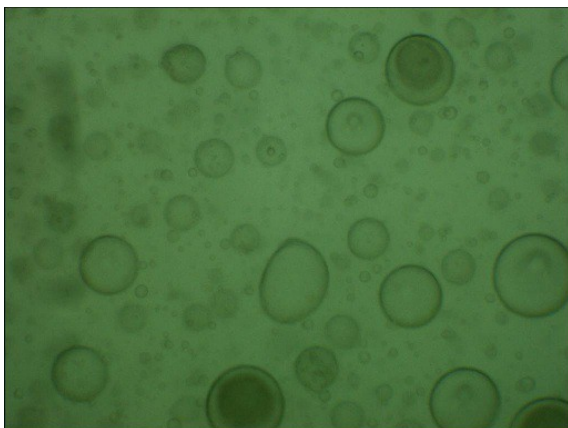
Fig. 25: 237.9 K

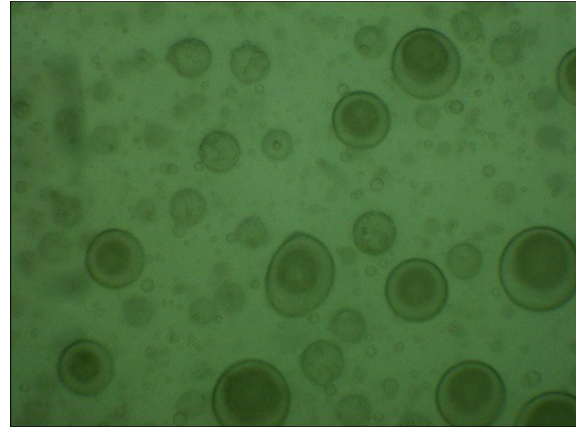**Fig. 26: 237.1 K**

58
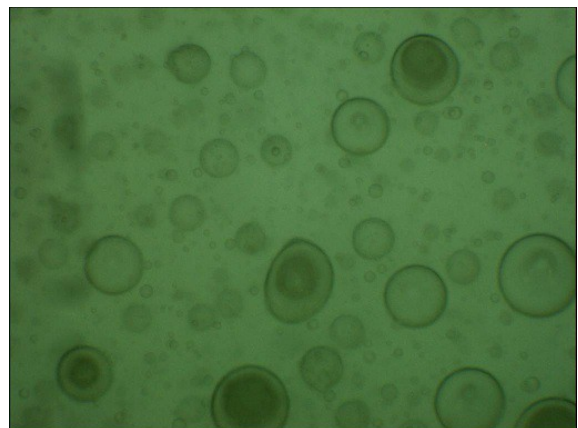
Fig. 27: 236.7 K
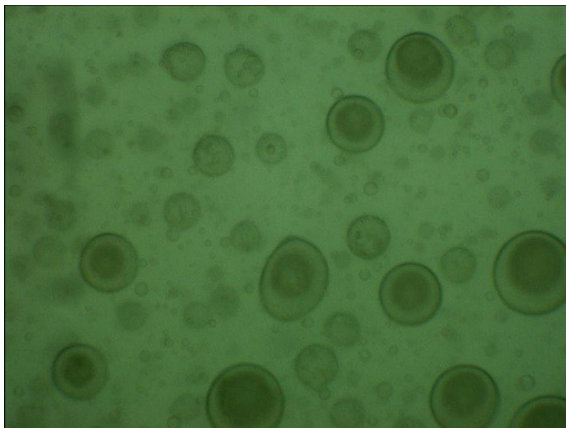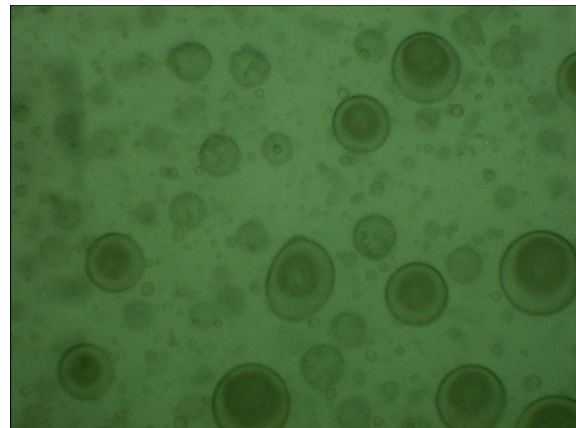

Fig. 28: 236.0 K

Fig. 29: 231.6 K

Fig. 30: 225.4 K

The number of frozen droplets was counted in every picture, listed and divided by the total droplet number, which is the number of frozen droplets at the minimum temperature. In most cases, the freezing was clearly visible by a transformation of a clear droplet to one with dark internal structures, like dots, rings, edges or cubes. Only droplets in the diameter range from 10 to 200 μm were counted. On average, almost 50% of counted droplets were smaller than 35 μm, while only about 10% were larger than 100 μm.

- Droplets smaller than 10 μm were difficult to count and assign, since the internal structures were too small to be visible. Furthermore, these small droplets cannot immerse particles that are larger than themselves.

- Droplets larger than 200 μm were not of interest, since cloud droplets are smaller (very large droplets would begin to precipitate). Furthermore, since the observation window has a defined size, larger droplets demand more space, so fewer droplets fit into that area. However, fewer countable

droplets lead to worse statistical quality of the results. Furthermore, the shapes of very large droplets often deviate severely from sphericity.

The counting results for the model curve in to are shown in Tab. 3:

T [K]	273.5	247.9	246.0	243.8	241.9	241.6	240.1	238.8
$\#_{ice}$	0	0	0	0	0	1	1	3
f_{ice} [%]	0.0	0.0	0.0	0.0	0.0	3.7	3.7	11.1

T [K]	237.9	237.1	236.7	236.0	231.6	225.4
$\#_{ice}$	6	11	19	27	27	27
f_{ice} [%]	22.2	40.7	70.4	100.0	100.0	100.0

Tab. 3: Frozen droplet counting results. $\#_{ice}$ is the number of counted frozen droplets, f_{ice} is the normalized frozen fraction.

These data are plotted in a nucleation spectrum, with the temperature as x-axis and the percentage of frozen droplets as y-axis.
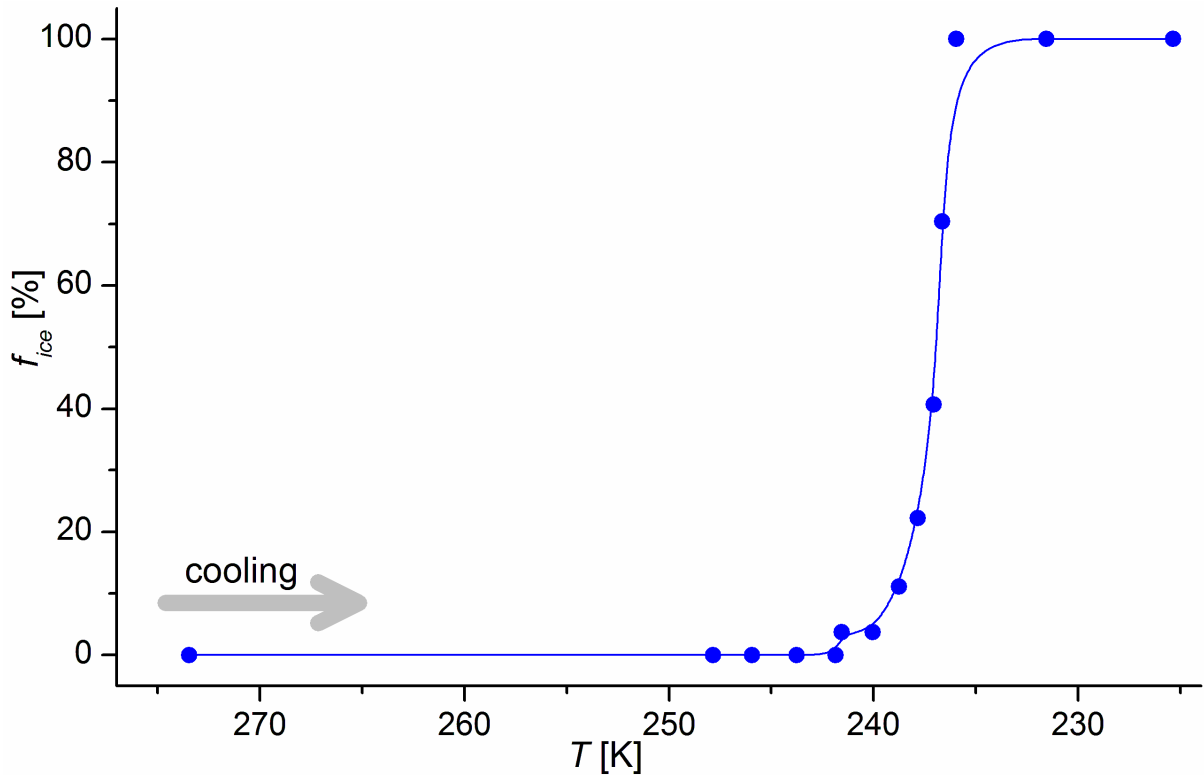

Fig. 31: The corresponding nucleation spectrum of the pure water emulsions.

To make different nucleation spectra easily comparable, they are reduced to one numeric value. Two different approaches for characterization have been developed in the past, namely the initial freezing temperature and the median freezing temperature [Diehl et al. 2001]. The initial freezing temperature is the

one, where the first droplet freezes. However, since it is statistically very unreliable, and is very sensitive towards sample contamination, it is not appropriate for determining the IN activity of a sample in a reliable way. The median freezing temperature T_{50}, which is the temperature at which half of all droplets is frozen (equivalent to f_{ice}=50%), is statistically far more robust. In this study the numeric values of all median freezing temperatures were rounded to whole Kelvin.

To measure the IN* activity of fungal spores, the emulsion was spiked with about 20 mg/ml in relation to the water content. As references, Snomax and two types of mineral dust (Kaolinite and Arizona Test Dust) were prepared the same way, also with concentrations of 20 mg/ml. By mixing a droplet of emulsion with a bit of sample on a glass slide, the aerosol particles are immersed in the water droplets. Photos were taken to record the nucleation spectra. The median freezing temperatures were determined and plotted in Fig. 36. The whiskers were set at the points, where 25% and 75% of the droplets were frozen. So half of all droplets froze in the encompassed range. These errors, same as the T_{50} values, were also rounded to whole Kelvin.

Tab. 4 shows the statistical data for pure water and the reference samples. The statistical data for the spores either grown on agar (*Ascomycota*), or directly purchased from MRCA (*Basidiomycota*, marked with an asterisk) are given in Tab. 5. The statistical data for the spores from food molds (*Ascomycota*) or from a mushroom cultivation set (*Basidiomycota*, marked with an asterisk), are shown in Tab. 6. The median freezing temperatures of all samples are visualized in Fig. 36.

name	# curves	# droplets	T_{50}	T_{25}	T_{75}
Snomax	4	250	268	269	267
ATD	2	214	252	255	249
Kaolin	3	212	250	251	248
blank	20	654	237	238	236

Tab. 4: Statistical data of reference samples.

name	# curves	# droplets	T_{50}	T_{25}	T_{75}
F. avenaceum	4	301	264	267	256
L. edodes *	6	523	247	249	245
C. cladosporioides	8	1152	244	246	238
T. reesei	7	711	244	246	237
P. glabrum	4	462	243	245	239
Ag. bisporus *	12	1265	242	244	240
A. oryzae	6	730	242	245	239
F. oxysporum	4	335	240	245	237
P. digitatum	3	154	240	243	237
Pl. ostreatus *	4	391	240	244	237
A. fumigatus	4	230	239	240	238
P. chrysogenum	4	365	239	241	237
Ps. cubensis *	4	282	238	242	237
T. atroviride	3	217	238	240	236
A. niger	4	120	237	238	236
C. herbarum	5	145	237	238	236
E. album	2	157	237	244	236
T. virens	3	208	237	240	236

Tab. 5: Statistical data of agar-cultivated (AM) or purchased (BM) fungal spores.

name	# curves	# droplets	T_{50}	T_{25}	T_{75}
L. edodes *	6	469	243	237	235
P. chrysogenum	6	348	239	241	237
A. niger	6	501	239	242	237
P. citrinum	8	894	237	239	236

Tab. 6: Statistical data of naturally-grown fungal spores.

As a whole, most fungal spores showed no IN activity at all (Fig. 32). Only a few show a slight IN* activity, which lies still below the IN* activity of the mineral dust reference samples. Only *F. avenaceum* is a highly potent exception, which shows IN* activity close to that of Snomax. The long whisker towards the low temperature site can be explained by the fact that these cultures had been grown for several generations before they sporulated. As it has been found out before, the IN* activity is lost after some generations of laboratory cultivation

[Tsumuki et al. 1995]. In fact, this sample also lost its IN* activity within time. Further attempts to reactivate the expression of the INP failed (see chapter 4.1.).
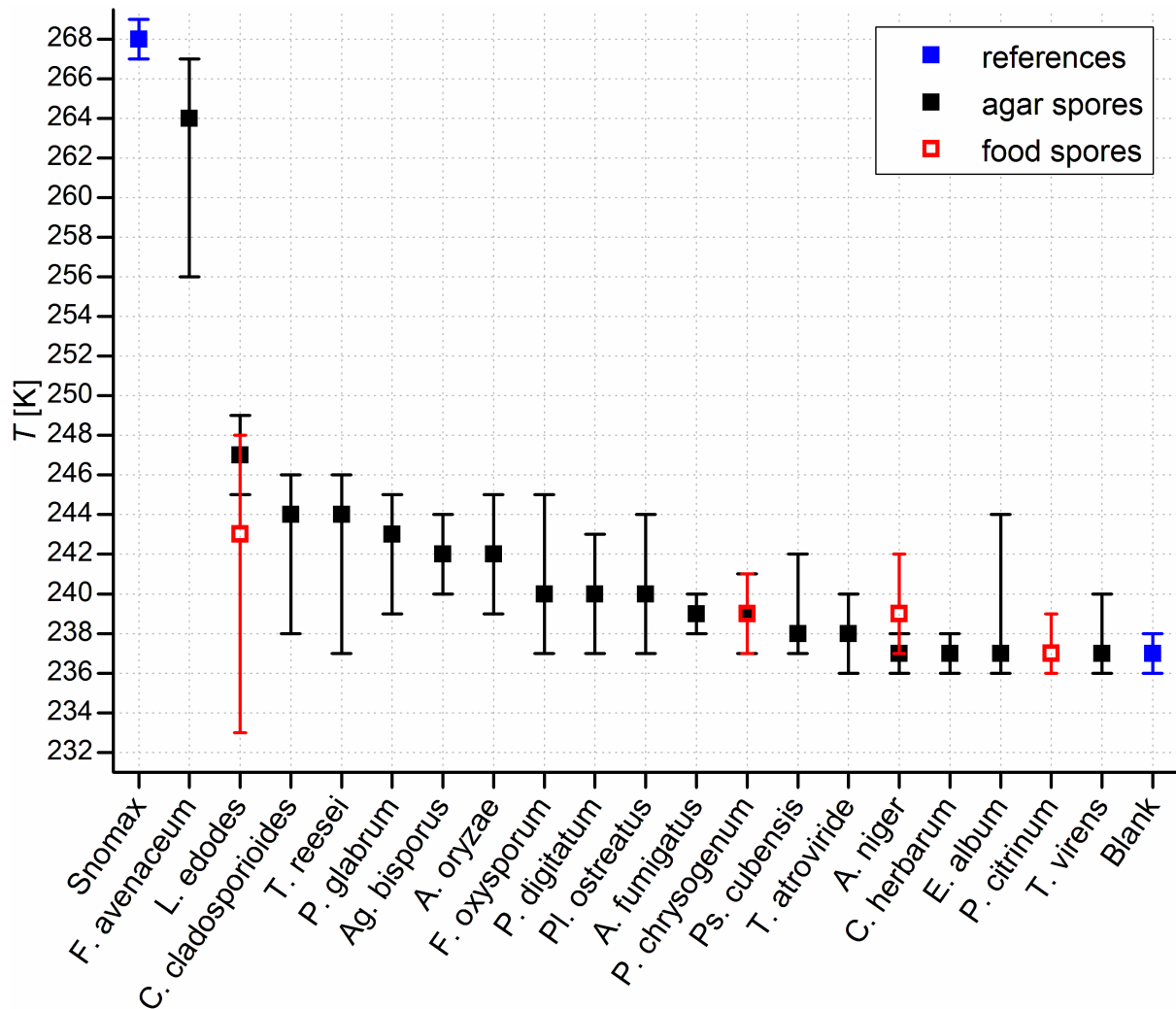

Fig. 32: Median freezing temperatures of fungal spores. The whiskers include the temperature region, where half of all droplets freezes. The red datapoints stand for the mold grown on food and the *L. edodes* from the mushroom cultivation set.

The data of the *L. edodes* show a rather strange behavior. First, the difference of T_{50} between the purchased and the self-grown species is the largest of all samples, and second, the nucleation curve is very broad. One could speculate about the reason for this behavior, as well as about the differences between the other fungal species. However, since all those T_{50} values are rather low, their relevance for ice nucleation is most certainly negligible. Furthermore, the lower the median freezing temperature of a sample is, the more sensitive it reacts towards contamination. If, for example, an IN* negative sample is contaminated by a few weakly IN* active particles – and these are ambient – they will cause

nucleation at temperatures higher than the homogeneous freezing temperature, and so broaden the nucleation spectrum. This is a further reason, why the median freezing temperature is a more reliable parameter than the initial freezing temperature, which can be severely altered by only one single IN* active contaminant.

The IN* activity of pollen was determined in the same way as that of fungal spores. Since they are much bigger than the other samples, the emulsion had to be spiked with about 50 mg/ml in relation to the water content in order to force enough pollen into the droplets. In the optimum scenario, most droplets contained 1-3 pollen grains. Since many pollen grains either stayed in the oil phase due to their hydrophobic exine, or formed larger agglomerates, the concentrations had to be high to cover the losses. The results of pollen measurements are given in Tab. 7.

name	# curves	# droplets	T_{50}	T_{25}	T_{75}
Betula pendula	15	457	254	256	251
Juniperus communis	5	53	252	253	249
Pinus sylvestris	13	62	253	255	252
Juniperus chinensis	10	98	248	251	246
Salix caprea	5	125	247	249	243
Corylus avellana	9	110	246	251	244
Urtica dioica	2	24	248	252	244
Agrostis gigantea	5	137	248	252	244
Taxus baccata	5	83	250	251	248
Thuja orientalis	6	47	242	248	238
Platanus orientalis	4	84	246	248	244
Ambrosia artemisiifolia	7	149	240	243	239
Zea mays	5	19	242	246	241

Tab. 7: Statistical data of pollen grain IN* measurements.

It turned out that not only pollen themselves act as ice nuclei, but also aqueous pollen extracts. So it is releasable material from the pollen that causes their IN*

activity. The released fraction made up 30-40% of the initial pollen mass (see chapter 3.1.). Because of this, the chosen concentrations of 50 mg/ml for pollen and 20 mg/ml for other aerosols can be considered consistent.

Therefore, pollen were suspended in water at a concentration of 50 mg/ml for several hours and mixed occasionally to prevent sedimentation. The concentration was chosen to make the results directly comparable to the pollen grain data. Then the pollen grains were filtered off. The aqueous fraction, the pollen water, was then applied for the preparation of emulsions, and then their IN* activity was measured (see Fig. 33).
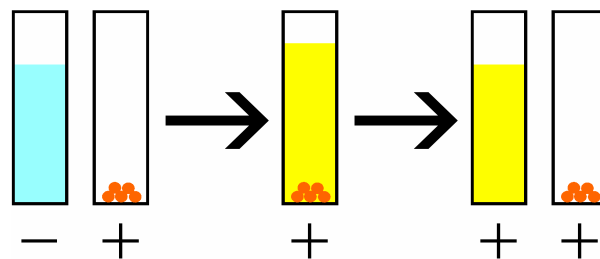

Fig. 33: The procedure for preparing IN*-positive pollen waters.

In most cases the median freezing temperatures between whole pollen grains and pollen waters differed by a few Kelvin or not at all. So it is not the whole pollen grains that are responsible for the IN* activity, but some submicron sized structures that can be extracted with water. Fig. 34 shows typical nucleation spectra of pure water, birch pollen water and hazel pollen water. In this plot the region below 241 K is interpreted as homogeneous ice nucleation, while freezing above is defined as heterogeneous ice nucleation. In some cases, every droplet of the pollen water emulsion freezes at elevated temperatures. However, in most cases, as can be demonstrated at the example of hazel, some of the droplets do not freeze at the expected heterogeneous freezing temperature. Only a certain fraction shows heterogeneous activity. The remaining droplets do not freeze until the homogeneous freezing range is reached. so these curves show two steps, which are in the ideal case separated by a horizontal plateau. This can be explained by the fact that the IN number is too low that every droplet contains an ice nucleus. To determine the median freezing temperatures, only the height

of the heterogeneous step is taken into account. However, in most cases the median freezing temperature would not significantly change, if the sum of both steps was taken into account, since the heterogeneous steps are very high and have a steep slope.
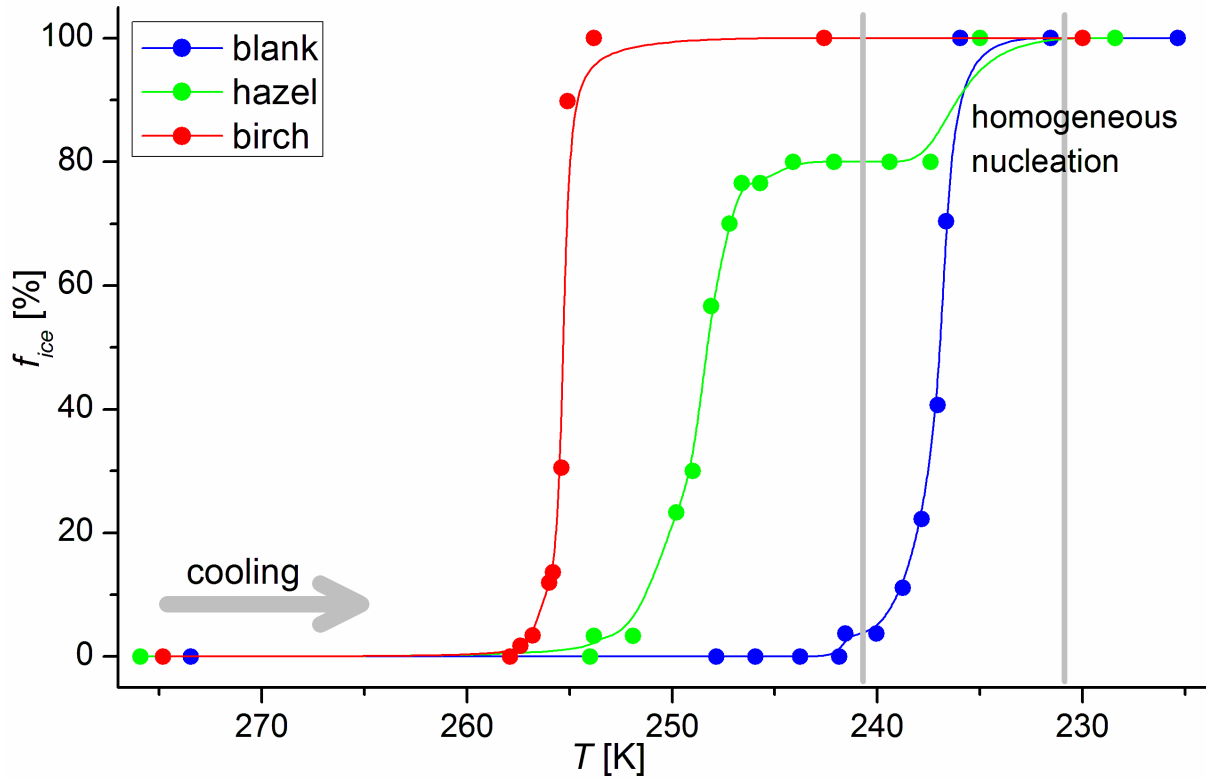

Fig. 34: IN* spectra of three individual measurements: Pure water, hazel and birch I pollen water.

Some pollen species, like ragweed, show a very weak heterogeneous IN* activity, with small active fractions that individually differ from curve to curve. Furthermore, there is no IN* activity above 250 K at all. Therefore, the assumption is made that these pollen are in fact IN* negative, and that the sporadic freezing events are caused either by traces of contamination, or are statistical outliers, as in accordance with the statistical nature of ice nucleation theory. The pollen waters of ragweed and corn show an even lower median freezing temperature than pure water, because all pollen waters contain not only the IN, but all components that can be washed off the pollen. Some of these, like low-molecular sugars and salts, are known to decrease the freezing point of water (see Eq. 1). The statistical data of the pollen water samples are given in Tab. 8:

name	# curves	# droplets	T_{50}	T_{25}	T_{75}	% active
Betula pendula	13	408	255	256	254	100
Betula occidentalis	4	202	254	255	253	100
Juniperus communis	6	145	253	254	251	100
Pinus sylvestris	9	229	252	253	251	62
Rumex acetosa	8	785	252	253	250	84
Ulmus americana	7	524	250	251	249	100
Juniperus chinensis	4	199	249	250	248	100
Salix caprea	6	211	249	251	247	34
Corylus avellana	8	288	249	251	247	77
Thuja occidentalis	4	152	248	251	246	48
Urtica dioica	6	355	248	250	245	62
Agrostis gigantea	5	134	248	250	241	58
Artemisia absinthium	11	695	247	249	245	63
Carpinus betulus	3	214	246	249	243	42
Taxus baccata	6	268	246	250	244	74
Thuja orientalis	5	292	245	247	243	38
Triticum aestivum	4	152	245	248	239	100
Platanus orientalis	6	258	244	245	243	59
Lolium perenne	3	186	238	240	237	0
Plantago lanceolata	3	192	237	238	236	0
Ambrosia artemisiifolia	11	325	236	240	235	0
Zea mays	5	357	235	236	234	0

Tab. 8: Statistical data of pollen water IN* measurements.

Fig. 35 shows some examples of accumulated sum curves for pollen species with different IN* activity. The birch pollen water spectrum shows a very steep slope and a perfectly flat plateau, thus making the interpretation straightforward. The pine spectrum shows two separated steps. However, since some droplets nucleated at random temperatures between these steps, the plateau of the sum curve shows a slight positive slope. For the calculation of the active fraction, this plateau was divided in the middle, and the corresponding f_{ice} was interpreted as the heterogeneously nucleating fraction, in this case 62%. For the calculation of T_{50}, the temperature where half of this fraction, in this case 31%, was frozen, was

read out. For pine it was 252 K (see Tab. 8). The curve of ragweed shows a broad onset of the nucleation curve and a steep slope at homogeneous freezing temperatures. This slight ascent at temperatures between 250 and 237 K cannot be interpreted as a step, and so no active fraction can be determined. Furthermore, the initial freezing temperature, as well as the precise shape of this onset region varies individually in the single measurement curves. The low reproducibility suggests that these IN* events are not caused by a specific ice nucleus, but rather by a heterogeneous mixture of everything that was extracted from the pollen. The small fraction that nucleated also suggests that this activity might have been caused by any kind of contaminants in the sample, since at these temperatures many chemical compounds can initiate freezing. However, their activity is far too low to be significant in nature. Consequently, the whole curve was interpreted as one step with a median freezing temperature around the homogeneous freezing point. It is therefore justified to specify the ragweed pollen as being IN* negative.
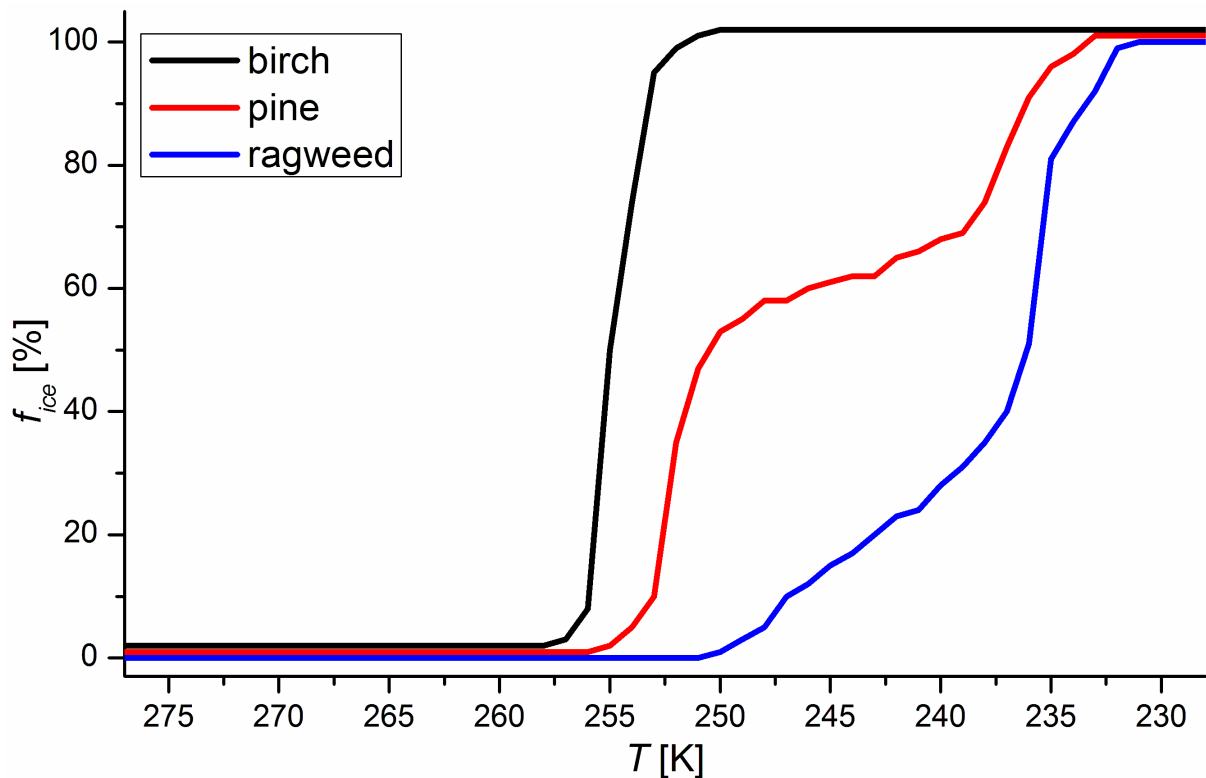

Fig. 35: Accumulated sum curves of three different pollen waters. Note: To prevent overlapping of the data points, each curve was shifted vertically by 1% relative to its neighbor.

The determined median freezing temperatures of both pollen grains and pollen waters are visualized in Fig. 36, which is constructed analogously to Fig. 32.
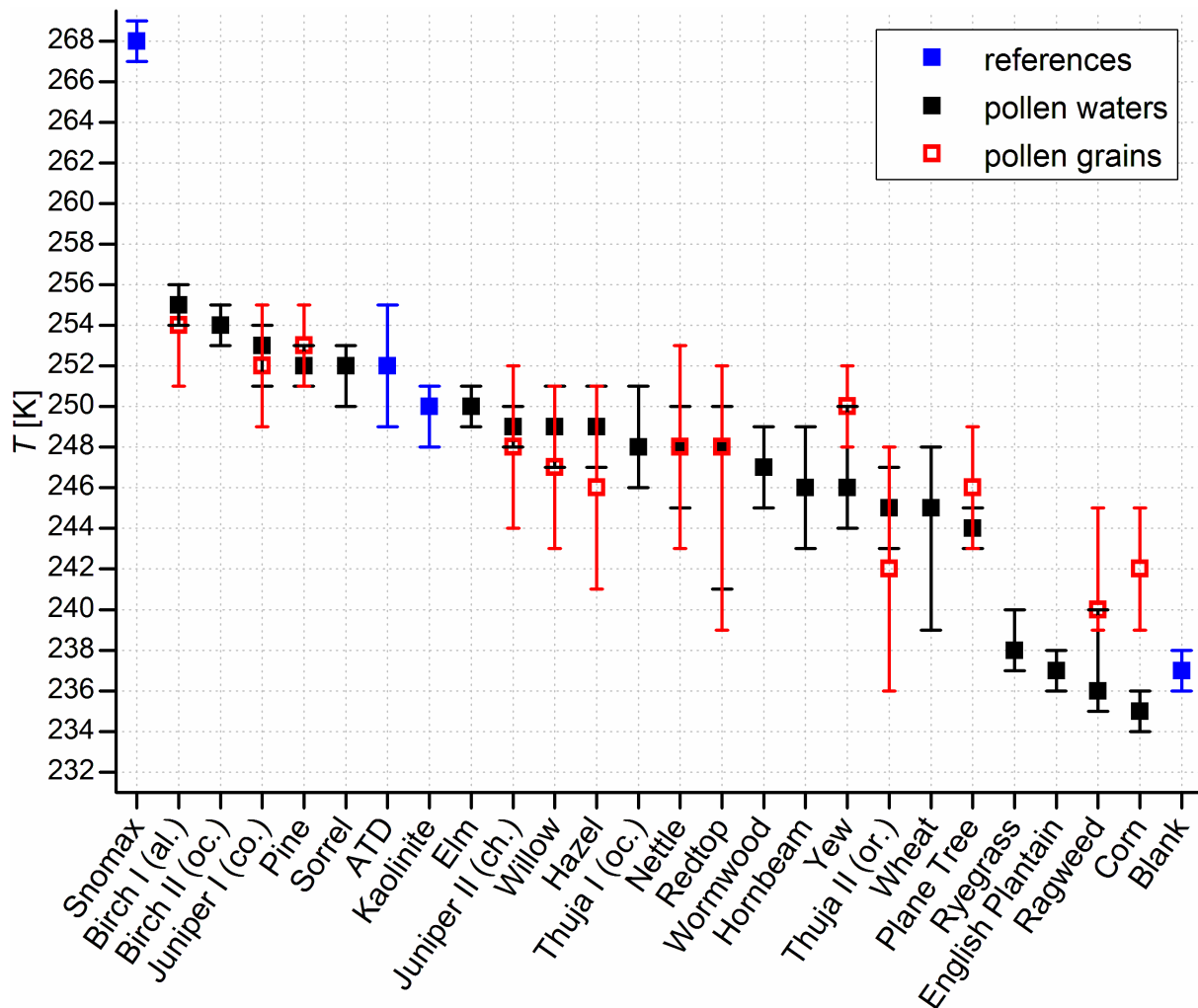
Fig. 36: Median freezing temperatures of emulsion with pollen grains and pollen waters.

The median freezing temperatures of pollen grains and pollen waters match in most cases [Pummer et al. 2012]. Most pollen show nucleation in the range from 242 to 250 K. The four species with lower freezing temperatures can be considered to be IN* negative, since their freezing range overlap with the homogeneous freezing range. Five species nucleate at higher temperatures. Four of these, namely silver birch, water birch, common juniper and Scots pine, are native in rather cold environments.

The extractability of the PIN is highly advantageous for handling and measuring of the samples, since the preparation of emulsions becomes a far more convenient task: It allows the reproducible adjustment of a given IN concentration, which is essential for comparison, because a large number of

small macromolecules distributes more smoothly in the emulsion than a far smaller number of relatively large pollen grains. As shown in Fig. 36, the error bars of the pollen grain measurements are always larger than those of the pollen water measurements. Furthermore, the pollen grain measurements have one more critical parameter, namely the distribution of the pollen grains. Since the grains tend to agglomerate, most droplets contain either many pollen grains, or none at all. Furthermore, since the droplets are in the same diameter range as the pollen, it is difficult to immerse the pollen in the droplets. This way the pollen force the droplets together to form very big (>200 µm) droplets, which are too large to be of interest. So only few droplets fulfill all conditions to be taken into account in the statistics. This can be seen by comparing the average number of droplets per curve in Tab. 7 and Tab. 8. Especially for the very large pollen, like corn and pine, this advantage is highly visible.

Another interesting feature is that both, the error bars and the differences between grains and waters, tend to grow with decreasing median freezing temperature. The higher IN* activity of ragweed and corn pollen grains in comparison to the waters is most probably caused by the presence of a large heterogeneous surface itself. Especially the vast difference for the corn pollen, which are also the largest pollen in this study (see Tab. 1), support this hypothesis. Furthermore, the T_{50} values of the most active sample are not affected by contamination. The reason is the high activity, which surpasses the IN activity of possible contaminants. The lower the temperature, the more particles become IN* active, so the more possible contaminants exist that may adulterate the data. For example, at 255 K only birch pollen showed IN* activity, so possible contaminants would be activated at temperatures where the sample was already fully frozen. So they would have no impact on the freezing temperature. On the other hand, if the median freezing temperature of a sample lies close to or below possible contaminants, it surely will be corrupted, if the

reagents and preparation are not clean enough. Consequently, the lower the expected T_{50} is, the higher are the demands for cleanliness.

In addition, nucleation spectra of self-collected *Pinus nigra* (black pine) pollen were recorded. The sum spectrum showed a steep slope in the temperature range between 263 and 255 K, which reached to about 55% f_{ice}. In the lower range the slope was gentle until the range of homogeneous nucleation, where another step reaching to 100% f_{ice} occurred. The active fraction is 70% with a median freezing temperature of 261 K. The collected pollen were visibly contaminated and were not cleaned up like the purchased pollen, so the high activity could indeed be caused by microbial contaminants. The closeness to the freezing temperature of the IN* positive *F. avenaceum* (T_{50} = 268 K) would suggest this interpretation.

2.3. Nucleation rate measurements

Since nucleation is a stochastic process depending on both time and droplet volume or active surface (see chapter 1.2.), the impact of these factors was also investigated. Therefore, emulsions with pure water and with birch pollen water were chosen as model substances [Pummer et al. 2012].

In contrast to the measurements described in chapter 2.2., these measurements were isothermal, meaning that the emulsions were quickly cooled to a given temperature, which was then held over the necessary amount of time. Snapshots of the freezing emulsions were taken, and the dependence of the frozen fraction f_{ice} on the measurement time was determined. To count the total droplet number in the emulsion, which is necessary to calculate f_{ice}, the sample was cooled down at the end of each measurement to about 230 K to freeze the sample through. This is equivalent to an infinite measurement time, since f_{ice} exponentially approaches a value of 100% with increasing time.

T [K]	t [s]	f_{ice} [%]	J [cm^{-3}·s^{-1}]
236.5	0	0	
	1	50	$2.069 \cdot 10^7$
	2	100	
236.5	0	0	
	14	42	$1.149 \cdot 10^6$
	25	67	$1.312 \cdot 10^6$
	46	75	
238.0	0	0	$3.118 \cdot 10^5$
	45	38	$4.450 \cdot 10^5$
	93	75	$2.241 \cdot 10^5$
	223	81	
	407	84	
	909	84	
	2252	88	
	4190	88	
239.0	0	0	
	27	0	
	94	0	
	199	0	
	276	13	$1.548 \cdot 10^4$
	310	20	$2.149 \cdot 10^4$
	507	20	$1.314 \cdot 10^4$
	701	20	$0.950 \cdot 10^4$
	847	27	$1.093 \cdot 10^4$
	1239	33	$0.977 \cdot 10^4$
	1470	40	$1.037 \cdot 10^4$
	1772	40	$0.861 \cdot 10^4$
240.5	0	0	
	1440	2	
	18240	2	$2.751 \cdot 10^1$

Tab. 9: Time-resolved data plus calculated nucleation rates for pure water.

From these data, nucleation rate coefficients were calculated, as shown in chapter 1.2.. The results are listed in Tab. 9. Since most droplets freeze rather at the beginning of the measurement, the first time intervals are statistically more

reliable than the later ones. Individual droplets showing abnormal behavior are statistically less relevant when many droplets freeze at once than when only single droplets freeze. The data and results of a measurement with a pure water sample are given in the table below. The droplets had a median volume of $3.35 \cdot 10^{-8}$ cm^3, which is equivalent to a diameter of 40 μm. Only the nucleation rates that were taken into account for the averaging are presented in Tab. 9. Obviously, a calculation of nucleation rates at the start (t[s]=0) or with all droplets frozen (f_{ice}=100%) is mathematically impossible. In the first case, both sides of the equation are zero, so $J(T)$ could be any finite value, while in the latter case we have ln(0) on the left side, which results in negative infinity.

The data allow the application of a linear fit, as shown in Fig. 37. Additionally, kaolin data [Murray et al. 2011] are added after conversion into comparable dimensions by multiplication with 0.7162 cm^{-1}, which is the ratio of maximum particle surface per droplet and the average droplet volume.
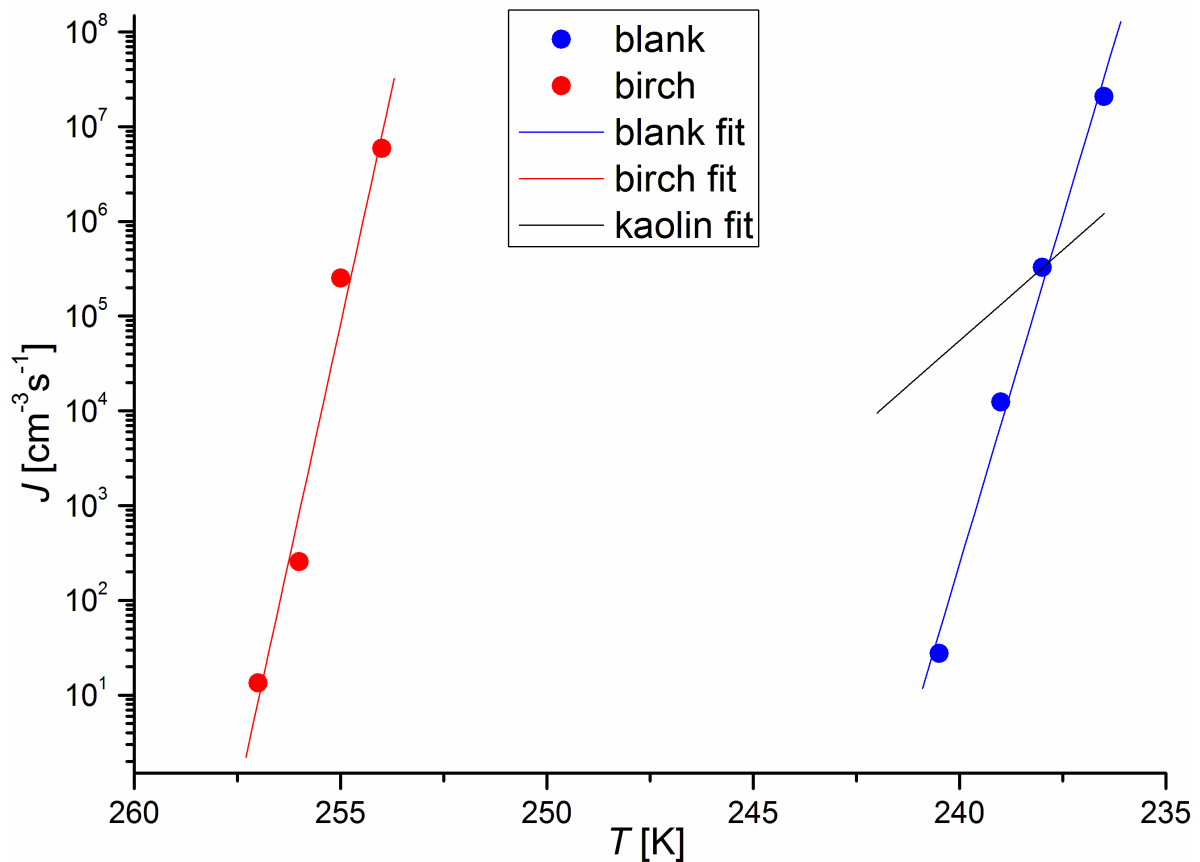

Fig. 37: A plot showing the nucleation rate coefficients as a function of temperature [Pummer et al. 2012, Murray et al. 2011].

The steep slopes of about 3 orders of magnitudes at every 2 Kelvin make the measurements robust towards slight variations in both droplet volume and measurement time, respectively cooling rates.

It has to be pointed out that linearising like in Fig. 37 is only possible within a small temperature range, since it relies on simplifications of classical nucleation theory (see chapter 1.2.), which cannot be applied for temperature intervals larger than a few Kelvin. For example, surface tension and density of water are considered to be temperature-independent, which is in reality only acceptable for temperature differences of a few Kelvin [Murray et al. 2010]. Additionally, it is impossible to measure reliably very low or high nucleation rates. If the nucleation rates are too low (at higher temperatures), then measurement time grows towards infinity. Measurement times longer than 1 day are not possible in a setup like this. Furthermore, if only a few droplets freeze at all, then the statistics are of very low quality. Very high nucleation rates (very low temperatures) show the problem that the cooling to the demanded temperature needs time. During this time temperatures with lower, but still relevant nucleation rates, have to be passed. Consequently, droplets in the sample already freeze before the starting of the measurement, which cannot be taken into account. So in fact only a fraction of the present droplets can be counted. Besides, the data might be afflicted with a systematical error, if an appreciable fraction of droplets is counted out this way. As not all droplets show the same IN* activity, it is to be expected that the more active ones are already frozen, while only the less active ones are statistically evaluable.

2.4. Smog chamber (LOTASC)

For verification of the results obtained in the oil immersion experiments in chapter 2.2., further measurements were carried out with a different setup: The LOTASC smog chamber is a glass vessel with an inner volume of 3.2 m^3, which is located at the BayCEER in Bayreuth (see Fig. 38[i]). Ice is detected via light

---

[i]   http://www.eurochamp.org/chambers/lotasc/

depolarization [Bleicher ands Zetzsch, 2012] – a setup that was inspired by the depolarization detector installed at AIDA [Möhler et al. 2003]. Therefore, a diode laser (Acculase lc, 635 nm, 5 mW) beam is transmitted across the lower third of the chamber. Aerosols in the chamber scatter the light back, which is then detected by a photomultiplier (Hamamatsu R374) setup at an angle of 175° relative to the laser beam direction. On the inlet of the photomultiplier a polarization filter is located, which is rotated by an electric motor. Because of this, the polarization filter oscillates between parallel and orthogonal orientation relative to the initial laser beam light. As light can only pass the filter, if the filter is parallel to the plane of light, the detector signal decreases when the filter is in orthogonal position. Thus the rotation of the filter is responsible for a sinus-shaped signal of light intensity at the detector versus time. If the laser beam is

Fig. 38: The glass tank of the LOTASC device.

scattered back on spherical aerosols, like liquid droplet, it remains polarized. However, if the aerosols are anisotropic, like ice crystals, the laser light is furthermore depolarized. Therefore, the difference between the minimum (orthogonal orientation) and the maximum (parallel orientation) of the detector signal decreases, since a part of the laser beam now is orthogonal towards the primary laser beam, and thus passes the filter in orthogonal position, while it is filtered in parallel position. The more anisotropic aerosols are present, the stronger is the depolarization. The depolarization degree D can be calculated by processing of the sinus signal (see Eq. 6):

$$D = \frac{I_{min}}{I_{min} + I_{max}}$$
Eq. 6

with I_{max} and I_{min} as maximum and minimum intensities of the time-dependent detector singal $I(t)$. The numeric values for D range from 0 for a fully polarized signal to 0.5 for a totally depolarized signal [Bleicher and Zetzsch, 2012]. The

LOTASC setup is the only one in this thesis, where artificial rainwater was applied as solvent instead of MilliQ water, because ultrapure water droplets would evaporate in the chamber. The salt concentration was: 0.04 mM Ca^{2+}, 0.02 mM Mg^{2+}, 0.04 mM Na^+, 0.10 mM K^+, 0.10 mM NH_4^+, 0.06 mM SO_4^{2-}, 0.09 mM NO_3^-, 0.04 mM Cl^-. The freezing point depression of such low salt concentrations is negligible in comparison to the accuracy of the measurement data.

For experiments, an aqueous suspension of pollen is nebulized into the uppermost third of the chamber by an ultrasonic nebulizer, until the relative air humidity is about 85%. The so-generated aerosol droplets slowly sink through the chamber. At the same time, the chamber is slowly precooled to about 5 K above the expected nucleation temperature. If the nucleation temperature is not known, several measurements with different precooling temperatures have to be carried out. Then the nebulizer is removed and the inlet is sealed. After that, the measuring program is started, which protocols measurement time, temperature, air pressure, the detector signal and the automatically calculated depolarization degree. For quick cooling, which is necessary for nucleation experiments, a vacuum pump evacuates the chamber from atmospheric pressure down to about 400 mbar and adiabatically cools the chamber inside for about 10 K – the maximum that is technically possible in LOTASC. For interpretation, $D(t)$ is plotted versus $T(t)$ in a diagram. Since the depolarization degree depends on the amount of frozen droplets, it is equivalent to f_{ice} as defined in chapter 2.2.. Therefore, the diagram shows a step between two more or less horizontal lines. The temperature at which D reaches the half height of this step is then interpreted as T_{50}.

Fig. 39 presents depolarization data for Snomax and pure water. The Snomax depolarization curve shows a steep slope around 270 K, while the curve of pure water remains relatively flat. The determined T_{50} were 270 K for Snomax, 261 K for birch I pollen, 244 K for hazel pollen and 243 K for ragweed pollen

[Pummer et al. 2011]. Since the setup could be cooled only down to 240 K, the homogeneous freezing temperature could not be reached. However, since no ice was observed down to that temperature, it can be regarded as upper limit for the nucleation of pure water.
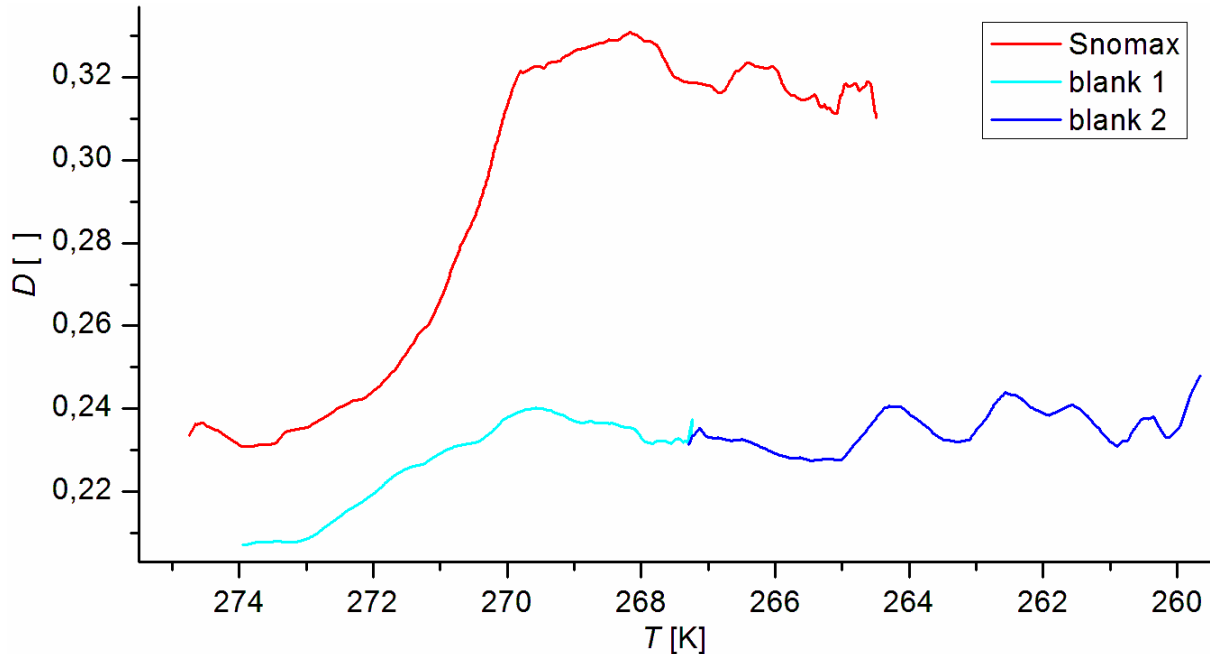

Fig. 39: Exemplary depolarization curves of Snomax and pure water.

In the given cases, the data agree passably with the data from the oil immersion setup. The deviations are acceptable, since LOTASC was not well equipped for droplet freezing measurements. The drawbacks it was afflicted with were:

- The particles deposited quickly in the chamber, so the pollen had to be crushed with a swing mill. However, this stress deactivated the more sensitive IN, like those of juniper pollen.
- Since it was not possible to fully clean the chamber after a measurement, the next sample might be altered by contaminations from the previous measurement.
- The detector cannot discriminate between primary and secondary nucleation. Furthermore, the change in the depolarization degree is very small in comparison with the signal noise.

- The droplet diameter could be neither controlled, nor predicted, since temperature, pressure and relative humidity change during the measurements.

- The depolarization degree is increased by background scattering, like from the chamber wall, respectively its ice cover. Even before aerosol freezing occurred, the depolarization degree was about 0.2.

- Liquid droplets in the chamber partly shield this background signal. However, if the aerosol concentration changes during the measurements (e.g. due to deposition, evaporation or the seeder-feeder mechanism), the depolarization degree is altered.

In general, these results are acceptable as approximate comparisons to confirm the results from chapter 2.2., but the uncertainty is too severe to apply them for further interpretation.

2.5. Flow tubes (LACIS and ZINC)

To acquire further comparative data, pollen waters as described in chapter 2.2. were prepared and inserted into two different devices, namely the Leipzig Aerosol-Cloud-Interaction Simulator (LACIS) at the Leibniz-Institute for Tropospheric Research, and the Zürich Ice Nucleation Chamber (ZINC) at the Swiss Federal Institute of Technology.

LACIS is a 7 meter long vertical flow tube (see Fig. 40[i] and 41[j]) with a circular lateral cut with a diameter of 15 mm. On its top, the aerosol of interest is inserted and pushed through together with sheat air of a given humidity content. The last 1-2 meters of the column are cooled down to the temperature, at which IN* is about to be
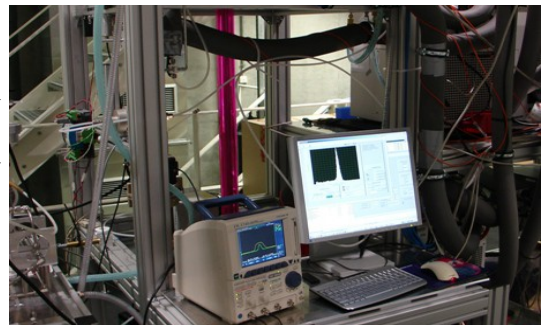

Fig. 40: A section of LACIS

---

[i]   http://www.eurochamp.org/chambers/lacis/
[j]   http://cloudlab.tropos.de/lacis/lacis.html

measured, so for each temperature in the nucleation spectrum, a separate measurement has to be carried out [Hartmann et al. 2011, Hartmann et al. 2012]. The cooled aerosol stream leaves the tube at its bottom, where an optical detection device, consisting of a laser beam and three photodetectors in a defined geometry can discriminate between liquid droplets and ice crystals. In fact, the setup can also differentiate between different crystal shapes [Kiselev et al. 2010, Clauss et al. 2013]. So the fraction that nucleated can be quantified by comparing the intensity of the liquid and the frozen signal.
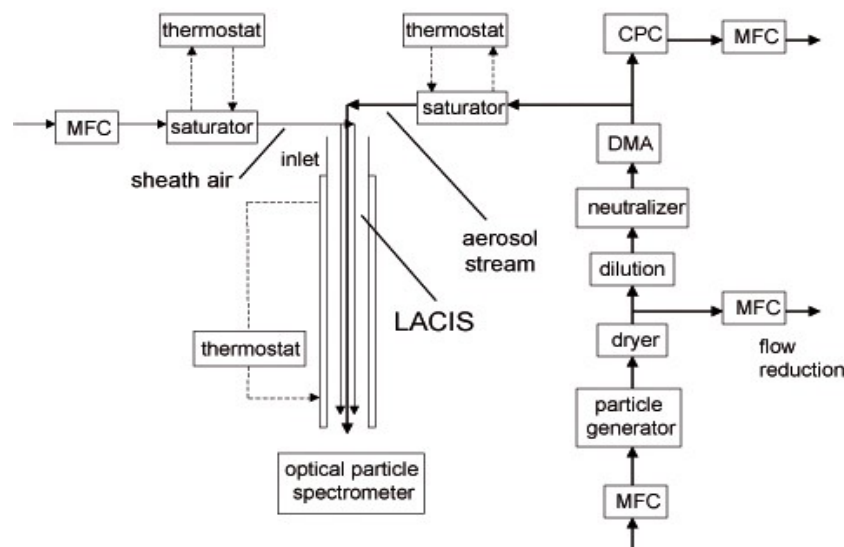
Fig. 41: Schematic overview of LACIS.

The data generation by LACIS differs from the other described setups (see chapter 2.2. and 2.4.) in three essential ways: First, the setup is isothermal, so to produce a full nucleation spectrum, several measurements have to be carried out at different temperatures. Second, the material content is kept very low by the insertion mechanism, which will be explained at the end of this chapter. As a consequence, both active fractions and median freezing temperatures are lower in comparison to other setups. Third, the sample aerosol is permanently renewed by the air flow. So droplets have to freeze within the 1-2 seconds during which they pass the last section, or else they will still be liquid, when they reach the detector. As nucleation is principally a time-dependent process, possible slower nucleation events are excluded from detection this way.

LACIS was applied to determine the IN* activity of different pollen waters [Augustin et al. 2012]. The insertion mechanism was constructed this way: First, pollen water was air-dispersed into small droplets of different sizes. These droplets were carried away by an air flow and dried in a diffusion dryer filled with silicagel, so that only the dried-up residues contained in the waters remained. The particle sizes follow a statistic distribution, which is determined by the concentration of the original suspension. Individual particles of the same size are expected to contain on average the same number of ice nuclei. Then the particle stream was passed through a

Fig. 42: ZINC

differential mobility analyzer (DMA) [Knutson and Whitby 1975], which selected one defined particle size for insertion into the flow tube. Because of this intermediate step, the results are independent of the initial pollen water concentration. The latter one onloy determines the absolute number of selected particles. The higher the pollen water concentration, the more large particles, which are more active, will be generated. Without the DMA, a more concentrated suspension would lead to generation of more and bigger particles and so show an increase in IN* activity – in consistency with the cryo-microscopic measurements (see chapter 2.2.). As all but one particle size are filtered with the DMA, and as only the fraction, not the absolute number of frozen droplets is of interest, the initial particle distribution is of no relevance. These particles were then inserted into the flow tube together with sheat air, which consists of a mixture of dry and water-saturated air, which allocates the water for CCN activation. By cooling the wall below the dew point of the air flow, water vapor was condensed on the particle surface to form liquid droplets again. However, since the air humidity was tuned as required, the droplet diameter was constantly 6 μm. These droplets were then sparged through the last

sections of the tube, where they are cooled down to the temperature of interest. Those droplets containing an IN active at this temperature will eventually freeze. Then both the remaining liquid droplets and the ice crystals leave the tube and reach the detector, where they are assigned.

Some results of these measurements are presented in Tab. 10 [Augustin et al. 2012]. As the birch I samples from AllergonAB$^©$ and Pharmallerga$^©$ showed a slight discrepancy in their IN activity, which was not detectable in the oil immersion device, their data sets were interpreted separately. For this purpose, the two different sources are labeled for discrimination with the first letter of the company name from which they were received, namely "A" for AllergonAB$^©$, and "P" for Pharmallerga$^©$.

As Tab. 10 shows, both the active fraction and the median freezing temperature are lower than their counterparts in the oil immersion setup and the smog chamber. Hazel pollen water, which was also tested, showed no heterogeneous nucleation in this device at all, although the detection limit for f_{ice} in LACIS is about 1%. Juniper I pollen water showed an active fraction of <2% for 500 nm particles. However, this seeming deviation is the result of the different IN concentrations per droplet in the two setups. In fact, the droplets in LACIS can be considered highly diluted in comparison to the emulsion. To verify this assumption, pollen waters of lower concentrations were generated and measured, as described in chapter 3.1..

sample	d [nm]	T_{50} [K]	f_{active} [%]
birch I$_A$	300	250	40
	500	250	80
	800	252	100
birch I$_P$	300	248	15
	500	249	35
	800	250	70

Tab. 10: Abridgment of the pollen water data acquired in LACIS: Both the median freezing temperature and the active fraction depend on both the sample and the selected residual particle diameter.

The differences between the birch I_A and I_P can be interpreted in different ways, either by variations in sequence or structure of the PIN, or by posttranslational modifications due to environmental impacts [Augustin et al. 2012].

ZINC is a flow tube [Stetzer et al. 2008] with a flat-rectangular lateral cut (see Fig. 42[i]). The pollen water was nebulized by an ultrasonic atomizer, dried up, and channelled through a DMA to select monodisperse particles. For growing droplets, a condensation chamber called Immersion Mode Cooling Chamber (IMCA) is attached before the ZINC. The sample is injected and encased by two streams of sheat air to keep the sample stream focussed. The air flow is humidified by a water-soaked filter paper stretching out over the chamber wall to condense droplets on the aerosols. When the sample jet is injected into the ZINC chamber, it is further encased by two streams of sheat air, which keep the droplet stream away from the chamber wall. A depolarization detector in the lower section of the tube quantifies the ice fraction. The total ZINC-IMCA-tube is only about 2 meters long. A further difference to LACIS is that particles need about 12 seconds to cross the cold section before they reach the detector, which is far longer than the 1-2 seconds in LACIS. Furthermore, the pollen waters had to be diluted to 1/50 of its original concentration, which is equivalent to a pollen water preparation with 1 mg/ml pollen, to prevent the overloading of ZINC with particles. However, since the results are independent of the initial concentrations due to the DMA, the results are still comparable.

Birch I_P pollen waters were chosen as a test sample. Aerosol particles with a selected diameter of 400 nm were investigated in the temperature range from 234 to 263 K. The determined active fraction was 73±14% and the median freezing temperature 250±1 K.

An important cognition of the LACIS campaign was the immensely high IN* active fraction in birch I pollen measurements. In comparison, the active fraction

---

[i]   http://www.iac.ethz.ch/groups/lohmann/research/lab/in/zinc

of mineral dusts or other pollen species never exceeded a few percent [Niedermeier et al. 2011b, unpublished data]. Of all samples investigated in LACIS up to now, only Snomax showed a similarly high active fraction, namely 20-50% for 650 to 800 nm particles [Hartmann et al. 2012]. Furthermore, the slight difference in the IN efficiency between birch pollen from two independent sources, namely the companies AllergonAB© and Pharmallerga©, was not detectable in the oil immersion setup.

2.6. Electron microscopy

Since surface topologies were held responsible for the IN* activity of bioaerosols in the past [Diehl et al. 2001], the pollen and spores were investigated by an electron microscope to look for correlations between texture and IN* activity. Scanning electron microscopy (SEM) measurements were carried out on a FEI Quanta™ 200 FEGSEM. Therefore, some pollen grains were placed on a sticky carbon tape, which itself was stuck to a sample carrier. The sample was then coated under argon atmosphere (sputtered) with a 4 nm thick film of a 6:4 Au-Pd alloy in a Sputter Coater Quorum Q50T S. This way the sample was made conductive to prevent charging of the sample, and so adulteration of the SEM image. Then the sample is inserted into the electron microscope and measured under high vacuum conditions ($\sim 10^{-6}$ mbar). The electron beam has a voltage of 5 kV, which is rather low, in order to prevent a potential manipulation of the sample.

An abridgment of captured fungal spore SEM images is shown from Fig. 43 to 45. The bars in the pictures are always 2.0 µm long. It can be seen that fungal species that are closely related produce the same type of spores.
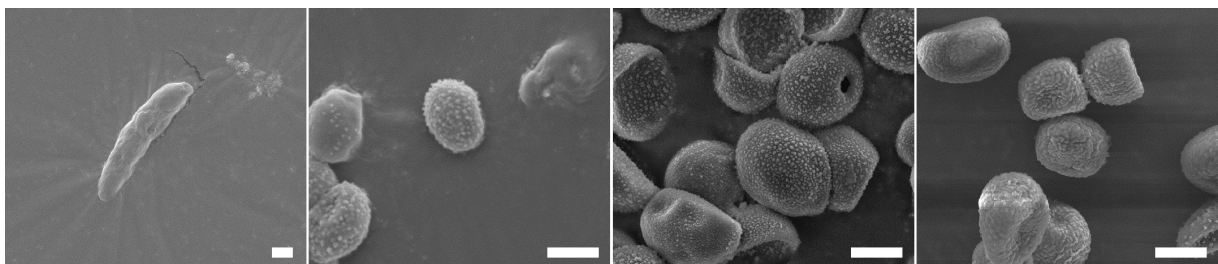

Fig. 43: Fungal spores of *F. avenaceum*, *T. atroviride*, *T. virens* and *P. citrinum* (from left to right).
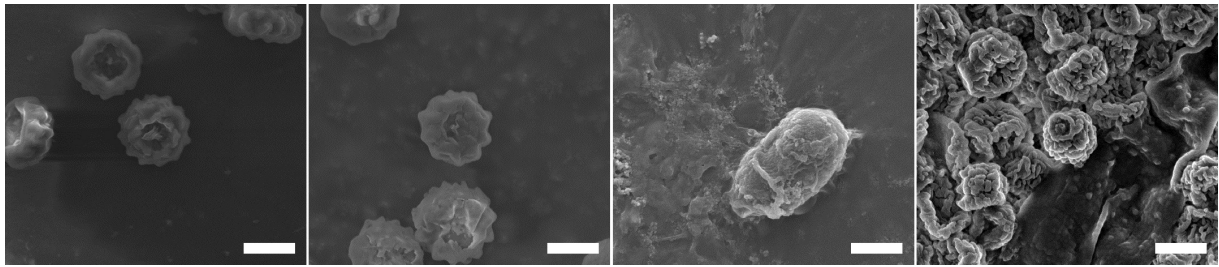
Fig. 44: Fungal spores of *A. fumigatus*, *A. niger*, *P. digitatum* and *P. glabrum* (from left to right).
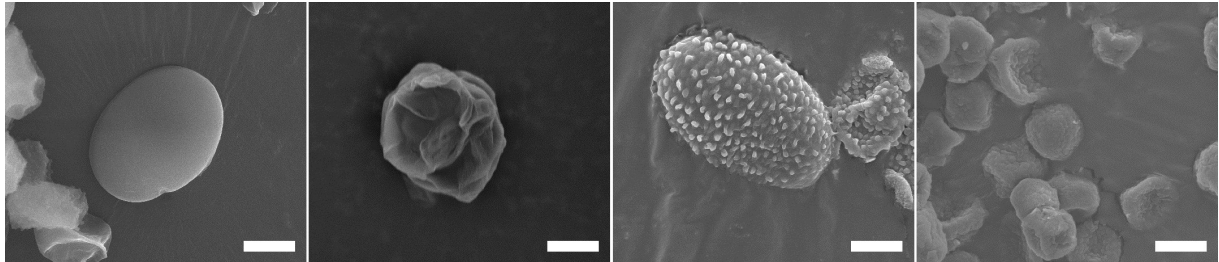

Fig. 45: Fungal spores of *Ag. bisporus*, *L. edodes*, *C. herbarum* and *E. album* (from left to right).

As it can be seen, the spores of the *Trichocomaceae* family all look quite alike, which is easily explicable by their close relation to each other. The *Fusarium* spores are characteristic, since they are very long and thin. It is important to point out that the appearance of the spores can severely vary with the growing conditions, same as the appearance of the whole fungus.

An abridgment of captured pollen SEM images is shown from Fig. 46 to 54. The first and third picture of every line show whole pollen grains. The pictures right of each grain image show details of the surface topology of the same pollen species. Only in the last line there are only whole pollen grain pictures of four different species. The bars in the pictures with whole pollen grains are 5.0 μm long, while those in the detail pictures are 0.5 μm long.

The surface topology of pollen is classified according to their appearance, which is only in few cases consistent with the genetic relationship between the species. The determined surface structures in these species were: rugulate (wrinkled) for pine, gemmate (gem-like) for the other conifers, reticulate (net-like) for willow and plane tree, echinate (spike-covered) for wormwood and ragweed, foveolate (pit-covered) for sorrel, tectate (tile-like) for elm and scrabate (nipple-covered) for all others. While the appearances of conifer pollen mirror the genetic relation of those species – meaning that closely related pollen look alike – the

appearances of angiosperm pollen can barely be correlated with species relationships.

All pollen showed a rich topology, and on some samples (*Pinus sylvestris*, *Ambrosia artemisiifolia*, *Plantago lanceolata*, *Ulmus americana*, *Rumex acetosa*) even the nanopores penetrating the exine were visible. However, there is no correlation visible between topological elements and IN* activity of the pollen. This alone makes the classic hypothesis explaining IN* ability with the topology very unlikely. Furthermore, this hypothesis cannot explain the IN* of the pollen waters, since they lack the pollen grains and so the surfaces.

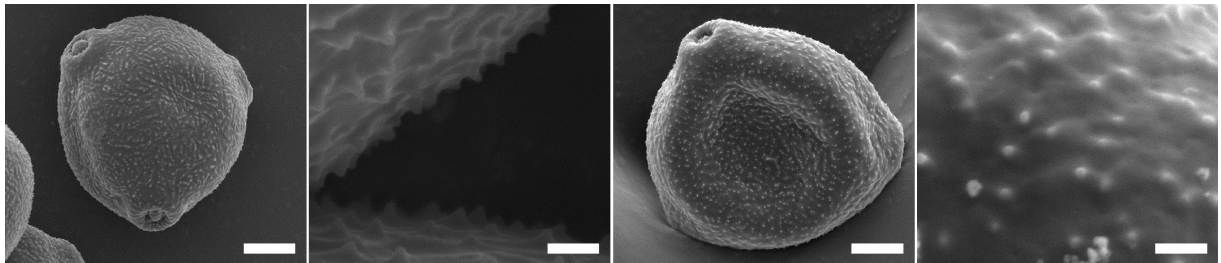**Fig. 46: Pollen SEM captions of *Betula pendula* (two left) and *Corylus avellana* (two right).**
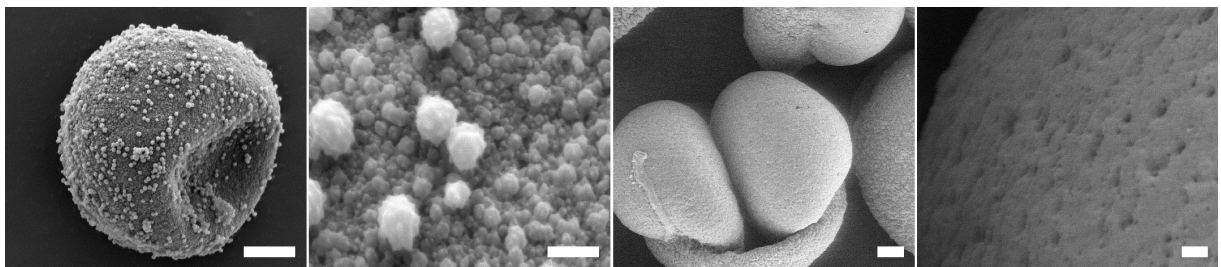
Fig. 47: Pollen SEM captions of *Juniperus chinesis* (two left) and *Pinus sylvestris* (two right).
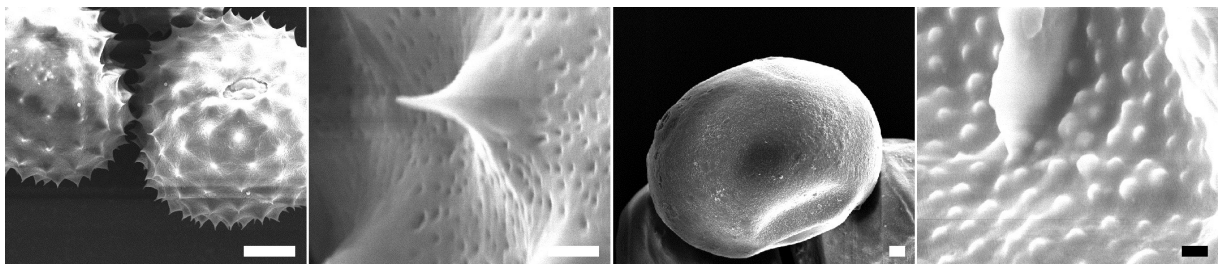
Fig. 48: Pollen SEM captions of *Ambrosia artemisiifolia* (two left) and *Zea mays* (two right).
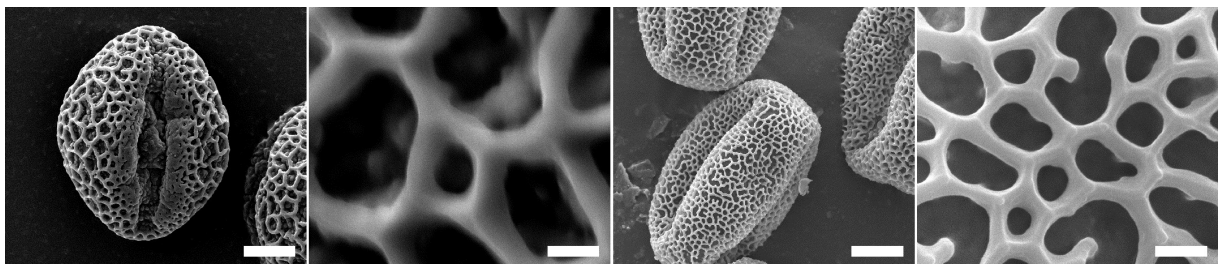
Fig. 49: Pollen SEM captions of *Salix caprea* (two left) and *Platanus orientalis* (two right).
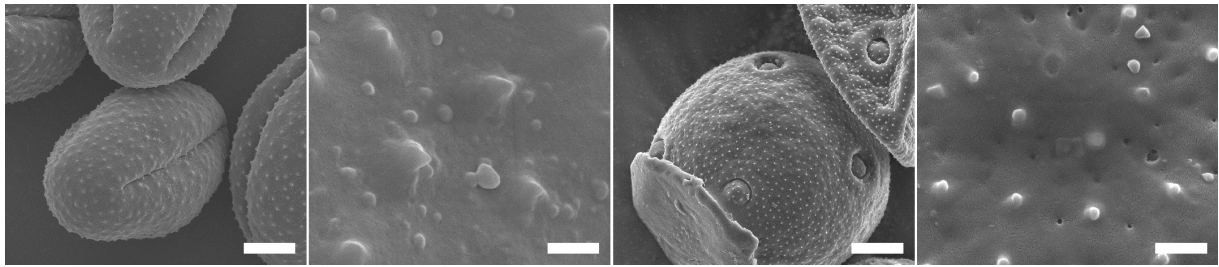
Fig. 50: Pollen SEM captions of *Artemisia absinthium* (two left) and *Plantago lanceolata* (two right).
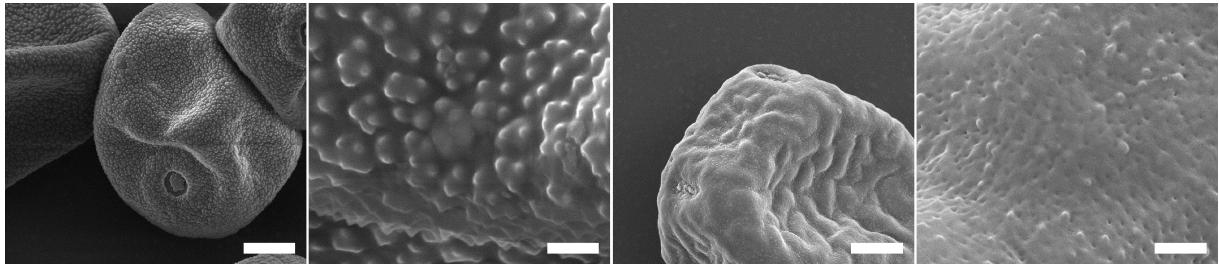
Fig. 51: Pollen SEM captions of *Agrostis gigantea* (two left) and *Ulmus americana* (two right).
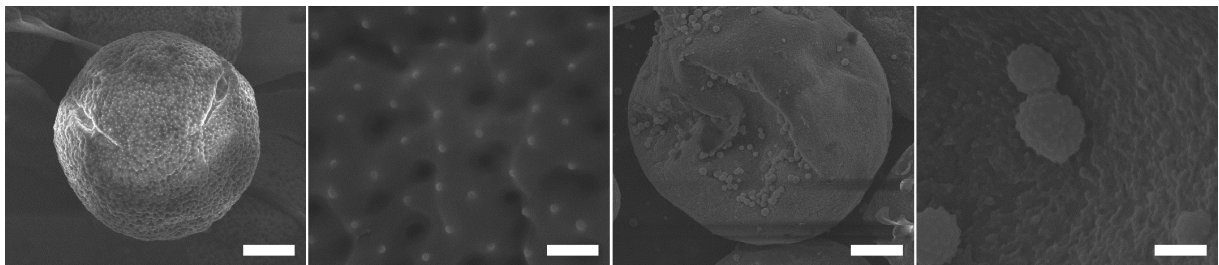
Fig. 52: Pollen SEM captions of *Rumex acetosa* (two left) and *Thuja orientalis* (two right).
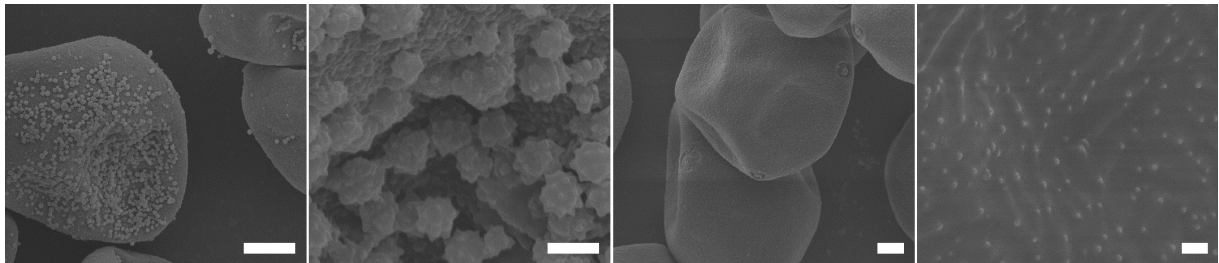
Fig. 53: Pollen SEM captions of *Thuja occidentalis* (two left) and *Carpinus betulus* (two right).
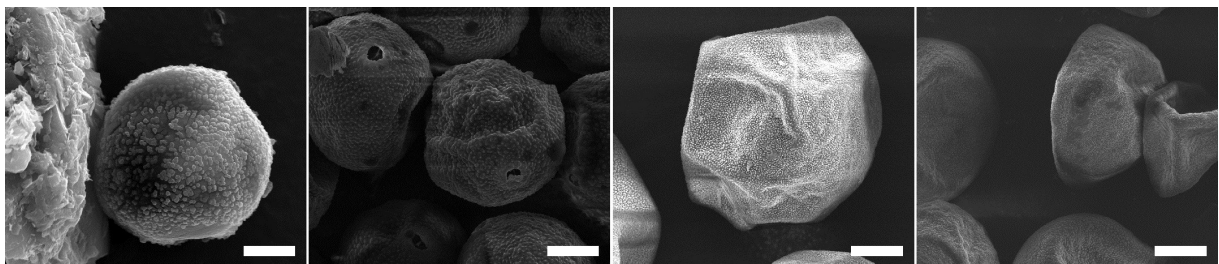
Fig. 54: Pollen SEM captions of *Taxus baccata*, *Urtica dioica*, *Triticum aestivum* and *Lolium perenne* (from left to right).

To check, if the pollen water contains submicron particles, which could be responsible for IN*, droplets of these were placed on a carbon-layered copper screen and left to dry up. The material contained in the water remained on the screen and formed a thin film. The samples were then placed under a FEI Tecnai

F20 transmission electron microscopy (TEM). This procedure was carried out with pollen waters of *Betula pendula*, *Pinus sylvestris*, *Ambrosia artemisiifolia*, *Juniperus communis* and *Salix caprea*.

The results were the same for all pollen species: The pollen material film was mostly homogeneous and amorphic down to a scale of a few nanometers. Higher resolution was not possible, since the background screen itself showed structures on the level of nanometers.
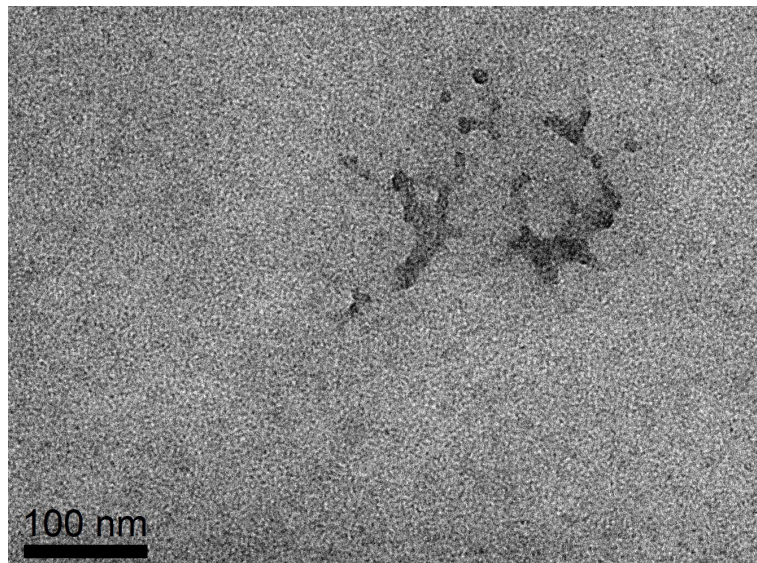
Fig. 55: A SEM image of birch pollen water residues.

Most parts of the layer were amorphous and homogeneous. The grainy look of Fig. 55 originates from the background, which is a carbon layer. Only occasionally anomalies like in the top right quarter of the image appear.

In addition, the elementary composition of the film was investigated by energy-dispersive X-ray spectroscopy (EDX), which was coupled to the TEM. By excitation with the TEM electron beam, inner shell electrons of atoms in the sample were removed. When relaxing, outer shell electrons, which contain higher shell energy, fill up the gaps, which are of lower shell energy. The energy difference is set free as X-ray photons with an energy content defined by the participating shells, which are in turn depending on the nucleus to which they are bound, and so on the chemical element.
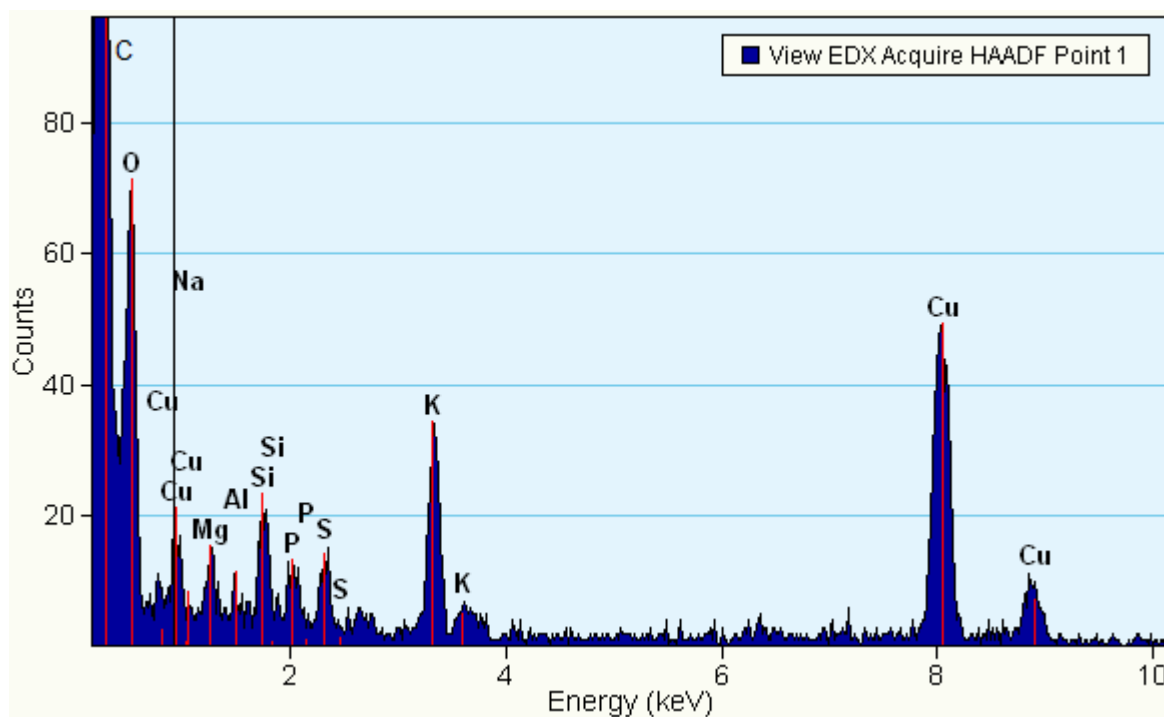
Fig. 56: An EDX spectrum of birch pollen water residues.

Same as the TEM measurements, the EDX spectra showed no difference between the investigated species. Therefore, an exemplary EDX spectrum of birch pollen residues is shown in Fig. 56. Unsurprisingly, the largest peaks correspond to carbon C and oxygen O, which are the basic elements of biological compounds (H cannot be detected by EDX due to its lack of electrons, respectively occupied shells). Consequently, the information that can be extracted from these data is minute. Furthermore, carbon C and copper Cu show signals originating from the sample carrier. Smaller signals could be assigned to typical quantity elements, like magnesium Mg, phosphorus P, sulfur S and potassium K. The latter one is the most important intracellular cation[i] and gives the largest of these signals.

Since pollen are spacious particles with a rich internal structure, they are exposed to fragmentation [Grote et al. 2001]. Consequently, chemical signatures of pollen can be detected in the atmosphere even in the absence of whole pollen grains [Solomon et al. 1983, Schäppi et al. 1999, Yttri et al. 2007]. This process might also boost atmospheric PIN concentrations in absence of the pollen

---

[i]   http://www.elmhurst.edu/~chm/vchembook/250fluidbal.htm

themselves [Pummer et al. 2012]. When the robust pollen exine breaks apart, the liquid inner life, the cytoplasm, leaks out. This way, the pollen micrometer-sized organelles are revealed. The most impressive organelles are starch granules, which function as nutrient storages. These granules were detected in some investigated grass pollen species via electron microscopy [Grote et al. 2001].

Pollen of *Betula pendula*, *Pinus sylvestris* and *Zea mays* were chosen for investigation. Suspensions of pollen grains were spread on a sticky carbon tape stuck on the sample carrier, vacuum-dried and sputtered with Au-Pd alloy (see chapter 2.6.). Then the sample was investigated with the FEGSEM. Four different preparation techniques were applied to fragment the suspended pollen.

- Method 1: Suspensions were generated in-situ on the carbon tape by placing dry pollen grains on it and adding a droplet of water with an Eppendorf pipet. After 10 min residence time the water was evaporated.

- Method 2: Pollen grains were suspended in water for some hours and occasionally shaken.

- Method 3: Dry pollen grains were crushed with a Retsch MM400 swing mill and suspended in water.

- Method 4: Pollen grains were suspended in water. The whole suspension was inserted into the swing mill and shredded.

While no fragmentation at all occurred with method 1, method 2 and 3 caused partial ripping of the pollen grains. The method 4 led to effective disintegration and released huge amounts of material. A selection of taken SEM pictures with disintegrated corn pollen is shown in Fig. 57. The picture on bottom left shows preparation by method 4, while the others show preparation by method 3. Fig. 57 shows that corn pollen contained huge numbers of organelles with about 2 μm diameter. These particles were interpreted as the starch granules. The severely disintegrated sample prepared by method 4 showed not only a huge number of released organelles, but also a covering of the pollen fragments with an amorphous layer. This film was obviously the same as it had been observed in

the TEM measurements. Obviously, it consists of the suspendable material that can be extracted from the pollen grains. Further characterization of the main components this layer consists of is presented in chapter 3.5..
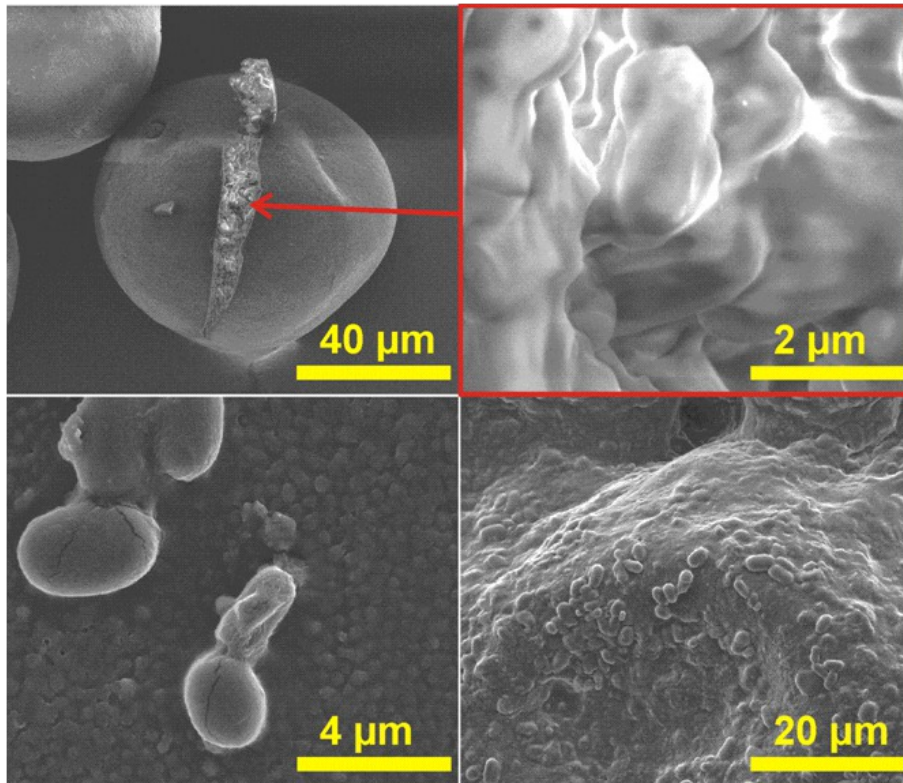
Fig. 57: SEM pictures of disintegrated corn pollen and released material. The 2-µm organelles were interpreted as starch granules.

Among the three species, only corn pollen released starch granules, which are commonly present in grass pollen [Grote et al. 2001]. Cereals, which are cultivated members of the *Poaceae* (sweet grass) family, are designed to build up huge amounts of starch to boost the nutrient content in the seeds, which are an essential source of food. Since corn is a type of cereal, the huge starch content is not surprising.

3. Pollen ice nuclei characterization

3.1. Quantification

To quantify the amount of material that is released by the pollen water preparation, pollen were suspended in water with concentrations of 25 mg/ml to generate the pollen waters. Then a glass slide was weighted. Droplets of a given pollen water were placed on the slide and left to dry. This procedure was repeated, until a total volume of 0.5 ml was spent. Then the glass slide was weighted again, and the difference to the original mass was attributed to the pollen material. The results are shown in Tab. 11. The percentage shows the mass that was extracted from the pollen relative to the whole pollen mass.

species	mg	wt.%	T_{50} [K]
birch I	5,2	42	255
juniper I	5,8	46	253
willow	4,4	35	249
hazel	4,7	38	249
ragweed	3,7	30	236
corn	4,6	37	235

Tab. 11: Determined masses of the pollen water residues.

The data presented in Tab. 11 show a surprisingly high fraction of extractable material. Since the residues were not actively dried (e.g. by heat or air stream) to prevent loss of material, they might contain remnants of incorporated water. Therefore, the determined masses can be considered as an upper limit for the real mass content. As a consequence, it is legitimate to compare pollen waters, where concentrations of 50 mg/ml pollen grains were applied, with 20 mg/ml Snomax or mineral dust, where the whole sample is in suspension.

The residues themselves are a heterogeneous mixture of all chemical compounds extractable from the pollen, like saccharides, lipids, proteins, carotenoids [Grote 1989, Ivleva et al. 2005, Schulte et al. 2008] and inorganic electrolytes.

While extracellular electrolytes mainly consist of Na^+, Ca^{2+} and Cl^- ions, intracellular electrolyte fluids mainly contain K^+, Mg^{2+} and $H_2PO_4^-/HPO_4^{2-}$ ions[i]. Since many of the extractable compounds, like the present monosaccharides and electrolytes, are excellently soluble in water, they are expected to decrease the freezing temperature. So in fact, only a minute fraction of the extracted pollen material can be considered as contributors to IN*. This is analogous to the bacterial IN, where only one protein out of many different chemical compounds of bacterial cell wall is responsible for the IN* activity [Kawahara 2002].

Inspired by the LACIS campaign (see chapter 2.5.), the question arose, if the made assumptions could be verified. It was suggested that the differences in the absolute numeric values of f_{ice} and T_{50} between the flow tube and the oil immersion measurements are caused by the differences in the IN concentration per droplet. As a consequence, the LACIS data should be reproducible in the oil immersion setup, if they are diluted. Therefore, pollen waters of different concentrations were prepared and measured via cryo-microscopy. This way, also the decrease of the IN activity with increasing dilution was determined.

Via dilution from higher to lower concentrations, pollen waters from the species with the highest median freezing temperatures were investigated, namely *Betula alba*, *Juniperus communis*, *Pinus sylvestris*, *Rumex acetosa* and *Ulmus americana*. The following pollen concentrations were applied: 50 mg/ml (original), 2 mg/ml, 0.1 mg/ml, 5 µg/ml, 0.5 µg/ml. Dilutions were measured until the IN* active fraction dropped to zero or negligible values of a few percents. The results for the median freezing temperatures are shown in Tab. 12, those for the active fraction in Tab. 13. Since these measurements were only carried out with birch from Pharmallerga©, it is again labeled as "birch I_P".

The relation between the active fraction and the concentration is non-linear. This is not surprising, since also T_{50} decreases with every dilution step. Consequently, triplets of concentration, active fraction and T_{50} have to be compared instead of

---

[i]   http://www.elmhurst.edu/~chm/vchembook/250fluidbal.htm

only pairs between concentration and active fraction. The dilution row furthermore shows that birch pollen exceed the others in their IN number by orders of magnitude.

	birch I_P	juniper I	pine	sorrel	elm
50 mg/ml	255	253	252	252	250
2 mg/ml	254	249	248	250	249
0.1 mg/ml	252	249	236	247	247
5 µg/ml	250	--	--	--	239
0.5 µg/ml	244	--	--	--	--

Tab. 12: Median freezing temperatures of the diluted pollen waters in Kelvin. The active fraction taken for analysis is given in Tab. 13.

	birch I_P	juniper I	pine	sorrel	elm
50 mg/ml	100	100	62	84	100
2 mg/ml	100	50	21	21	100
0.1 mg/ml	88	17	0	20	57
5 µg/ml	65	--	--	--	0
0.5 µg/ml	19	--	--	--	--

Tab. 13: IN* active fractions of the diluted pollen waters in %. For fractions without heterogeneous IN* activity (0%), the homogeneous IN* step was analyzed to determine the temperatures in Tab. 12.

The active fractions of the higher dilutions are comparable with those measured in the flow tubes (see chapter 2.5.). By correlating the active fraction with the particle diameter in Tab. 10, one can assign a theoretical particle diameter to a sample with a known active fraction in the pollen water. A comparison between the birch I_P pollen water data from Tab. 10, 12 and 13 gives a concentration of 0.5 µg/ml corresponding to a particle diameter of 300 nm, 5 µg/ml to 750 nm and 0.1 mg/ml to 1000 nm. The theoretical particle volume factor between the two lower concentrations is 15, while the concentration factor is 10. So these data are perfectly matching. The concentration increase to the highest concentration is a factor of 20, however, the theoretical volume increase is only a factor of 2. This discrepancy by a factor of 10 could be the result of the closeness to the saturation plateau, which leads to flattening of the curve, since active fractions obviously cannot exceed 100%.

Furthermore, these data demonstrate, why pine pollen water residues with particle sizes up to 800 nm showed no IN* activity in LACIS, because the pine pollen waters with concentrations up to 0.1 mg/ml were also negative in the cryo-microscopic measurements. The low active fraction of 500 nm juniper I in LACIS, namely <2%, correlates well with a concentration between 0.5 and 5 µg/ml, which is the same for the 500 nm birch I_P pollen.

Finally, birch I pollen were washed several times to determine, if the PIN can be either fully or just partly extracted. Therefore, a birch pollen suspension (50 mg/ml) was prepared and then filtrated. The generated pollen water was discarded, and the filter cake was suspended again in fresh water. This procedure was repeated to a total of 6 washing cycles. The last time, the suspension was not filtered, but mixed with oil for IN* measurements as described in chapter 2.2.. The median freezing temperature shifted from 254 K to 250 K. A frozen fraction of 100% was reached at temperatures above 243 K. This simple experiment shows that only a part of the IN is extracted by the washing procedure, so that even after several cycles there is still an appreciable IN* activity left. In reverse, the amount of IN on the pollen is higher than the amount of IN detectable in the pollen waters.

3.2.   Size analyzation

To confirm the hypothesis that PIN are macromolecules, pollen water samples were filtered through Vivaspin® columns (see Fig. 58), which are commercially available size exclusion filtration devices. Those are plastic tubes separated horizontally into two chambers by a porous polymer filter made of polyethersulfone, which retains everything larger than a defined mass limit, while it allows smaller compounds to pass through.

Tubes with mass limits of 300, 100, 50, 30, 10 and 5 kDa were applied for investigation of pollen waters [Pummer et al. 2012]. After the upper part was

filled with pollen water, the column was centrifuged at 4000 rpm to press the liquid through the filter. All molecules larger than the mass limit were held back by the polymer matrix. By measuring the IN* activity of the filtrate it could be decided, whether the IN were larger than the mass limit or not. If the filtrate was IN* negative, the IN had to be detained in the filter. The focus was laid on the three most active species, namely *Betula alba*, *Juniperus communis* and *Pinus sylvestris*.

filter	birch I	juniper I	pine
none	255 K	253 K	252 K
300 kDa	255 K	250 K	248 K
100 kDa	235 K	234 K	236 K
50 kDa	234 K	235 K	234 K
30 kDa	235 K	--	--
10 kDa	234 K	--	--
5 kDa	240 K	--	--

Tab. 14: Median freezing temperatures of pollen waters filtered through Vivaspin tubes.

As Tab. 14 shows, only the pollen waters filtered with the 300-kDa-filter kept their IN* activity, while all others became fully IN* negative. The conclusion is that the PIN masses have to be approximately between 100 and 300 kDa. This mass range belongs to the class of polymers, which are built up by a high number of low-molecular building blocks. In biochemistry, these are mostly amino acids, which build up proteins, and sugars, which build up saccharides.

Fig. 58: A Vivaspin tube (left) plus the individual constituent parts.

Considering that these units have masses between 75 Da (glycine) and 205 Da (arginine), a biopolymer of this size should consist of 500-5000 building blocks. The filtrate of the 5-kDa-column shows slightly higher IN* activity than the other IN* negative birch pollen filtrates, which might be caused by the release of

column material. Due to the smaller pore size and the quick congestion, the filtration with this column took far more time than with the others. This fact and the higher fragility of smaller structures might be the reason for a slight bleeding of the column.

The passage of the IN through the 300-kDa-filter shows that the IN are not adsorbed by the material itself, and are therefore able to pass the filter, if its pores are large enough.

3.3. Chemical and biochemical analysis

As BINP and FINP are already known to be proteinaceous compounds, it seemed likely that the PIN were also specially-structured nutrients.

Different assays were performed with pollen waters to determine the resistance of the PIN against heat, acidity, and specific nutrient-degenerating agents. After treatment, the samples were again checked for their IN* activity by cryo-microscopy (see chapter 2.2.). Apart from selected pollen species, blank water and Snomax were investigated to test the reliability of the method itself. *Betula alba*, *Juniperus communis* and *Pinus sylvestris* were tested in all assays [Pummer et al. 2012].

To determine the heat stability of the IN, washing extracts were heated to the proper temperature for 1h. Then the residue was resuspended in water. Heat tests were carried out at temperatures of 355, 385, 415, 445, 460 and 475 K, depending on the pollen species. The median freezing temperatures are listed in Tab. 15 and visualized in Fig. 59.

The differences in deactivation temperature ranges are distinguishable at a glance. So in fact, the IN* active sites have to differ between species as well. Furthermore, most PIN seem to be more stable than the BINP, since they were still very active at temperatures, where Snomax was already IN* negative. The

most stable ones were the birch PIN. The T_{50} curve of hazel and yew PIN, on the other hand, always lies below the Snomax curve.

	Snomax	birch I	juniper I	pine	willow	hazel	yew
none	268	255	253	252	249	249	246
355 K	262	254	249	--	--	249	245
385 K	263	254	249	251	248	250	240
415 K	235	250	246	249	241	236	237
445 K	236	247	237	241	241	236	--
460 K	--	236	234	236	236	--	--
475 K	--	236	--	--	--	--	--

Tab. 15: The listing of median freezing temperatures after sample heating. The numbers are temperatures in Kelvin. The first column lists the heating temperatures, the other columns list the measured T_{50}.
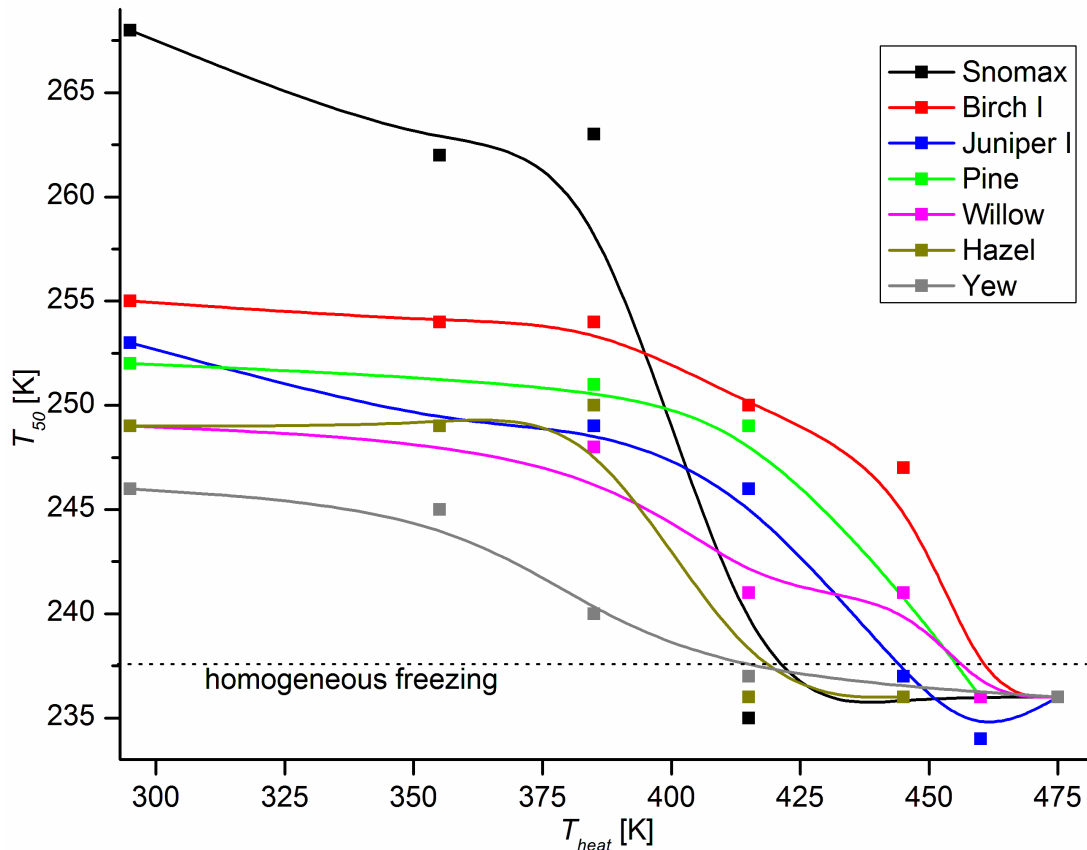
Fig. 59: The heat degeneration curves of Snomax and PIN. The x-axis is the temperature to which the sample was exposed before IN measurements, while the y-axis shows the median freezing temperature.

To test the impact of acidity on IN* activity, pollen were suspended in diluted sulfuric acid and warmed to a given temperature for a given time. The pollen water was then filtered and diluted to 0.5M H_2SO_4 to decrease the freezing point

depression caused by the acid itself. The diluted fraction was then taken for nucleation measurements.

Following acid concentration and conditions were applied:

- 0.5 M, 298 K, 1 h
- 2 M, 333 K, 3 h
- 5 M, 333 K, 1 h
- 10 M, 358 K, 1 h

When mixing pollen with 10 M acid the suspension color immediately changed from yellow to red, what can be explained by the oxidizing properties of highly-concentrated sulfuric acid. When tempering the sample, it turned black and coagulated within minutes due to dewatering and carbonization of organic compounds, what is accelerated at elevated temperatures. Results are presented in Tab. 16.

	birch I	juniper I	pine	willow	hazel	yew	corn	blank
none	255	253	252	249	249	246	235	237
0.5 M	252	248	244	--	--	--	--	232
2 M	254	--	--	--	--	--	--	--
5 M	240	236	234	242	236	234	237	232
10 M	231	--	--	--	--	--	--	232

Tab. 16: The results of the pollen water treatment with sulfuric acid. The numbers are T_{50} [K].

The general decrease of T_{50} in comparison to untreated samples is explicable by Raoult's law, according to which a soluble component always decreases the freezing point, depending on its concentration. Apart from that, all samples were fully deactivated after treatment with 5 M sulfuric acid. Again, birch I obviously carries the most robust PIN, since it is fully active after treatment with 2 M sulfuric acid, while the pine pollen seem to suffer IN* activity losses already at 0.5 M acid concentration.

As not all acid concentrations were investigated with all the pollen waters, Tab. 16 is quite sparse. However, since only little information can be extracted from these results, the focus was laid on other investigation techniques.

The presence of strong acids reduces the stability of the emulsions. Electrolytes increase the polaritiy of the aqueous phase, and so the polarity difference between the two phases. This speeds up the phase separation, and so destabilizes the emulsion. Additionally, esters are hydrolyzed under acidic conditions. Since lanolin, which stabilizes the emulsion in the first place, consists of fatty esters, it might be partly disintegrated.

For the enzymatic methods pollen water was spiked with enzyme and incubated for the given time at given temperature. After that the solution was measured for IN* activity. As the MilliQ water had a pH of about 5-6, only enzymes were chosen, which have their optimum more or less around that range. In all cases pure MilliQ water has been used as a reference.

The reaction media and conditions are the followings:
- Papain (A): 2 mg/ml, 338 K, 2.0 h (T_{opt}[K]=338, pH_{opt}=5-7)
- Papain (B): 2 mg/ml, 298 K, 4.0 h (T_{opt}[K]=338, pH_{opt}=5-7)
- Pancreas Lipase: 2 mg/ml, 308 K, 3.0 h (T_{opt}[K]=310, pH_{opt}=8)
- Spittle α-Amylase: 0.5 mg/ml, 313 K, 3.0 h (T_{opt}[K]=310, pH_{opt}=5-7)
- Pronase E: 5 mg/ml, 310 K, 4.0 h (T_{opt}[K]=310, pH_{opt}=7-8)
- Cellulase Onozuka: 5 mg/ml, 310 K, 4.0 h (T_{opt}[K]=313, pH_{opt}=4-5)

While papain and pronase E are proteases, which digest proteins, the amylase and the cellulase attack certain glycosidic bondings. Lipase splits the fatty acids from the backbone of lipidic compounds. The impact of all enzymatic assays on the IN* activity is shown in Tab. 17. The decrease of T_{50} after treatment with papain in proecedure A, which occurs in Snomax and juniper I pollen water, can be assigned to the thermal stress caused by the procedure. A comparison with Tab. 15 and Fig. 59, temperatures in this range already lower the T_{50} of the most sensitive samples for a few Kelvin. Therefore, the measurements were repeated with a different procedure at room temperature (procedure B), however, the T_{50} decrease was only 2-3 K for the conifer pollen. Since it is difficult to decide,

whether it is a negligible statistical effect, or already a slight degradation effect, a safe interpretation is not possible. All other chosen enzymes show maxcimum efficiency at lower temperatures, so this problem does not occur. Furthermore, all enzymes had their pH optimum close to that of pure MilliQ water, which was about pH=5, in order to avoid the necessity of pH adjustment. Therefore electrolytes are necessary, which would decrease T_{50} by freezing point depression, as well as by a potential sample modification. Because of this, very effective proteases, like pepsin, were inapplicable, since it is most efficient at pH=2.

	Snomax	birch I	juniper I	pine	blank
none	268	255	253	252	237
Papain A	262	254	249	249	237
Papain B	--	255	250	250	--
Lipase	--	253	253	250	238
Amylase	--	255	253	251	235
Pronase	263	255	252	251	237
Cellulase	265	--	251	251	237

Tab. 17: IN* activity after enzymatic treatments of selected samples. The numbers are T_{50} [K].

Since enzymes themselves are sensitive molecules, enzymatic deactivation is slower and less effective than chemical deactivation. Furthermore, most enzymes attack only specific sites on substrates. Neither the saccharases, nor the proteases applied in this study can break substrates down to the level of monomers.

The advantage of enzymatic assays is, that the method itself has no impact on T_{50}, as can be seen in the blank data column of Tab. 17. Furthermore, if a substrate is digested by a certain enzyme, this yields a lot of information about the nature of the substrate. On the other hand, if a substrate is not affected by an enzyme, the gain of information is lower, since one can only rule out the target class of this enzyme.

To answer the question, if the PIN are proteinaceous compounds, like the known INP of bacteria and fungi, pollen waters were spiked with guanidinium chloride, synonymously also known as guanindin hydrochloride, which is a salt consisting of a guanidinium cation (see Fig. 60) and a chloride anion. In biochemistry 6 M guanidinium chloride is commonly applied as universal denaturating agent for globular proteins, since it unfolds their secondary and tertiary structure [Makhatadze and Privalov 1992].

To determine the impact of protein denaturation, pollen waters were spiked with concentrations of 1 M or 6 M guanidinium chloride. Then emulsions were prepared, and their IN* activity was determined by cryo-microscopy. Results are shown in Tab. 18. Again, Raoult's law causes a systematic decrease of T_{50} with increasing electrolyte concentration.

$$\overset{+}{NH_2}$$
$$H_2N \diagdown \diagup NH_2$$
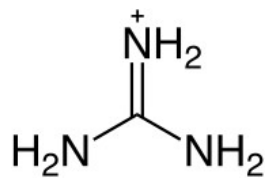
Fig. 60: Guanidinium

	Snomax			birch I			blank			pine	jun. I
	T_{50}	T_{25}	T_{75}	T_{50}	T_{25}	T_{75}	T_{50}	T_{25}	T_{75}	T_{50}	T_{50}
none	**268**	269	267	**255**	256	251	**237**	238	236	**252**	**253**
1 M	**263**	263	262	**252**	253	251	**232**	232	231	**249**	**249**
6 M	**226**	235	222	**239**	247	235	**223**	225	221	--	--

Tab. 18: Results of treatment with guanidinium chloride. The numbers are temperatures [K]. T_{50} are accentuated in bold letters.

According to these measurements, 6 M guanidinium chloride knocks out the BINP in Snomax. The T_{50} depression of the pollen waters is in the range of that of pure water, meaning that the PIN are not affected at all. Only Snomax shows a decrease far more drastical than it could be assigned to Raoult's law. In fact, the nucleation of Snomax in 6 M guanidinium chloride can be interpreted as purely homogeneous nucleation. The high stability of the PIN suggests that they are non-proteinaceous compounds. It has to be noted that the rising part of the nucleation curve covers a far broader temperature range after treatment with 6 M than before.

As PIN showed more resistance than Snomax, and as they are insensitive towards protein-denaturing enzymes and chemicals, they have to be a different kind of substance class. It is likely that they are polysaccharidic compounds, because sugars are quite abundant on the pollen surface [Grote 1989, Yttri et al. 2007]. In the past, mucilage, which are mainly polysaccharides, were correlated with IN* activity in the fluids of cacti [Goldstein and Nobel 1991, Goldstein and Nobel 1994]. Furthermore, BINP have glycosidic side chains attached, which contribute to the activity of the IN* complex. When they are removed, the IN* activity decreases [Kozloff et al. 1983, Kozloff et al. 1984]. The resistance against the saccharases in this study does not contradict this hypothesis, since these enzymes are very substrate-specific (see chapter 1.4.).

3.4. Environmental stress modification

As natural bioaerosols are exposed to and transformed by many natural stress sources, their impact on the IN* activity were investigated. Bioaerosols in the atmosphere are exposed to numerous stresses, like electromangetic radiation, electricity (lightning), acid droplets, extremes in temperature and humidity, as well as numerous trace gases, like ozone, nitrogen oxides, hydrogen sulfide and sulfur dioxide. To demonstrate the possible impact of these stresses, the sample were exposed to several selected stress scenarios to
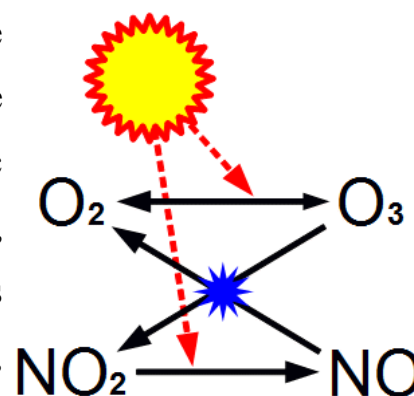
Fig. 61: A scheme showing the connections between ozone, nitrous gases and solar radiation. Note that this graphic does not include all relevant atmospheric processes.

determine the impact. More precisely, the effect of UVA light, ozone and nitrogen dioxide on the IN* activity was investigated.

Although the ozone layer filters out much of the solar ultraviolet light reaching the Earth, most of the UVA light (315-395 nm) reaches the planetary surface. With rising height the UV exposure increases. Furthermore, some atmospheric

aerosols scatter light and so increase the radiation load pollen are exposed to. UV light is very aggressive, since it can excite electrons and so damage sensitive molecules. Furthermore, radiation of this high energy is converted into huge amounts of heat, which may cause severe damage, for example skin burns. The destructive force of UV light can also be sapplied for sterilizing food, since it also kills of germs, however, it has to be taken care that the food itself is not damaged by the process.

To determine the impact of UV light on the PIN, tubes filled with pollen water were stored in an UVA-oven for 30 min. Then the remaining IN* activity was measured. The results are listed in Tab. 19.

NO_2 is a common pollutant in the atmosphere, mainly due to combustion processes [Mohnen 1988] and agriculture [Hulpke et al. 1993]. In reaction with hydrocarbons it can either serve as an oxidant due to the high oxidation level of the nitrogen, or as an electrophilic subsitutent [Vollhardt and Schore 2003]. In the latter, one H atom in an aromatic ring is replaced by an NO_2 molecule. Since nitration of pollen allergenes increases their allergenic potential [Franze et al. 2005], it was of interest, if exposure to nitrous gases would also change the PIN activity.

Therefore, pollen were put into an impinger and suspended in as little water as possible. Then NO_2 from a gas cylinder was piped through the impinger for 60 min. The gas stream caused enough turbulences in the suspension to stir up pollen and expose them. Then the impinger was ventilated with technical air. The suspension was then diluted to the standard concentration of 50 mg/ml, filtrated and analyzed. The results are presented in Tab. 19. By pH indicator paper (pH range 2.5-5.5) it was determined that the pH of the filtrate was well below the lower range limit of pH=2.5. This means that the sample was acidified strongly due to the reaction shown in Eq. 7:

$$2\,NO_2 + H_2O \rightarrow HNO_2 + HNO_3$$

Eq. 7
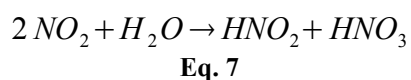
The reaction of nitric oxides and other acidic gases with water in the atmosphere is responsible for the decrease of the rain water pH, a phenomenon that is widely known as acid rain [Mohnen 1988]. Since this reaction disturbs the nitration process itself, the procedure was repeated with dry birch pollen grains that were exposed to NO_2.

Ozone is an essential component of our atmosphere [Hulpke et al. 1993], since it shields Earth's surface out high-energy solar radiation and triggers oxidation of hydrophobic atmospheric contaminants, which eventually leads to their wash-out. On the other hand, ozone levels close to the ground are increased due to anthropogenic emissions [Hulpke et al. 1993]. Atmospheric aerosols are exposed to the oxidative potential of ozone and suffer surface modifications, which might also affect the PIN.

Pollen were inserted into an impinger and suspended in little water. The impinger was attached to an ozone generator of the type OZ500 from Fischer Engineering GmbH. The generator, which was supplied by a stream of oxygen, was put into operation, and the leaving air stream was inserted into the impinger for 150 min. Then then impinger was ventilated with technical air. The suspension was then diluted to the standard concentration of 50 mg/ml, filtrated and analyzed. The results are put together in Tab. 19.

	Snomax	birch I	juniper I	pine	ragweed	corn
none	268	255	253	252	236	235
UV	253	255	245	247	239	--
NO_2	--	246	236	--	233	--
O_3	267	256	250	--	236	236

Tab. 19: Impact of environmental stresses on the IN* activity of pollen waters. The numbers are T_{50} [K].

The UV light treatment reduces the IN* activity of all samples except that of birch I. By comparison with the heat degeneration data in Fig. 59, the UV exposure resembles a heating to 400-425 K. The conclusion is that the UV light

is converted into heat and so causes thermal damage to the samples. Therefore, UV exposure is expected to decrease the IN* activity the more, the less heat stable the IN is.

The NO_2 treatment decreased the IN* activity by two effects which are in causal connection with the acidification: First, the freezing point depression, and second the chemical denaturation. Again, the birch PIN seems to be relatively stable. When comparing the T_{50} with those of the sulfuric acid treatment in Tab. 16, it resembles an exposure of at least 1 M acid. Comparison of the data with higher-concentrated H_2SO_4 are not sensible, since they were diluted after treatment, what alters the impact of Raoult's law. Furthermore, H_2SO_4 is a diprotic acid, while HNO_3 is a monoprotic acid. Of course, the mentioned acidification process severely adulterates the results in comparison to what a dry NO_2 exposure would show. However, since water is ambient in the atmosphere, this process is likely to occur there as well. Altogether, one can expect that the activity of PIN is reduced by the presence of acidic gases like NO_2, in the laboratory as well as in nature. The result of the dry nitration was a T_{50} of 235 K, which is surprisingly even lower than for the wet nitration. This could mean that nitration is more harmful for the PIN than acidification. Alternatively, it might be that the PIN were not as releasable any more after NO_2-induced sample modification. It was noticed that the pollen were agglomerated far stronger after the treatment.

The ozone treatment led to no change in IN* activity. However, conditions in the atmosphere might be different, where ozone molecules are activated due to ultraviolet radiation. The high oxidative potential of the atmosphere is in fact caused by hydroxyl radicals, which are generated by photo-induced chemical reactions between ozone and water [Thompson 1992, Hulpke et al. 1993]. Since these radicals could not be generated with this setup, oxidative stress in the atmosphere is expected to be stronger than under laboratory conditions.

3.5. Vibrational spectroscopy

Chemical bonds between atoms can be modeled as springs. The strength of these springs corresponds to the electron configuration of the bonding. As a consequence, distances and angles in a molecule behave like an oscillator. Since the laws of quantum mechanics are decisive on the molecular level, only defined levels of vibration energy are allowed for the springs. By uptake or release of energy the system can skip between the different vibration states, respectively energy levels. This can be realized by interaction with photons, which are absorbed, emitted or scattered in the process. Depending on the kind of interaction process, each of which corresponding mathematically to a certain multipole momentum, selection rules decide, transitions between which levels are allowed. As a result, functional chemical groups show a certain energy level scheme. The energy differences in vibration states of molecular bonds match the energy content of infrared photons. Therefore, the system can take up or emit amounts of energy in this order of mangitude.

In infrared (IR) spectroscopy, a sample is exposed to a white spectrum of infrared light. Since the functional groups in the sample absorb photons of certain energies, the light intensities at the corresponding frequencies decrease, while the intensities at other frequencies are transmitted or reflected. The ratio of the light after and before interaction with the sample is plotted versus the frequency ν, respectively the wavenumber $k[\text{cm}^{-1}]$. The relations are demonstrated in Eq. 8:

$$k = \frac{\nu}{c} = \frac{\Delta E}{h \cdot c}$$

Eq. 8

with ν as the photon frequency, c as the vacuum light speed constant, h as the Planck constant and ΔE as the energy difference between two vibration levels of an oscillator. Overall, a certain absorption band in the spectrum corresponds to a certain functional group in the sample.

Alternatively, in Raman spectroscopy, the sample is exposed to a light beam of photons with an energy far beyond the energy differences between the sample's oscillator energy levels. Depending on the scientific question, lasers of near-infrared (NIR), visible (VIS) or ultraviolet (UV) light are applicable. Some of the laser photons are scattered on the sample, which are then detected. Since the probability of a process decreases with an increasing number of photons participating in an elementary process (see Tab. 20), the scattering intensity is far weaker than absorption. While principally every photon can be scattered, only photons with an energy matching the energy differences in the oscillator can be absorbed. Therefore, beyond the absorption ranges, scattering is the dominant interaction between oscillators and photons. Besides the dominant process of elastic scattering, where neither the photons, nor the oscillators change their energy, inelastic scattering occurs: Here the oscillators are excited to a higher (or relaxed to a lower) level during the scattering process. The energy difference is compensated by the scattered photons, which then have a lower (or higher) frequency than before the process. The difference between the frequency of the elastically and the inelastically scattered light is then translated into oscillator energy differences and to theoretical IR absorption wavenumbers. This way, the spectra of IR and Raman spectroscopy are converted into the same units and can be directly compared.

An overview over the features of these two methods is given in Tab. 20:

spectroscopy	number of photons	momentum	physical magnitude	physical process	selection rules: Δn
Infrared	1	dipole	polarity	absorption (emission)	±1
Raman	2	quadrupole	polarizability	inelastic scattering	±2

Tab. 20: Overview over the characteristics of the most common oscillator-photon-interaction processes.

To determine, if the IN of pollen can be correlated with the integral chemical surface composition, Raman spectra of pollen grains and waters were measured and compared. Full pollen grains have already been investigated before [Ivleva

et al. 2005, Schulte et al. 2008, Schulte et al. 2009, Schulte et al. 2010], however, no work on the aqueous extracts has been carried out before. In vibrational spectroscopy, different chemical substance classes show characteristic absorption bands. The most dominant signals in the spectra of both former research groups were interpreted in two different ways: They were either assigned to the sporopollenin [Ivleva et al. 2005], or to carotenoids [Schulte et al. 2008]. Therefore, they were named "S+C", short for "sporopollenin and carotenoids", in this thesis.

Carotenoids, which are present in the pollen exine, are hydrocarbons with about 40 carbon atoms and many conjugated double bonds. As a consequence, their electronic absorption bands shift into the range of blue light, what makes them appear red, orange or yellow. Due the structural similarity and the concurrence of vibrational spectroscopic bands, it seems likely that sporopollenin is a product of carotenoid polymerization. However, it was discovered that sporopollenin is not generated the proposed way [Prahl et al. 1986]. It is most likely synthesized mainly from phenols and fatty acids, and is therefore similar to other sturdy plant biopolymers, like lignin, cutin and suberin [Scott 1994].

Six species were investigated in this study, namely *Pinus sylvestris*, *Corylus avellana*, *Ambrosia artemisiifolia*, *Zea mays*, *Betula pendula* and *Betula occidentalis*. For preparation of grain spectra, pollen were suspended in very little water and spread on a glass slide. Pollen waters for the spectra were prepared as described in chapter 2.2. and dripped onto a glass slide. After that the water was evaporated in an air stream. The residues formed an amorphic, glue-like layer on the slides.

The sample slides were inserted into an inVia Reflex Raman spectroscope (RENISHAW) of 250 mm focal length, which is connected to a free-space-microsocpe of the type Olympus BXFM. The sample is excited by the beam of a laser diode (RENISHAW) with a wavelength of 785 nm. The application of an

NIR laser is advantageous to minimize the disturbance of background fluorescence [Ivleva et al. 2005].

A holographic grating of 1200 grooves per millimeter and a Peltier-cooled front-illuminated CCD detector (576×400 pixels) enables a spectral resolution of 2.5 cm^{-1}. Calibration was against the line of a silicon wafer at 520.4 cm^{-1}. Spectra were gathered by accumulation of 4-5 single measurements in the range from 200 to 4000 cm^{-1}. After baseline correction, in order to eliminate the background fluorescence, which covered most of the spectrum, the spectra were rescaled for a convenient comparison with each other. All measured Raman spectra are shown in Fig. 63. The ranges from 1700 to 2800 cm^{-1} and above 3100 cm^{-1} were cut out, since they contained no signals. Band assignments were adopted from literature [Ivleva et al. 2005, Schulte et al. 2008].

Raman spectra with exception of those from pine pollen showed a high fluorescence background, which exceeded the intensity of the Raman bands themselves, and had to be substracted therefore. Alternatively, photo-bleaching with ultraviolet or visible light could be performed [Ivleva et al. 2005], however, since the sample is adulterated in the process, it was avoided.

species	grain color	water color
pine	pale yellow	none
hazel	bright yellow	yellow
ragweed	pale yellow	yellow
corn	dark yellow	opaque white
birch I	bright yellow	nearly none
birch II	bright yellow	nearly none

Tab. 21: colors of pollen grains and waters.

The signal that dominated each grain spectrum was the S+C-peak at 1603 cm^{-1}. In the pollen waters, however, these peaks were significantly reduced or even eliminated. The only spectra which still showed a signal were those of hazel and ragweed. If we compare with the color data in Tab. 21, these pollen waters were the only ones showing an impressive yellow color. A sporopollenin is a robust

hydrophobic biopolymer, it is unlikely that the S+C bands and the color of the pollen waters can be asssignet to it. It is most likely that these effects are caused by the low-molecular carotenoids alone, while the relative increase in the grain spectra can be assigned to the sporopollenin. The lack of the S+C band at 1600 cm^{-1} in the pollen waters of the other four species suggests either that carotenoid concentrations are significantly lower in these species, or that they are tighter incorporated into the sporopollenin, and so non-extractable.

In contrast to the S+C-peaks, the bands originating from typical pollen nutrients, like saccharides, lipids and proteins, did not diminish in the pollen water spectra. It shows demonstratively that these compounds can be extracted from the pollen grains in reasonable amounts. Furthermore, these are the potential candidates for being the sought-after PIN molecules. The huge complexity of the mixture, however, makes it impossible to pick out the PIN by Raman spectroscopy alone. Nevertheless, the spectral data further affirmate that the IN* activity of pollen is caused by certain PIN molecules, which are most likely nutrients.

The spectra of water birch and silver birch are very much alike, which is explicable by their close relatedness. The spectra of pine pollen differ from the others in several ways (see Fig. 63). First, the bands are sharper than in the other spectra, which points at a higher level of structural order. Since the bandwith in Raman spectra of solids is determined by the vibration anharmonicity, the peak broadenings in the other samples might be caused by a lower degree of structural order. Another feature is the absence of the carbonyl band at 1650 cm^{-1}, but instead the presence of

Fig. 62: Cinnamic acid

two bands at 1630 cm^{-1} and 1690 cm^{-1} . The signal at 1630 cm^{-1} could be explained by the presence of coumaric acid [Cunha et al. 2012], which is a hydroxy-derivative of cinnamic acid (see Fig. 62). The lack of the band at 1650 cm^{-1} was surprising, since it was assigned to the amides of the protein backbone [Ivleva et al. 2005, Schulte et al. 2008]. Since proteins are ubiquitous on the
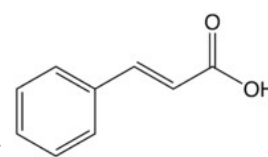
pollen surface, this band might be interpreted another way: Possibly, it originates from another hydroxycinnamate that is not coumaric acid.

A further approach to characterize pollen grains and waters was the gathering of infrared spectra, which is complementary to Raman spectroscopy. This kind of technique was already applied on whole pollen grains, mainly in order to discriminate between species via their characteristic signal pattern [Dominguez et al. 1999, Pappas et al. 2003, Dell'Anna et al. 2009, Zimmermann 2010].

Here, five species were investigated, namely *Pinus sylvestris*, *Corylus avellana*, *Ambrosia artemisiifolia*, *Zea mays* and *Betula pendula*. These are the same species as were investigated by Raman spectroscopy (see chapter 3.5.), with exception of *Betula occidentalis*.

Pollen grains were placed on a Spectra Tech micro compression diamond cell from Thermo Scientific and analyzed using a confocal Hyperion 3000 IR microscope LH2MCT, which was attached to a Tensor FTIR spectrometer with a single point liquid nitrogen cooled MCT detector from Bruker Optics. Spectra were gathered by accumulation of 32 scans per sample, in the transmission mode with a 15× augmentation objective and 4 cm^{-1} resolution. For the generation of a pollen water spectrum, 50 µl of it were pipetted onto a 2 mm thick CaF_2 window and left to dry up. Then a 150×150 µm rectangular section of the sample was measured in transmission using the same technical parameters as for the pollen grain spectra.

Each sample was measured in the range from 600 to 4000 cm^{-1}. Six measurement cycles as described above were performed per sample to test the reproducibility. Results are shown in Fig. 64. Regions without any significant informations, more precisely below 800 cm^{-1}, above 3800 cm^{-1} and from 1800 to 2600 cm^{-1}, were cut out.
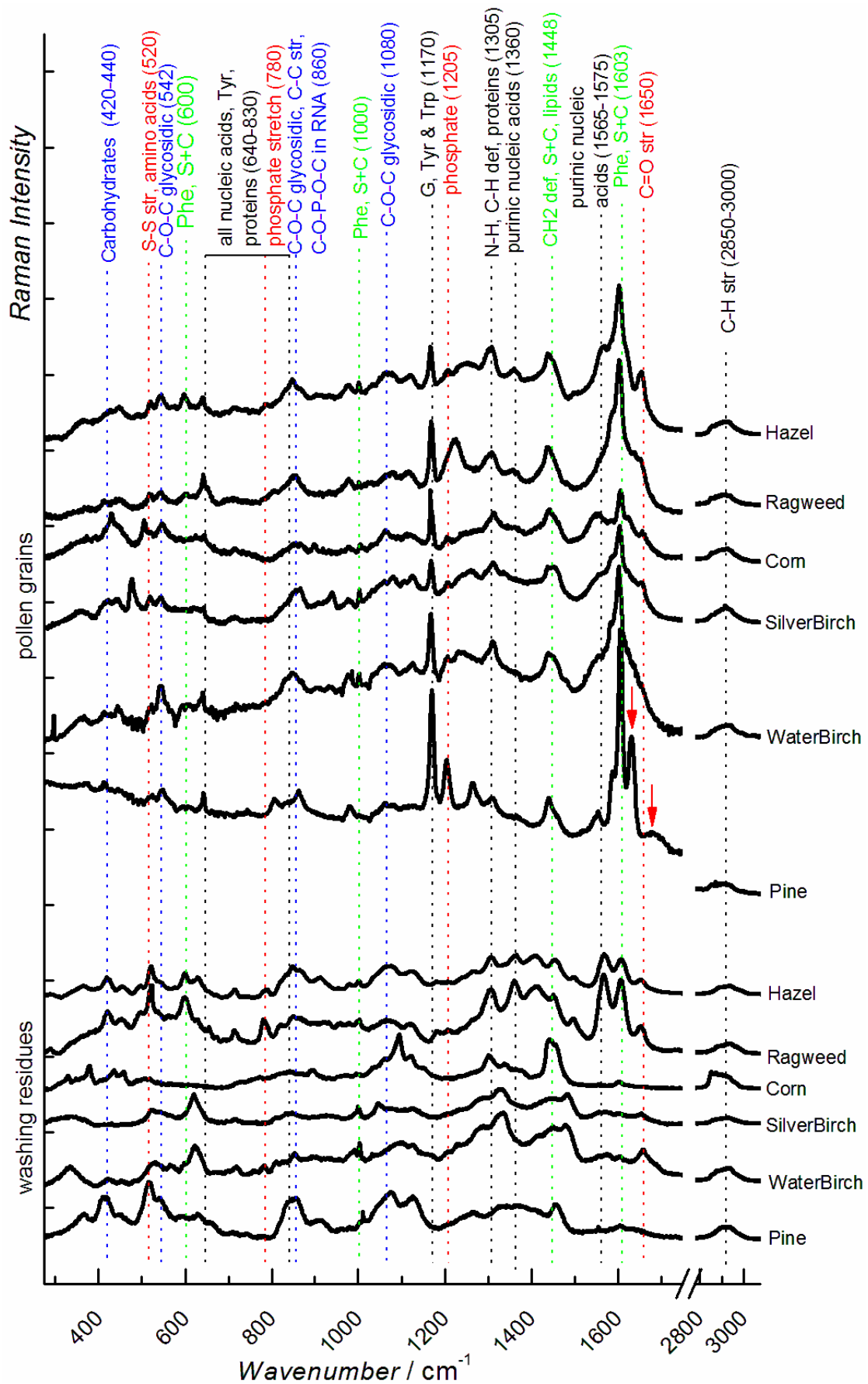
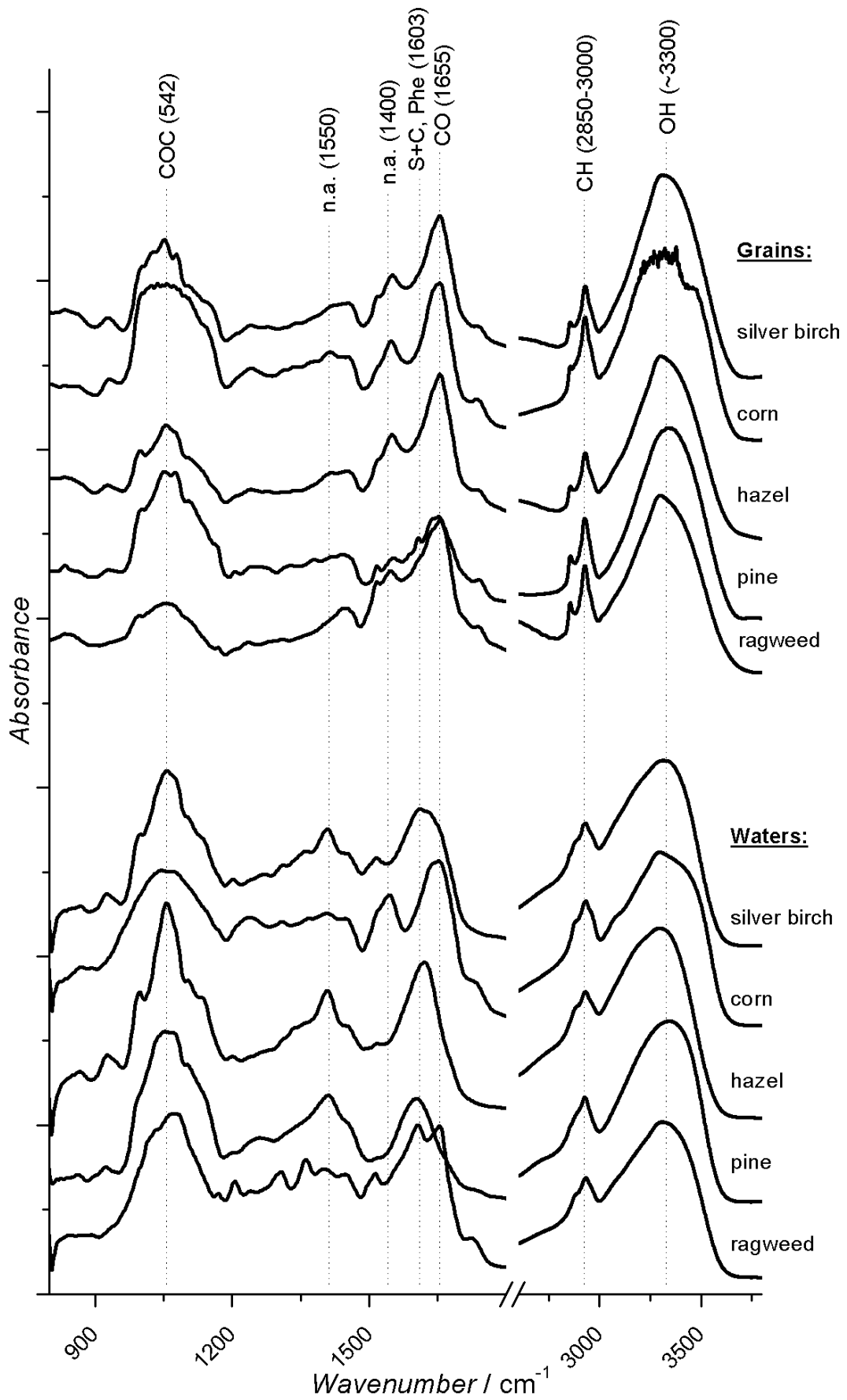**Fig. 63: Raman spectra of investigated pollen species.**

Fig. 64: IR spectra of investigated pollen species.

Sine the selection rules for IR absorption differ from those for Raman scattering [Atkins 2001], the IR spectra show other characteristic bands. For example, the dominant signal in each spectrum is the broad hydroxyl stretching band with its maximum at about 3300 cm^{-1}, which does not appear in the Raman spectra at all (see Fig. 63). The signal originates from functional OH groups in the sample, e.g. sugars, alcohols and organic acids. Furthermore, the bands in the IR spectrum are generally broader, what leads to overlapping of signals. Therefore, detailed interpretation as in the Raman spectra is not possible. For example, the S+C-peak at 1603 cm^{-1} overlaps with the carbonyl peak at 1655 cm^{-1}.

3.6. Solid phase extraction

Further investigation of the PIN was carried out in cooperation with the Helmholtz Institute of Munich. Therefore, the pollen water was fractionated with different types of commercially available solid phase extraction (SPE) tubes. On the one hand, the obtained fractions were tested for their IN* activity, and on the other investigated with mass spectrometry to determine their chemical composition. Therefore, pollen water of *Betula alba* was applied, since it contains the highest amount of PIN.

All chemicals used for this procedure were of ultrapure grade. The pH of pollen water was adjusted to pH=2 with hydrochloric acid. Two SPE tubes of a kind were conditioned with 1 ml methanol, 5 ml MilliQ water and 1 ml pH=2 hydrochloric acid, then 1 ml sample was inserted. After that the column was washed with 1 ml pH=2 hydrochloric acid and 2 ml MilliQ water. Then the sample was eluted with methanol-water, starting with 0.5 ml 10 vol.% methanol and increasing it for further 10 vol.% each step of 0.5 ml, until 100 vol.%. So the total elution volume is 5 ml. The different fractions are collected separately and united with the same fraction of the second column. Then the methanol is evaporated, and every fraction is diluted with MilliQ water to a total volume of

1.5 ml. Differences between the fractions were visible even with the naked eye, since the material residues before dilution varied in amount and color.

Five different types of Varian Bond Elut (Agilent) SPE columns were applied. These are plastic tubes packed with porous packing material which was functionalized to achieve certain retention behavior[i]. Details of the five different types of applied tubes are given below:

- C2: very non-polar, silica-based, $-O-Si(CH_3)_2(nC_2H_5)$
- C18: non-polar, silica-based, $-O-Si(CH_3)_2(nC_{18}H_{37})$
- CNE: rather non-polar, silica-based, $-O-Si(CH_3)_2(nC_3H_6CN)$
- PH: very non-polar, silica-based, $-O-Si(CH_3)_2(Ph)$
- PPL: very polar, polymer (styrene-divinylbenzene)

A full set of eluted fractions with each column was prepared and investigated by cryo-microscopy (see chapter 2.2.). To check the reproducibility, extractions with the CNE and the PPL column were carried out independently at Helmholtz Institute of Munich, delivered to Vienna and further investigated. The determined median freezing temperatures of all fractions are shown in Tab. 22 (preparation in Vienna) and Tab. 23 (preparation in Munich). As the total amount of extracted material delivered from Munich was significantly lower than that available from Vienna, the concentration in the oil emulsion were also lower. The consequences are evident in terms of the lower T_{50} in Tab. 23. The high material amount in the Vienna samples obviously overloaded the columns. Since extraction is based on a finite non-zero distribution ratio between two phases, IN can also spread into a phase, where their residence probability is low, if total IN concentrations are high enough. Because of this, most fractions showed critically higher IN* activity than homogeneous freezing would. As the fractions with the highest T_{50} contained the highest amount of IN, these were of interest.

In comparison, the IN concentration in the fractions from Munich was very low, which was advantageous in this case: Since there was no overloading of the

---

[i]   http://de.scribs.com/doc/39863374/92/Bond-Elut%C2%AE-PPL

column, the lower number of IN was focused in one fraction per elution row. All other fractions showed significantly lower T_{50}. In most cases, T_{50} is in the range of homogeneous freezing.

% MeOH	C2 [K]	C18 [K]	CNE [K]	PH [K]	PPL [K]
10	252	251	251	245	252
20	255	253	250	250	248
30	245	253	251	246	251
40	242	246	245	241	251
50	252	234	246	252	254
60	252	247	245	252	247
70	245	251	243	250	244
80	250	235	236	249	241
90	238	232	234	245	231
100	242	<225	245	234	237

Tab. 22: Median freezing temperatures of different elutes in Kelvin. Sample preparation in Vienna. The most active fractions (252-255 K) are marked in red.

% MeOH	C2	C18	CNE	PH	PPL
10	--	--	242	--	238
20	--	--	238	--	236
30	--	--	238	--	237
40	--	--	237	--	239
50	--	--	237	--	248
60	--	--	237	--	237
70	--	--	237	--	242
80	--	--	236	--	234
90	--	--	237	--	237
100	--	--	236	--	238

Tab. 23: Median freezing temperatures of different elutes in Kelvin. Sample preparation in Munich. The relatively most active fraction of both columns is marked in red.

In both cases, the 50%-MeOH fraction is the most active one from the PPL column. The highest T_{50} of the CNE-elutes is reached by the 10%-MeOH-fraction. Since it is significantly lower than the maximum T_{50} for the other four columns, it seems likely that the PIN are hardly retained by the CNE-tube at all.

The presence of two T_{50} maxima among the C2 fractions cannot be explained by the current state of knowledge. A speculative explanation might be the presence of two different types of PIN present on the birch pollen, as it was suggested from the LACIS data [Augustin et al. 2012]. Another explanation might be the generation of fragments, which still show IN* activity, but differ in some other properties, what changes their retention behavior in the SPE columns.

The most active fractions in Tab. 23 were further investigated with high-resolution electrospray fourier transformation mass spectrometry (ESI-FT-MS) and compared to measurements of IN* negative fractions, as well as to corn pollen water. Spectra were gathered in the positive and the negative ion mode. Those compounds unique for the active fractions were interpreted via MassTRIX data filtering and Netcalc calculation, plotted in van Krevelen and Kendrick Plots, and finally assigned to certain chemical compounds (see Fig. 65 to 68). Since the currently used device has an upper mass limit of 900 Da, only the low-molecular compounds could be investigated. In future research, the macromolecular mass range, where the IN are located (see chapter 3.2.) has to be covered, but the data still demonstrate that ESI-FT-MS allows to generate a characteristic molecular fingerprint of a sample, in this case birch pollen water. Furthermore, the elementary constitution of the macromolecules, which consist of smaller building blocks (see chapter 1.4.) is expected to be similar to those in the low-molecular mass range that was investigated in this study.

In a van Krevelen plot, the ratio of hydrogen to carbon atoms in a detected fragment is plotted against the ratio of oxygen to carbon atoms. The position in the diagram gives information about the chemical nature of the fragment, but since the information is not unambiguous, more information is necessary for assignment. For example, both ethanol and dimethyl ether have the sum formula C_2H_6O. Therefore, their H/C-ratio is 3.0, and their O/C-ratio is 0.5. The

advantage of such a plot is that higher homologues of one type of chemical species, which show similar chemical properties, appear as one signal. For example, all monosaccharides have the formula $C_nH_{2n}O_n$ and so, independent of n, the same H/C- and O/C-ratio.

For a Kendrick Plot, a chemical group has to be assigned as a reference, in this case CH_2. The real mass, 14.01565 Da, is rounded to an integer value, which is defined as Kendrick Mass (KM), here 14 KM. The mass of any detected ion in Dalton is then multiplied with the ratio of the masses of the reference group in Nominal Kendrick Mass and Dalton (see Eq. 9).

$$ion\,mass\,[KM] = ion\,mass\,[Da] \cdot \frac{ref.\,mass\,[KM]}{ref.\,mass\,[Da]} = ion\,mass\,[Da] \cdot \frac{14.00000}{14.01565}$$
Eq. 9

The mass calculated by Eq. 9 is then rounded to integer values, the nominal mass (NM). The difference, the Kendrick Mass Defect (KMD), is characteristic for a series of homologues of the reference group. The KMD (see Eq. 10) is then plotted versus NM in the Kendrick Plot.

$$KMD = KM - NM$$
Eq. 10

For example, the extension of an alkyl chain by a CH_2 unit does not change the KMD, while the insertion of a nitrogen atom, which has the same nominal, but a different real mass (14.00670 Da), causes a change. Therefore, all homologues of a series lie on a horizontal line in the plot with constant distances. The combination of a Kendrick Plot and a Van Krevelen Plot allows in many cases the identification of a fragment's chemical constitution.

The plots in Fig. 65 to 68 show that the fraction still contains a mixture of a broad spectrum of different compounds. Most of them consist of the elements carbon, hydrogen, oxygen and nitrogen (CHON), or of these elements plus sulfur (CHONS). Some contain neither nitrogen, nor sulfur (CHO). If the suggested hypothesis that PIN are saccharides, they have to be CHO (sugars) or

CHON (aminosugars). The CHON and CHONS signals might also originate from proteinaceous compound fragments.
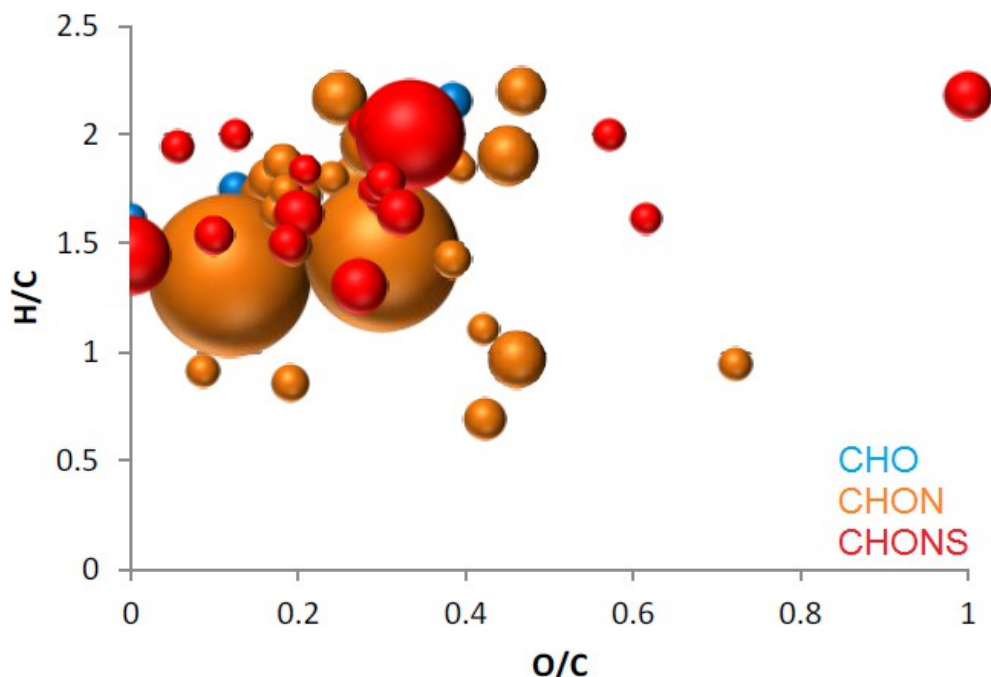
Fig. 65: Van Krevelen Plot of the positive ions. The size of the balls correlates with the signal intensity in the MS, and so with the concentration.
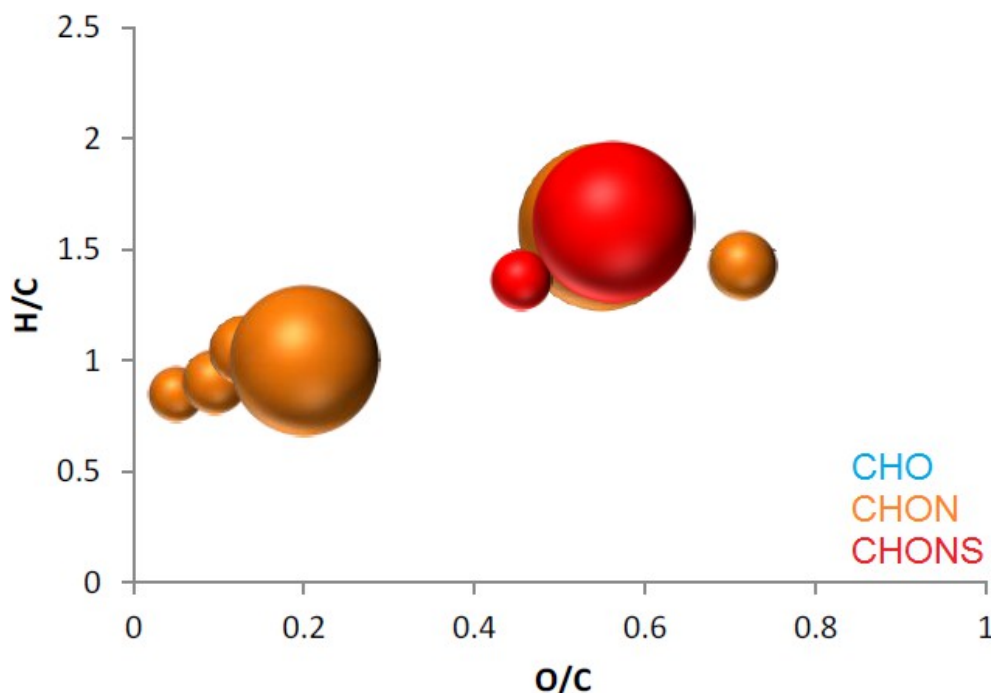
Fig. 66: Van Krevelen Plot of the negative ions. The size of the balls correlates with the signal intensity in the MS, and so with the concentration.

The suggested method opens new pathways of analysis. Although extraction with one of the columns still leads to a mixture of possible candidates for being the PIN, a serial extraction of one pollen water with different columns (orthogonal fractioning) plus analyzation with MS might enable identification of

the birch PIN. On the one hand, the application of more extraction steps is expected to confine the number of compounds in the pollen water, but increase the total material loss, which multiplies with each extraction step.
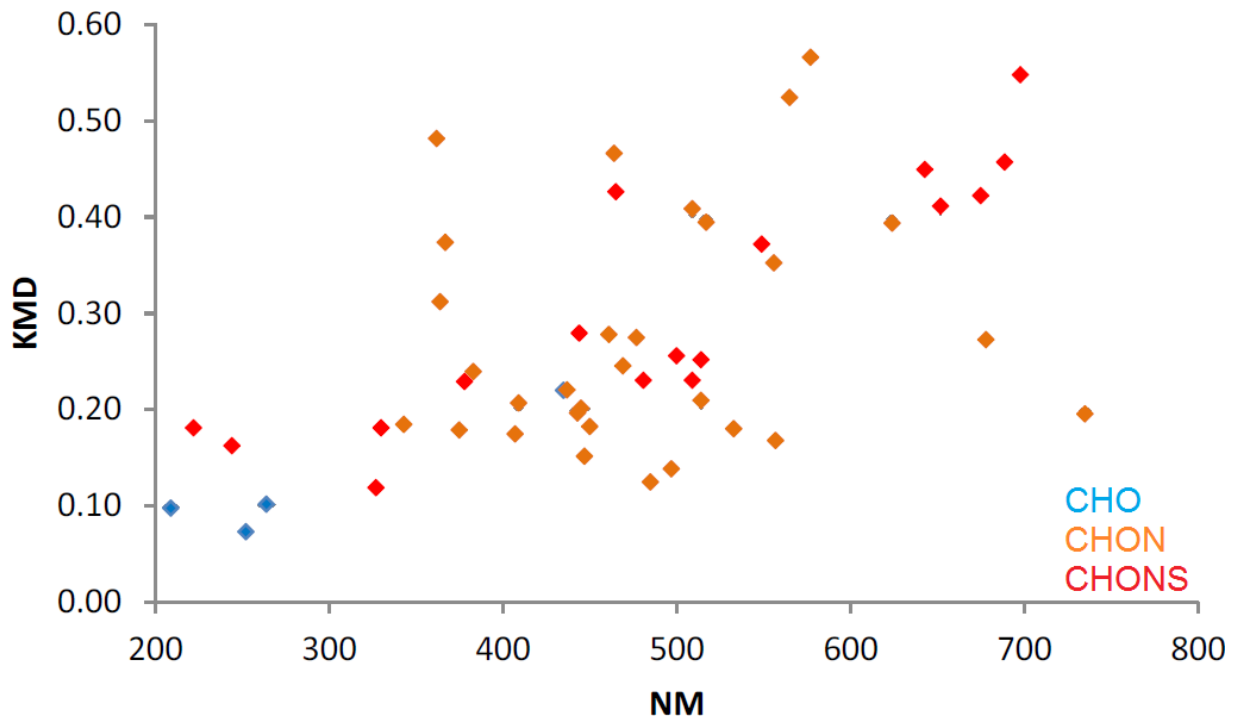
Fig. 67: Kendrick Plot of the positive ions.
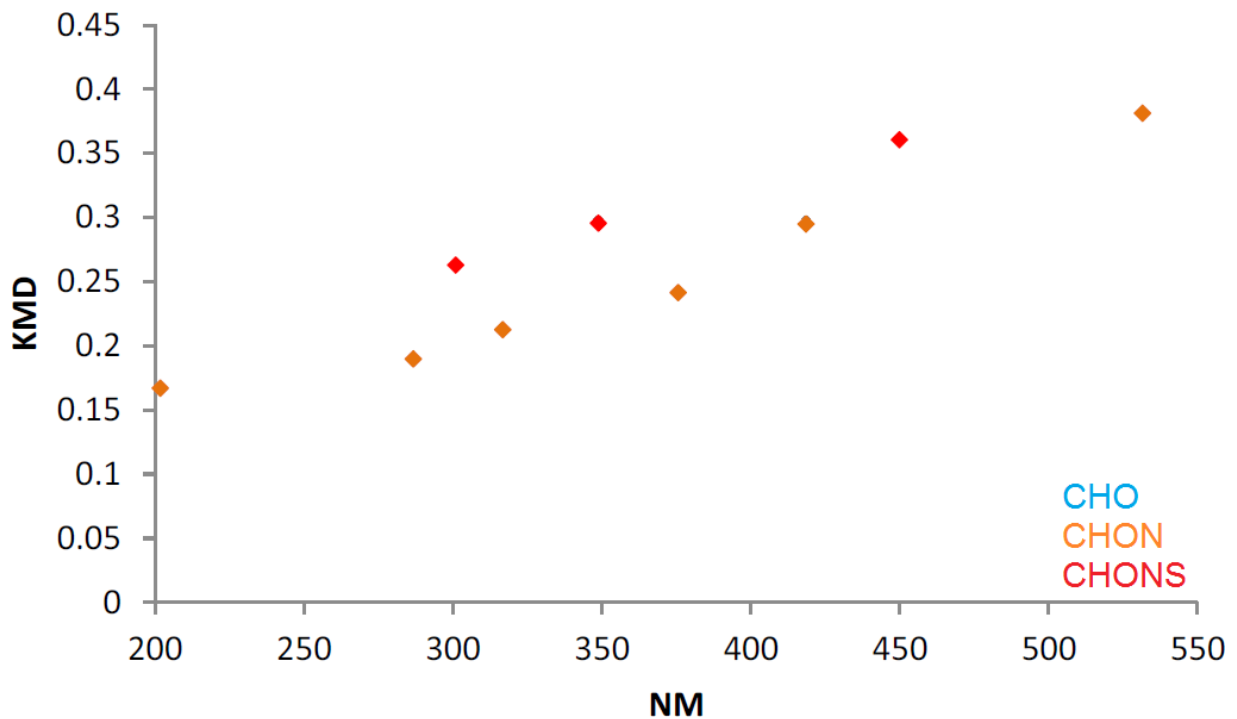
Fig. 68: Kendrick Plot of the negative ions.

4. Fungal ice nuclei expression

4.1. Cultivation conditions

Since IN* activity is interpreted as a cryoadaptive mechanism, the impact of freezing was also of interest. Therefore, a set of different strains of *Fusarium* and *Trichoderma* species was selected for cultivation (see Tab. 24).

The *Fusarium* species were acquired from BOKU. Genetic sequencing showed that the cultures with serial numbers beginning with "Fx" were not *F. avenaceum*, but other *Fusarium* species, which could not be assigned distinctly. According to the available data, they are strains of *F. oxysporum*, *equiseti* or another close relative. The *Trichoderma* strains were sampled at four sites belonging to different climate zones to check them for a possible impact of temperature and other climate parameters on the IN* activity.

Of every chosen sample, four plates of PDA were inoculated and grown. While two of these plates were cultivated exactly the same as described in chapter 2.1., the other two were exposed to subzero temperatures several times over night to induce freezing stress. Then two plates per species – one with, one without freezing events – were harvested as described in chapter 2.1..The gathered spores were then measured in the oil immersion mode as described in chapter 2.2.. Results are presented in Tab. 24. The strain Ta-0626 is the same strain as *T. atroviride* in chapter 2.2..

Surprisingly, the occasional freezing did not alter the IN* ability of the fungal species. An explanation could be that cold temperatures alone are not sufficient to boost IN expression. It is possible that either other stresses, like starvation or other microbial competitors, or only a combination of several disadvantageous conditions, with freezing as just one of them, leads to an increase in IN* activity [Rogers et al. 1987, Nemecek-Marshall et al. 1993, Gurian-Sherman and Lindow 1995, Fall and Fall 1998]. This would make perfect sense, since the main

purpose of IN expression in fungi is believed to be the release of nutrients from host plants, which is especially necessary when nutrients are scarce. A typical agar medium, on the other hand, is designed to make nutrients easily available for the culture. Therefore, cultivation on a nutrient-poor agar might be necessary to boost IN* activity.

sample	BOKU code	species	origin	T_{50}	T_{50}*
Fa-4237	none	*F. avenaceum*	Austria	237	238
Fx-4686	MA1255	*F.* sp.	unknown (rye)	238	237
Fx-4682	MA1255	*F.* sp.	unknown (rye)	237	237
Fx-4683	MA2594	*F.* sp.	Austria (soil)	235	--
Fx-4684	MA1275	*F.* sp.	England (dianthus)	236	--
Fx-4685	MA1220	*F.* sp.	Austria (rhizoplane)	235	--
Ta-0626	none	*T. atroviride*	Ethiopia	239	237
Tl-1301	none	*T. longibrachiatum*	Antarctica	240	238
Ta-3001	none	*T. atroviride*	marine	240	239
Ta-1680	none	*T. atroviride*	Slovenia	238	238

Tab. 24: Classification and IN* activity of different fungal samples. T_{50} marks the median freezing temperatures of samples without, T_{50}* those with freezing events during cultivation.

4.2. Bradford measurements

Since the FINP are proteinaceous [Kieft and Ruscetti 1990, Pouleur et al. 1992, Tsumuki and Konno 1994], it was of interest, if the freezing stress leads to some overall impact on protein expression in the fungi. A common biochemical method to quantify the total protein content, is the Bradford assay [Bradford 1976], which is a colorimetric method: The dye Coomassie Brilliant Blue (see Fig. 69[i]) is an organic compound with a
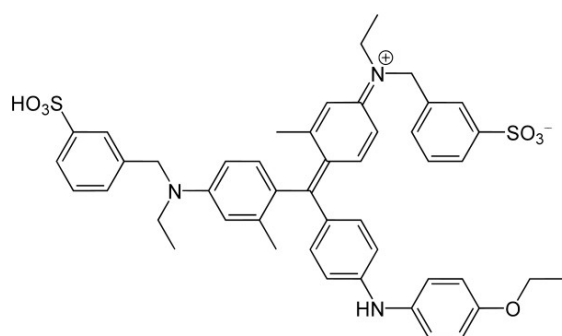
Fig. 69: Chemical formula of Coomassie Brilliant Blue G-250.

large delocalized π-electron network which absorbs visible light. The sulfonate anion has its absorption maximum at 595 nm, what leads to an intense blue

---

[i]   http://en.wikipedia.org/wiki/Coomassie_Brilliant_Blue

color. When the dye molecule binds to a protein, the anion is stabilized, while in free aqueous solution there is an equilibrium with the protonized form that shows maximum absorption at 470 nm. Therefore, a solvent of unbound dye is brown. The intensity of the blue color, which is quantified via the absorption at 595 nm in a photometer, is a measure for the total protein amount in the sample. Since the assay is very sensitive towards the system parameters, calibration with standard protein dilutions is essential.

Most of the fungal species in Tab. 24 (with exception of Fx-4683, Fx-4684 and Fx-4685) were cultivated as described in chapter 4.1.. The two plates that were not applied for IN* measurements (one with, one without freezing events) were harvested analogously, but with water as a solvent instead of ethanol. The spores were then left in suspension.

fungal culture	E [ ], freezing events	
	no	yes
blank	0.217±0.006	
Fa-4237	0.526±0.002	0.479±0.006
Fa-4686	0.481±0.002	0.429±0.004
Fa-4682	0.493±0.005	0.446±0.004
Ta-0626	0.405±0.012	0.400±0.015
Tl-1301	0.370±0.002	0.424±0.003
Ta-3001	0.373±0.002	0.395±0.003
Ta-1680	0.410±0.005	0.405±0.007

Tab. 25: Extinction data E of the Bradford measurements.

To guarantee the same spore concentration in every sample, spore suspensions were diluted accordingly via measurement of the light transmission. A vial of pure water (70% transmission) was provided, and spores suspensions were slowly added, until the transmission dropped to 36-38%. Then 1 ml of the suspension was mixed with 0.5 ml of Bradford solution, which was prepared by diluting commercially available Bradford solution to the five times of its volume. For each sample and the blank three vials were prepared and measured.

We measured the absorbance at 565 nm to quantify the total protein content. The extinction data are presented in Tab. 25, and the calculated concentrations in Tab. 26.

From these data, a total protein amount was determined: After fitting a linear regression curve through the standard data, the protein content was calculated back from the absorption data. After subtraction of the background signal, the protein concentration was calculated by insertion into the formula for the regression curve:

$$616.4 \cdot (E - E_0) - 17 = C$$

E is the extinction from Tab. 25, E_0 the extinction of the blank and C the total protein concentration in µg/ml. Results are shown in Tab. 26.

fungal culture	C [µg/ml], freezing events	
	no	yes
blank	6±2	
Fa-4237	173±1	144±2
Fa-4686	145±1	113±1
Fa-4682	153±2	124±1
Ta-0626	99±4	96±5
Tl-1301	77±1	110±1
Ta-3001	79±1	93±1
Ta-1680	102±2	99±2

Tab. 26: Total protein content of the suspensions in µg/ml.

Tab. 26 demonstrates that the total protein expression in the *Fusarium* strains was significantly decreased by the occurrence of freezing events, while it remained unaltered for *Trichoderma atroviride*. The Antarctic *Trichoderma longibrachiatum* even showed a considerable increase in total protein content as a response to freezing. This finding could be indeed related to a cryoadaptation of this strain which has to dwell in a very cold environment. Fig. 70 shows the total protein content C versus T_{50}. Although the data seem to show a slight tendency, it has to be considered that the scaling of the y-axis is very narrow.

Since in Tab. 24 no impact of freezing on the IN* activity could be seen, the expression of the FINP does not correlate with the total protein expression.
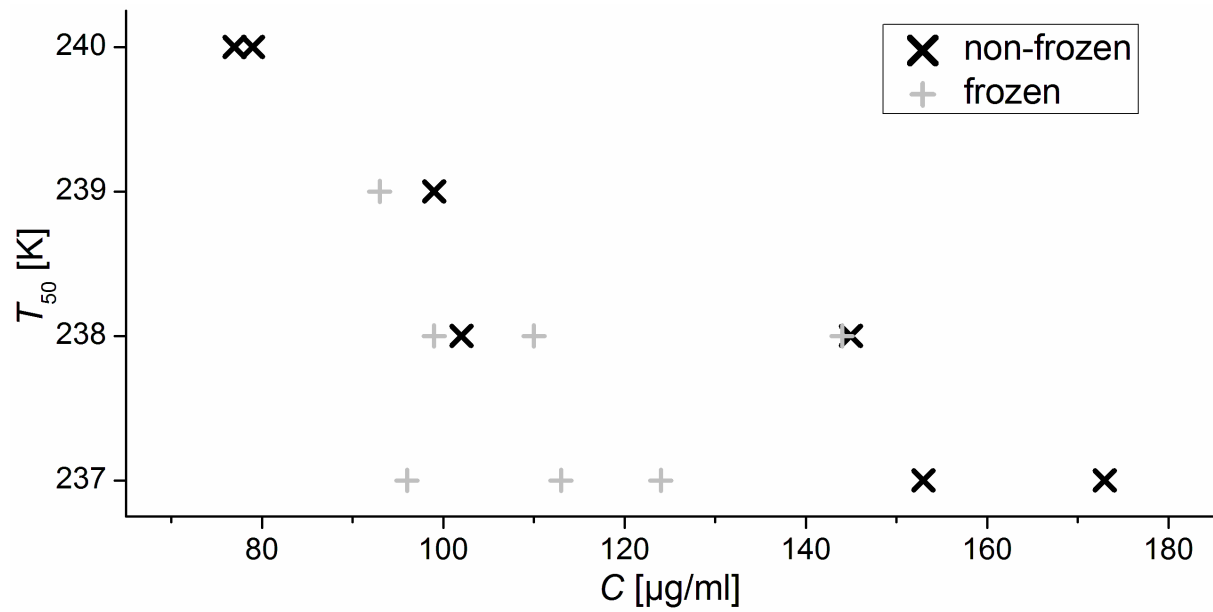
Fig. 70: The correlation between median freezing temperature and total protein content *C*. Note that the y-axis shows a very narrow range, so the differences on this axis are in fact negligible.

5. Discussion and Conclusions

5.1. Evaluation of results

The cryo-microscopic setup as described in chapter 2.2. shows some immense advantages, which make it a very attractive method of determining IN* activity:

- The setup is cheaper and more compact than others. The demands on the infrastructure are very low, so the system can be easily installed.

- It can conveniently be operated by one person. Furthermore, the handling of the equipment is very intuitive. Once the standards of proceedings are optimized, they can be easily passed on – also to inexperienced staff.

- Both the launching of the setup and the measurements themselves are quicker than for most other existing setups.

- The isolation of the droplets from each other suppresses secondary ice nucleation effects.

- The sample consumption is far lower, since only 1-2 ml of aqueous suspension are necessary for sample preparation. In other setups, 50-200 ml of suspension have to be invested. This can be the limiting factor, if precious samples, like difficultly cultivable fungal species, are of interest.

On the other hand, the method is or might be afflicted with some drawbacks, which are discussed below:

- The oil embedding the droplets is suspected to change the surface tension of the droplets and so IN* activity. However, the reference measurements with airborne droplets (see chapters 2.4. and 2.5.) showed comaptible results. Furthermore, the reference data of Snomax and pure water were in good agreement with literature date. As a whole, the thermodynamic effect of the oil fraction seems to be negligible.

- The sample is distributed between the two non-miscible phases. This way, IN* active material is lost to the oil phase. Since the distribution

126

coefficient varies between substances, respectively samples, the exact IN concentration is afflicted with an uncertainity.

- The variation in droplet size, ergo material-content per droplet, leads to a broadening of the nucleation spectrum.

- The sample handling itself, as well as the application of various reagents (e.g. the oil), is a potential source of contamination and therefore adulteration of results. Therefore, cleanliness is important. On the other hand, keeping the setup clean is far easier than in the more bulky other setups.

- The setup does not allow the measurement in the deposition or the condensation mode, since the droplets are present from the beginning.

- Due to the embedding of the droplets in the oil, impacts of air humidity and pressure on IN* cannot be investigated.

Since the pollen were sampled in nature, the question arises, if their IN* activity is merely caused by contamination. If we consider birch PIN, this hypothesis can be ruled out:

- The reference mineral dust at a concentration of 20 mg/ml nucleate at 250-252 K, while birch pollen water with the same content nucleates at 255 K. It is impossible that traces of mineral dust in an IN* negative sample cause a far higher IN* activity than the pure mineral dust.

- If the pollen were contaminated by IN* active bacteria, they would nucleate at far higher temperatures. If the bacterial contamination was low, it would rather strongly decrease the ice-active fraction rather than shift temperatures that dramatically. However, the steep slope of the birch nucleation spectrum suggests a high IN number, what was confirmed in chapter 3.1..

- Snomax, which is a bacterial ice nucleus, behaved differently from the birch PIN in the assays. Even, if we regard the enzymatic measurements

as disputable, and suggest that the PIN is in fact a fragment of a BINP, the heat and the guanidinium chloride treatment contradict this hypothesis, since the nucleation temperature of Snomax falls below that of birch pollen after certain treatments. This could never be the case, if the birch PIN was in fact a denatured BINP fragment.

- Enzymatic treatments show a significant effect on the IN* activity of bacteria and fungi [e.g. Kieft and Ruscetti 1990], but no effect on birch PIN was observed (see chapter 3.3.).

For those pollen with rather low IN* activity, namely significantly below the mineral dust references, any kind of contamination as a source for ice nucleation might be possible. The occasional freezing events above the homogeneous freezing temperature in IN* negative samples, like ragweed and corn, are surely caused by contaminants and not by the pollen themselves. The low number of IN in these samples (less than 1 per pollen grain) and the low freezing temperatures (if T_{25} lies below 245 K) point strongly at contamination.

The huge spread in the median freezing temperatures (see chapter 2.2.), the different number concentrations (see chapter 3.1.) and the individual sensitivity towards heat (see chapter 3.3.) suggest that PIN have to differ between the species. The dissimilarity could occur on different levels:

- Conformation: It might be that all PIN show the same molecular sequence, but can fold in different ways. It is known that the folding determines the biological activity of macromolecules [e.g. Pan et al. 1993], so this could be also the case for PIN.

- Functionalization: Chemical reactions of a macromolecule with reactive compounds of the surrounding change the occurrence of functional groups on its surface [e.g. Franze et al. 2005].

- Mutation: Substitutions of monomers in the sequence can severely alter the properties of the macromolecule [e.g. Takahashi et al. 1994], since it

might change conformation and functionalization. Mutations occur commonly and are a major drive of evolution.

- Different molecules of one class: The PIN could be different exponents of one class of compounds, for example polysaccharides.

- Molecules of different classes: PIN of different species might not even belong to the same class of substances. IN* can be catalyzed by proteins, saccharides, organic and inorganic compounds. According to the concept of convergent evolution, different approaches from different lifeforms can lead to the very same results.

- Proprietary versus deposited: While the birch PIN have to orginate from the pollen themselves, as it was stated earlier in this chapter, the weak activity in samples like wheat, plane tree and thuja II, could be in fact related to traces of deposited external contaminants.

Since all hypotheses are theoretically possible, and might be valid in some cases, further discussion of this topic is rather speculative. Only the eventual characterization of the PIN will allow an evaluation of these hypotheses.

5.2. Comparison with literature

The results of this thesis are compared with earlier works about IN* of pollen and fungi [Kieft 1988, Pouleur et al. 1992, Tsumuki et al. 1995, Jayaweera and Flanagan 1982, Diehl et al. 2001, Diehl et al. 2002]. The results by Diehl et al. are in the same range as from the smog chamber measurements at BayCEER, but the oil immersion measurements show lower median freezing temperatures. The study by Jayaweera and Flanagan showed very high nucleation temperatures for some fungal species, but a homogeneous freezing point of 248 K, which is higher than in the setups applied in this study. Therefore, comparison of the absolute median freezing temperatures is not possible. At last, the samples of this study might be individually different from those used by others. As research

by Tsumuki showed, differences between strains of the same fungal species can be vast.

In former immersion studies the material loading per droplet was higher than in this thesis. Although the droplet diameter itself is not relevant for heterogeneous IN*, larger droplets are expected to contain more IN (see chapter 1.2.). Since the droplet volumes are easily available, they are utilized for comparison: In the oil immersion of this thesis (see chapter 2.2.) investigated droplets had a volume between 0.5 pl (10 µm) and 4.2 nl (200 µm). Droplet volumes in the work of Diehl et al. were in the range 8.8-27 nl (256-372 µm), while Jayaweera and Flanagan had droplets with a volume of 0.5 µl. Kieft and Pouleur et al. used 10 µl droplets.

5.3. Comparison of methods

Three different methods for measuring IN* activity were presented in this thesis, namely the cryo-microscopy (see chapter 2.2.), the smog chamber LOTASC (see chapter 2.4.) and the flow tubes LACIS and ZINC (see chapter 2.5.). The characteristics of all setups show different facettes of IN*, which are complementary to each other. The features, as well as pros and cons of the methods are discussed by direct comparison in the following section:

LACIS versus ZINC:

The results in the LACIS and the ZINC setup differ only slightly from each other and can therefore be considered comparable. The comparison between flow tube and cryo-microscopy data seems to be contradictory at a first glance, however, the deviations are an intrinsic artifact of the methods. Both T_{50} and f_{ice} are lower in the flow tubes in comparison to the oil immersion, but if the data are rescaled with the system parameters (e.g. material concentration per droplet), they are fully comparable. The lower absolute values for T_{50} and f_{ice} in

comparison with the oil immersion setup had already been noticed in studies of other IN* active samples [Niedermeier et al. 2011b, Hartmann et al. 2012].

LOTASC versus flow tubes:

The ensemble of droplets within a spacious smog chamber is closest to a real cloud and therefore should be the least adulterated by artifacts. However, in the case of LOTASC, the equipment was not optimized for freezing measurements, which led to the drawbacks already discussed in chapter 2.4..

In LACIS the diameters of both the aerosols and the droplets could be tuned, while in LOTASC they could not even be measured. Furthermore, a chamber cannot discriminate between primary and secondary nucleation, as droplets float along and can interact with each other. Neither the oil immersion, where droplets are separated by oil, nor the flow tubes, where fresh droplets are generated permanently, face this drawback. Furthermore, the laser beam of LOTASC can also be backscattered at the vis-a-vis chamber wall. Since glass also depolarizes light, the LOTASC data are adulterated with a background signal, which depends on the optical density of the fog in the chamber, which changes during the measurement. This is also the reason for the pumping peak described above. Furthermore, the disturbing impact of icing of the chamber wall cannot be quantified.

So in general the LOTASC setup needs much improvement before it is applicable for IN* measurements. Other chambers, like the AIDA (Aerosol Interaction and Dynamics in the Atmosphere) at KIT are larger and better equipped, and therefore more applicable for generation of reference data.

Cryo-Microscopy versus other setups:

The main drawback of the cryo-microscopic setup is the presence of an oil matrix surrounding the droplets, which is in contrast to natural conditions. Further details about the quality of this setup were already discussed in chapter

5.1.. In all cases, the absolute numeric values of T_{50} differed severely, e.g. for birch pollen it was 6-7 K higher in LOTASC and 3-6 K lower in LACIS and ZINC. Nevertheless, if the differences in the integral system parameters (e.g. the IN concentration per droplet) are considered appropriately, the data are perfectly compatible.

5.4. Impact of results

The two most important findings of this work are:

- the pollen of different species differ strongly in their IN* behavior
- the IN* of pollen can be derived from macromolecules placed on the pollen surface, which can be easily separated from the pollen body

Up to now pollen have been rejected as important atmospheric ice nuclei, as they are too heavy to reach higher altitudes. If it does not need the whole pollen grain, but some macromolecules, which can split off, to cause nucleation, the story looks quite different: After separation these much lighter macromolecules might be carried up to far higher altitudes than the pollen they come from. So the impact of pollen on atmospheric IN* might have been underestimated before.

The huge differences in IN* activity of different pollen species raises the question, if it is a specific evolutionary protection mechanism. In fact, the most active species are silver and water birch, Scots pine and common juniper, which grow as far North as the Northern timberline. Birch is additionally an early bloomer, which means, that birch pollen might suffer from a temperature drop, as it can happen in late winter or early spring. So in fact the IN on the pollen surface could be a cryoprotective mechanism to cover the pollen with an ice shell and prevent frosting damage.

On the other side of the scale ragweed, corn and plane tree are placed, which originated in subtropical regions and are late bloomers (May or even later). So the species least threatened by frosty weather are also the least IN* active ones.

The most important parameters to determine the possible importance of these pollen are T_{50} and the active fraction (see Tab. 8). Since the pollen species significantly differ from each other concerning these features, their impact should show the same variability. According to the measurements in this study, most pollen species should be negligible concerning their impact on atmospheric ice nucleation. However, a few of them, especially birch pollen, will have to be investigated further, since they might have an impact.

In retrospect it is not surprising that the IN* activity of pollen is caused by extractable macromolecules, since the pollen surface, which consists of the very hydrophobic sporopollenin, is covered with many different chemical species, like proteins, lipids, carotenoids, low- and high-molecular saccharides and other components. Many of these are only loosely attached to the surface, and most are more hydrophilic than the sporopollenin itself. These compounds determine the impact of pollen on their environment, not only concerning ice nucleation, but also cloud condensation nucleation [Dingle 1966] and allergenic potential [Swoboda et al. 1995, Franze et al. 2005]. These effects altogether depend on the interaction with water. For example, pollen allergenes have to be suspended in human mucous membranes, which mainly consist of water, to cause an allergic reaction in the human being [Swoboda et al. 1995]. And it is obvious that catalyzing a phase transition of water, no matter if condensation or freezing, depends on interaction with water molecules.

An additional convenience resulting from the extractability is the fact that by preparing pollen waters, the extracted chemical components can be investigated independently of the pollen bodies themselves. This eliminates, or at least reduces, the dominant signals of the sporopollenin in chemical characterization data, which overshadow those of other components. As it can be seen in Fig. 63, the pollen grain spectra are determined by the sporopollenin peaks, which is not the case in the pollen water spectra.

The practical advantage in sample preparation and handling is also worthy of discussion, since many experimental techniques can be applied easier on liquids than on grains. As an example, transmission spectra are adulterated by light-scattering or -intransparent particles. Since pollen grains are both, other techniques have to be applied to gain sensible information. The chemical compounds in the pollen waters, however, are too small to function as scattering centres for VIS and IR light, so transmission measurements are possible. Furthermore, micrometer-sized particles cannot be applied on a chromatographic column, since they are too large. Finally, enzymatic assays only show reliable results, if enzymes can interact unhinderedly with their reaction partners. This interaction might be disturbed by the shielding effect of a heterogeneous surfaces. Additionally, the pollen grains are expected to deliver further material into the aqueous phase over time, therefore, the enzymes are not able to fully metabolize the substrate. Summing it up, all these techniques can be applied in future investigation of PIN.

Whereas the most efficient ice nucleating pollen are not as effective as bacteria or fungi, they seem to be more active than fresh soot [von Blohn et al. 2005]. Pollen are rather heavy and have relatively high sink velocities, nevertheless, those with advantageous aerodynamical properties can reach altitudes of 3 km and higher [Gregory 1978]. Since they are not that abundant as mineral dust or bacteria, they have not been in the focus of research for many years. Recent model calculations [Hoose et al. 2010] suggest pollen concentrations below 100 m^{-3} above the continental surface and about 0 m^{-3} above the oceans, but as experimental data are too scarce to attest these calculations, their concentrations could be much higher in reality than expected. An alternative study [Jacobson and Streets 2009] estimates that global pollen emissions should be twice as high. Additionally, pollen concentrations can locally and temporarily vary by several orders of magnitude, e. g. in a forest during pollination seasons. Concentrations

higher than 1000 m^{-3} can occur [Golovko et al. 1997] and cause intensive Mie scattering of the sunlight, leading to the so-called pollen corona [Mims 1998]. A further variable is the annual global emission, as in so-called mast-years pollen concentrations can severely exceed the long-term average [Kelly 1994].

Pollen concentrations strongly decrease with the altitude, as they are rather large particles, so they are not expected to reach the upper troposphere in noteworthy numbers. However, as this thesis shows, it does not need whole pollen grains to trigger appreciable ice nucleation, but just some easily-extractable surface macromolecules, which are much lighter and can be elevated and distributed far easier than the heavy pollen bodies. This opens a new pathway, which would increase the impact of pollen on atmospheric ice nucleation drastically – meaning that pollen have been underestimated up to now. This hypothesis is supported by the fact, that material from the pollen surface can easily leave the pollen body and be distributed independently. As a consequence, pollen allergic subjects feel intense symptoms after a rainfall, which washes out the pollen, but releases the allergenes [Solomon et al. 1983, Schäppi et al. 1999]. Not only allergenes, but also sugars can be removed from the bulk of the pollen grains and spread independently [Yttri et al. 2007].

5.5. Outlook

The most important outcomes of this work are summarized below:

- The cryomicroscopic oil immersion setup was evaluated and directly compared with other methods to determine the IN* activity of samples. It proved itself to be a strong and convenient way of measuring IN*.

- A broad spectrum of pollen and fungal spore species was investigated to facilitate estimations about the atmospheric impact of these types of aerosols.

- The IN* activity of pollen was tracked down to extractable macromolecules, which were further investigated.

- Furthermore, this finding changes our understanding of the atmospheric distribution of biological IN, since cell rupture causes generation of fragments that show a different spreading pattern than whole cells.
- The possibility to extract relevant pollen components and not to dependend on the whole grains opens further pathways of sample handling and analyzation.
- The hypothesis that relevant IN* activity is a rather exclusive property of only a few species has been confirmed.

However, this thesis also raises several new questions, which will have to be answered in order to understand biological IN*.

- Other lifeforms, like species from different algal and protozoic phyla, as well as more bacterial and fungal species, will have to be investigated in order to find more IN* active species.
- Systematic patterns of IN distribution among species have to be found in order to make the previous task more efficient.
- Different reference samples (especially mineral dust and soot) have to be investigated and compared with the bioaerosol data.
- The chemical nature of all IN* active sites on aerosols has to be investigated for understanding and quantification of atmospheric IN*. Especially the knowledge about the IN* active sites on soot and mineral dust particles has to be augmented.
- More field measurements shall verify the laboratory measurements under natural conditions and inspire more experiments based on their findings.
- Model calculations have to be refined with the improved database.

6. Listings

6.1. Citations

- Abe K., Watabe S., Emori Y., Watanbe W., Arai S.: FEBS Letters 258, p.297-300 (1989)

- Alpert P., Aller J., Knopf D.: Physical Chemistry Chemical Physics 13, p.19882-19894 (2011)

- Ariya P.A., Sun J., Eltouny N.A., Hudson E.D., Hayes CT, Kos G: International Reviews in Physical Chemistry 28, p.1-32 (2009)

- Atanasova L., Druzhinina I.S.: Journal of Zhejiang University Science B 11, p.151-168 (2010)

- Atkins P.W.: *Physikalische Chemie, 3rd edn.*, ISBN[10] 3527302360; Wiley-VCH Verlag, Weinheim, D (2001)

- Augustin S., Hartmann S., Pummer B.G., Grothe H., Niedermeier D., Clauss T., Voigtländer J., Tomsche L., Wex H., Stratmann F.: Atmospheric Chemistry and Physics Discussions 12, p.32911-32943 (2012)

- Aunaas T.: Cellular and Molecular Life Sciences 38, p.1456-1457 (1982)

- Baltes W.: *Lebensmittelchemie, 6th edn.*, ISBN[13] 9783540381815; Springer-Verlag, Berlin/Heidelberg, D (2007)

- Bauer H., Kasper-Giebl A., Löflund M., Giebl H., Hitzenberger R., Zibuschka F., Puxbaum H.: Atmospheric Research 64, p.109-119 (2002)

- Benton M.: *When Life Nearly Died*, ISBN[13] 9780500285732; Thames & Hudson, London (2003)

- Bingemer H. et al.: Atmospheric Chemistry and Physics 12, p.857-867 (2012)

- Bleicher S., Zetzsch C.: 16th International Conference on Clouds and Precipitation, P.10.24 (2012)

- Bradford M.M.: Analytical Biochemistry 72, p.248-254 (1976)

- Breiteneder H., Pettenburger K., Bito A., Valenta R., Kraft D., Rumpold H., Schreiner O., Breitenbach M.: EMBO Journal 8, p.1935-1938 (1989)

- Brush R.A., Griffith M., Mlynarz A.: Plant Physiology 104, p.725-735 (1994)

- Burrows S.M., Elbert W., Lawrence M.G., Pöschl U.: Atmospheric Chemistry and Physics 9, p.9263-9280 (2009)

- Clausse D., Bouabdillah D., Cochet N., Luquet M.P., Pulvin S.: Pure & Applied Chemistry 63, p.1491-1494 (1991)

- Calderon C., Lacey J., McCartney H.A., Rosas I.: Grana 34, p.260-268 (1995)

- Cheftel J.C., Lévy J., Dumay E.: Food Reviews International 16, p.453-483, (2000)

- Chen J.P., Hazra A., Levin Z.: Atmospheric Chemistry and Physics 8, p.7431-7449 (2008)

- Christner B.C., Cal R., Morris C.E., McCarter K.S., Foreman C.M., Skidmore M.L., Montross S.N., Sands D.C.: Proceedings of the National Academy of Sciences 105, p.18854-18859 (2008)

- Christner B.C.: Apllied Microbiological Biotechnology 85, p.481-489 (2010)

- Clarke A., Gleeson P., Harrison S., Bruce Knox R.: Proceedings of the National Academy of Sciences USA 76, p.3358-3362 (1979)

- Clauss T., Kiselev A., Hartmann S., Augustin S., Pfeifer S., Niedermeier D., Wex H., Stratmann F.: Atmospheric Measurement Techniques 6, p.1041-1052 (2013)

- Constantinidou H.A., Menkissoglu O.: Journal of Experimental Botany 43, p.585-591 (1992)

- Corrigan C.E., Novakov T.: Atmospheric Environment 33, p.2661-2668 (1999)

- Costanzo J.P., Claussen D.L.: Journal of Experimental Zoology 254, p.228-232 (1990)

- Cunha V.R.R., Constantino V.R.L., Ando R.A.: Vibrational Spectroscopy 58, p.139-145 (2012)

- Dell'Anna R., Lazzeri P., Frisanco M., Monti F., Malvezzi Campeggi F., Gotthardini E., Bersani M.: Analytical and Bioanalytical Chemistry 394, p.1443-1452 (2009)

- DeMott P.J.: Atmospheric Research 38, p.63-99 (1995)

- Diehl K., Mitra S.K.: Atmospheric Environment 32, p.3145-3151 (1998)

- Diehl K., Quick C., Matthias-Maser S., Mitra S.K., Jaenicke R.: Atmospheric Research 58, p.75-87 (2001)

- Diehl K., Matthias-Maser S., Jaenicke R., Mitra S.K.: Atmospheric Research 61, p.125-133 (2002)

- Dingle A.N.: Journal de Recherches Atmosphériques 2, p.231-237 (1966)

- Dominguez E., Mercado J.A., Quesada M.A., Heredia A.: Sex Plant Reproduction 12, p.171-178 (1999)

- Duman J.G., Horwath K.: Annual Review of Physiology 45, p.261-270 (1983)

- Duman J.G., Morris J.P., Castellino F.J.: Journal of Comparative Physiology B 154, p.79-83 (1984)

- Duman J.G., Neven L.G., Beals J.M., Olson K.R., Castellino F.J.: Journal of Insect Physiology 31, p.1-5 (1985)

- Duman J.G., Wu D.W., Wolber P.K., Mueller G.M., Neven L.G.: Comparative Biochemistry and Physiology Part B 99, p.599-607 (1991)

- Duman J.G., Olsen T.M.: Cryobiology 30, p.322-328 (1993)

- Duman J.G., Li N., Verleye D., Goetz F.W., Wu D.W., Andorfer A., Benjamin T., Parmelee D.C.: Journal of Comparative Physiology B 168, p.225-232 (1998)

- Ebeling W., Hennrich N., Klockow M., Metz H., Orth H.D., Lang H: European Journal of Biochemistry 47, p.91-97 (1974)

- Elliott W.H., Elliot D.C.: *Biochemistry and Molecular Biology, 3rd edn.*, ISBN[10] 0199271992, Oxford University Press, New York, USA (2005)

- Fall A.L., Fall R.: Current Microbiology 36, p.370-376 (1998)

- Franze T., Weller M.G., Niessner R., Pöschl U.: Environmental Science and Technology 39, p.1673-1678 (2005)

- Fröhlich-Nowoisky J., Pickersgill D.A., Després V.R., Pöschl U.: Proceedings of the National Academy of Sciences 106, p.12814-12819 (2009)

- Fröhlich-Nowoisky J., Burrows S.M., Xie Z., Engling G., Solomon P.A., Fraser M.P., Mayol-Bracero O.L., Artaxo P., Begerow D., Conrad R., Andreae M.O., Despres V., Pöschl U.: Biogeosciences 9, p.1125-1136 (2012)

- Frischmann A., Neudl S., Gaderer R., Bonazza K., Zach S., Gruber S., Spadiut O., Friedbacher G., Grothe H., Seidl-Seiboth V.: Journal of Biological Chemistry 288, p.4278-4287 (2013)

- Fukuta N.: Journal of the Atmospheric Sciences 23, p.191-196 (1966)

- Gao W., Smith D. W., Sego D.C.: Cold Regions Science and Technology 29, p.121-133 (1999)

- Gavish M., Popovitz-Biro R., Lahav M., Leiserowitz L.: Science 250, p.973-975 (1990)

- Giebl H., Berner A., Reischl G., Puxbaum H., Kasper-Giebl A., Hitzenberger R.: Journal of Aerosol Science 33, p.1623-1634 (2002)

- Goldstein G., Nobel P.S.: Plant Physiology 97, p.954-961 (1991)

- Goldstein G., Nobel P.S.: Plant Physiology 104, p.675-681 (1994)

- Golovko V.V., Kirov E.I., Koutzenogii P.K.: Journal of Aerosol Science 28, p.591-592 (1997)

- Gorbunov B., Hamilton R., Clegg N., Toumi R.: Atmospheric Research 47-48, p.271-283 (1998)

- Govindarajan A.G., Lindow S.E.: Journal of Biological Chemistry 263, p.9333-9338 (1988)

- Graether S.P., M.J. Kuiper, Gagné S.M., Walker V.K., Jia Z., Sykes B.D., Davies P.L.: Nature 406, p.325-328 (2000)

- Graether S.P., Jia Z.: Biophysical Journal 80, p.1169-1173 (2001)

- Green R.L., Warren G.J.: Nature 317, p.645-648 (1985)

- Gregory P.H.: Pure and Applied Geophysics 116, p.309-315 (1978)

- Griffin D., Westphal D., Gravy M.: Aerobiologia 22, p.211-226 (2006)

- Gross D.C., Proebsting E.L., Maccrindle-Zimmermann H.: Plant Physiology 88, p.915-922 (1988)

- Grote M.: Journal of Histochemistry and Cytochemistry 37, p.981-987 (1989)

- Grote M., Vrtala S., Niederberger V., Wiermann R., Valenta R., Reichelt R.: Journal of Allergy and Clinical Immunology 108, p.109-115 (2001)

- Guadet J., Julien J., Lafay J.F., Brygoo Y.: Molecular Biology and Evolution 6, p.227-242 (1989)

- Gurian-Sherman D., Lindow S.E.: Cryobiology 32, p.129-138 (1995)

- Hartmann S., Niedermeier D., Voigtländer J., Clauss T., Shaw R.A., Wex H., Kiselev A., Stratmann F.: Atmospheric Chemistry and Physics 11, p.1753-1767 (2011)

- Hartmann S., Augustin S., Clauss T., Voigtländer J., Niedermeier D., Wex H., Stratmann F.: Atmospheric Chemistry and Physics Discussions 12, p.21321-21353 (2012)

- Hasegawa Y., Ishihara Y., Tokuyama T.: Bioscience Biotechnology Biochemistry 58, p.2273-2274 (1994)

- Hayes D.R., Loomis S.H.: Cryo-Letters 6, p.418-421 (1985)

- Heggemann C., Budke C., Schomburg B., Majer Z., Wißbrock M., Koop T., Seewald N.: Amino Acids 38, p.213-222 (2010)

- Hon W.C., Griffith M., Chong P., Yang D.S.C.: Plant Physiology 104, p.971-980 (1994)

- Hon W.C., Griffith M., Mlynarz A., Kwok Y.C., Yang D.S.C.: Plant Physiology 109, p.879-889 (1995)

- Hoshino T., Odaira M., Yoshida M., Tsuda S.: Journal of Plant Research 112, p.255-261 (1999)

- Hoose C., Kristjansson J.E., Burrows S.: Environmental Research Letters 5, no.0254009 (2010)

- Huang T., Duman J.G.: Plant Molecular Biology 48, p.339-350 (2002)

- Huffman J.A. et al.: Atmospheric Chemistry and Physics Discussions 13, p.1767-1793 (2013)

- Hulpke H., Koch H.A., Wagner R.: *Römpp Lexikon Umwelt, 9th edn.*, Georg-Thieme-Verlag, Stuttgart, D (1993)

- Humphreys T.L., Castrillo L.A., Lee M.R.: Current Microbiology 42, p.330-338 (2001)

- Iannone R., Chernoff D.I., Pringle A., Martin S.T., Bertram A.K.: Atmospheric Chemistry and Physics 11, p.1191-1201 (2011)

- Imshenetsky A.A., Lysenko S.V., Kazakov G.A.: Applied and Environmental Microbiology 35, p.1-5 (1978)

- Ivleva N.P., Niessner R., Panne U.: Analytical and Bioanalytical Chemsitry 381, p.261-267 (2005)

- Jacobson M.Z., Streets D.G.: Journal of Geophysical Research 114, no.D08118 (2009)

- Jaeger E.J., Neumann S., Ohmann E.: *Botanik, 5th edn.*, ISBN[10] 3827409217; Spektrum Akademischer Verlag, Heidelberg, D (2003)

- Jaenicke R.: Science 308, p.73 (2005)

- Jann A., Lundheim R., Niederberger P., Richard M.: US Patent no.5665361 (1997)

- Jayaweera K., Flanagan P.: Geophysical Research Letters 9, p.94-97 (1982)

- Kärcher B., Möhler O., DeMott P.J., Pechtl S., Yu F.: Atmospheric Chemistry and Physics 7, p.4203-4227 (2007)

- Kawahara H.: Journal of Bioscience and Bioengineering 94, p.492-496 (2002)

- Kelly D.: Trends in Ecology and Evolution 9, p.465-470 (1994)

- Kieft T.L.: Applied and Environmental Microbiology 54, p.1678-1681 (1988)

- Kieft T.L., Ahmadjian V: Lichenologist 21, p.355-362 (1989)

- Kieft T.L., Ruscetti T.: Journal of Bacteriology 172, p.3519-3523 (1990)

- Kieft T.L.: US Patent no.5169783 (1992)

- Kieft T.L.: in *Biological Ice Nucleation and its Application, 1st edn.*, (Ed. Lee R.E., Warren G.J., Gusta L.V.) ISBN[13] 9780890541722; American Phytopathological Society Press, St. Paul, USA (1995)

- Kiselev A., Clauss T., Niedermeier D., Hartmann S., Wex H., Stratmann F.: EGU General Assembly 2010, p.10236 (2010)

- Knopf D.A., Alpert P.A., Wang B., Aller J.Y.: Nature Geoscience 4, p.88-90 (2011)

- Knutson E.O., Whitby K.T.: Journal of Aerosol Sciences 6, p.75-76 (1975)

- Koop T., Zobrist B.: Physical Chemistry Chemical Physics 11, p.10839-10850 (2009)

- Kovacik L., Plitzko J.M., Grote M., Reichelt R.: Journal of Structural Biology 166, p.263-271 (2009)

- Kozloff L.M., Schofield M.A., Lute M.: Journal of Bacteriology 153, p.222-231 (1983)

- Kozloff L.M., Lute M., Westaway D.: Science 226, p.845-846 (1984)

- Kozloff L.M., Turner M.A., Arellano F.: Journal of Bacteriology 173, p.6528-6536 (1991)

- Kristiansen E., Pedersen S., Ramlov H., Zachariassen K.E.: Journal of Comparative Physiology B 169, p.55-60 (1999)

- Krog J.O., Zachariassen K.E., Larsen B., Smidsrod O.: Nature 282, p.300-301 (1979)

- Kubicek C.P. et al.: Genome Biology 12, no.R40 (2011)

- Kuhs W.F., Hansen T.C.: Geophysical Research Abstracts 11, EGU2009-3607-1 (2009)

- Kulkarni G., Dobbie S.: Atmospheric Chemistry and Physics 10, p.95-105 (2010)

- Kumble K.D., Demmer J., Fish S., Hall C., Corrales S., DeAth A., Elton C., Prestidge R., Luxmanan S., Marshall C.J., Wharton D.A.: Cryobiology 57, p.263-268 (2008)

- Latge J.P.: Trends in Microbiology 9, p.382-389 (2001)

- Laube M., Höller H.: 5.1. Clouds, in *Physical and Chemical Properties of the Air*, Springer Berlin Heidelberg, p.1-7 (1988)

- Leinala E.K., Davies P.L., Jia Z.: Structure 10, p.619-627 (2002)

- Lindow S.E., Arny D.C., Upper C.D.: Plant Physiology 70, p.1084-1089 (1982a)

- Lindow S.E., Hirano S.S., Barchet W.R., Arny D.C., Upper C.D.: Plant Physiology 70, p.1090-1093 (1982b)

- Lindow S.E.: Cryobiology 32, p.247-258 (1995)

- Liou Y.C., Thibault P., Walker V.K., Davies P.L., Graham L.A.: Biochemistry 38, p.11415-11424 (1999)

- Liou Y.C., Tocilj A., Davies P.L., Jia Z.: Nature 406, p.322-325 (2000)

- Lohmann U.: Geophysical Research Letters 29, no.1052 (2002)

- Lundheim R.: Marine Biology 128, p.267-271 (1997a)

- Lundheim R.: Journal of Phycology 33, p.739-742 (1997b)

- Lundheim R.: Philosophical Transactions oft he Royal Society B 357, p.937-943 (2002)

- Madison D.L., Scrofano M.M., Ireland R.C., Loomis S.H.: Cryobiology 28, p.483-490 (1991)

- Makhatazde G.I., Privalov P.L.: Journal of Moelcular Biology 226, p.491-505 (1992)

- Maki L.R., Willoughby K.J.: Journal of Applied Meteorology 17, p.1049-1053 (1978)

- Marcolli C., Gedamke S., Peter T., Zobrist B.: Atmospheric Chemistry and Physics 7, p.5081-5091 (2007)

- Marshall C.B., Daley M.E., Graham L.A., Sykes B.D., Davies P.L.: FEBS Letters 529, p.261-267 (2002)

- Mims F.M.: Applied Optics 37, p.1486-1488 (1998)

- Meyer K., Keil M., Naldrett M.J.: FEBS Letters 447, p.171-178 (1999)

- Mishcenko M.I., Rossow W.B., Macke A., Lacis A.A.: Journal of Geophysical Research 101, p.16973-16985 (1996)

- Möhler O., Stetzer O., Schaefers S., Linke C., Schnaiter M., Tiede R., Saathoff H., Krämer M., Mangold A., Budz P., Zink P., Schreiner J., Mauersberger K., Haaw W., Kärcher B., Schurath U.: Atmospheric Chemistry and Physics 3, p.211-223 (2003)

- Möhler O., Field P.R., Connolly P., Benz S., Saathoff H., Schnaiter M., Wagner R., Cotton R., Krämer M., Mangold A., Heymsfield A.J.: Atmospheric Chemistry and Physics 6, p.3007-3021 (2006)

- Möhler O., Hoose C.: Nature Geoscience 4, p.76-77 (2011)

- Mohnen V.A.: Scientific American 259, p.30-38 (1988)

- Morris C.E., Georgakopoulos D.G., Sands D.C.: Journal de Physique IV France 121, p.87-103 (2004)

- Mugnano J.A., Lee R.E., Taylor R.T.: Journal of Experimental Biology 199, p.465-471 (1996)

- Murray B.J., Broadley S.L., Wilson T.W., Bull S.J., Wills R.H., Christenson H.K., Murray E.J.: Physical Chemistry Chemical Physics 12 p.10380-10387 (2010)

- Murray B.J., Broadley S.L., Wilson T.W., Aitkinson J.D., Wills R.H.: Atmospheric Chemistry and Physics 11, p.4191-4207 (2011)

- Nemecek-Marshall M., LaDuca R., Fall R.: Journal of Bacteriology 175, p.4062-4070 (1993)

- Neven L.G., Duman J.G., Low M.G., Sehl L.C., Castellino F.J.: Journal of Comparative Physiology B, Biochemical Systemic and Environmental Physiology 159, p.71-82 (1989)

- Niedermeier D., Shaw R.A., Hartmann S., Wex H., Clauss T., Voigtländer J., Stratmann F.: Atmospheric Chemistry and Physics 11, p.8767-8775 (2011a)

- Niedermeier D. et al.: Atmospheric Chemistry and Physics 11, p.11131-11144 (2011b)

- O'Gorman C.M., Fuller H.T., Dyer PS: Nature 457, p.471-474 (2009)

- Olsen T.M., Duman J.G.: Journal of comparative Physiology B 167, p.105-113 (1997)

- Orser C., Staskawicz B.J., Panopoulos N.J., Dahlbeck D., Lindow S.E.: Journal of Bacteriology 164, p.359-366 (1985)

- Pan K.M., Baldwin M., Nguyen J., Gasset M., Serban A., Groth D., Mehlhorn I., Huang Z., Fletterick R.J., Cohen F.E., Prusiner S.B.: Proceedings of the National Academy of Science USA 90, p.10962-10966 (1993)

- Pappas C.S., Tarantilis P.A., Harizanis P.C., Polissiou M.G.: Applied Spectroscopy 57, p.23-27 (2003)

- Pearce D.A., Bridge P.D., Hughes K.A., Sattler B., Psenner R., Russell N.J.: FEMS Microbiology Ecology 69, p.143-157 (2009)

- Peter T., Marcolli C., Spichtinger P., Corti T., Baker M.B., Koop T.: Science 314, p.1399-1402 (2006)

- Pinti V., Marcolli C., Zobrist B., Hoyle C.R., Peter T.: Atmospheric Chemistry and Physics 12, p.5859-5878 (2012)

- Pouleur S., Richard C., Martin J.G., Antoun H.: Applied and Environmental Microbiology 58, p.2960-2964 (1992)

- Prahl A.K., Springstubbe H., Grumbach K., Wiermann R.Z.: Zeitschrift für Naturforschung C 40, p.621-626 (1986)

- Pratt K.A., DeMott P.J., French J.R., Wang Z., Westphal D.L., Heymsfield A.J., Twohy C.H., Prenni A.J., Praether K.A.: Nature Geoscience 2, p.398-401 (2009)

- Prospero J., Blades E., Mathison G., Naidu R.: Aerobiologia 21, p.1-19 (2005)

- Pruppacher H.R., Klett J.D.: *Microphysics of Clouds and Precipitation, 2nd edn.*, ISBN[10] 0792342119; Kluwer Academic Publishers, Dordrecht, NL (1997)

- Pummer B.G., Bauer H., Bernardi J., Bleicher S., Grothe H.: Atmospheric Chemistry and Physics Discussions 11, p.27219-27241 (2011)

- Pummer B.G., Bauer H., Bernardi J., Bleicher S., Grothe H.: Atmospheric Chemistry and Physics 12, p.2541-2550 (2012)

- Richard C., Martin J.G., Pouleur S.: Phytoprotection 77, p.83-92 (1996)

- Rogers J.S., Stall R.E., Burke M.J.: Cryobiology 24, p.270-279 (1987)

- Sattler B., Puxbaum H., Psenner R.: Geophysical Research Letters 28, p.239-242 (2001)

- Saxena P., Hildemann L.M.: Journal of Atmospheric Chemistry 24, p.57-109 (1996)

- Schäppi G.F., Taylor P.E., Pain M.C.F., Cameron P.A., Dent A.W., Straff I.A., Suphioglu C.: Clinical and Experimental Allergy 29, p.633-641 (1999)

- Schmid D., Pridmore D., Capitani G., Battistutta R., Neeser J.R., Jann A.: FEBS Letters 414, p.590-594 (1997)

- Schnell R.C., Vali G.: Nature 236, p.163-165 (1972)

- Schnell R.C., Vali G.: Journal of the Atmospheric Sciences 33, p.1554-1564 (1976)

- Schnell R.C.: American Geophysical Union, fall meeting 2009, no.A11B-0091 (2009)

- Schoffelmeer E.A.M., Klis F.M., Sietsma J.H., Cornelissen B.J.C.: Fungal Genetics and Biology 27, p.275-282 (1999)

- Schüller E.: *Vergleichende mikroskopische und molekularbiolog. Untersuchungen von Pilzsporen in Feinstaubproben*, MSc Thesis, BOKU Vienna, Austria (2008)

- Schulte F., Lingott J., Panne U., Kneipp J.: Analytical Chemistry 80, p.9551-9556 (2008)

- Schulte F., Mäder J., Kroh L.W., Panne U., Kneipp J.: Analytical Chemistry 81, p.8426-8433 (2009)

- Schulte F., Panne U., Kneipp J.: Journal of Biophotonics 3, p.542-547 (2010)

- Scott R.J.: Scott R.J., Stead A.D., *Molecular and Cellular Aspects of Plant Reproduction*, Cambridge University Press, Cambridge, UK (1994)

- Sesartic A., Lohmann U., Storelvmo T.: Environmental Research Letters 8, no.014029 (2013)

- Shaw R.A., Durant A.J., Mi Y.: Journal of Physical Chemistry B 109, p.9865-9868 (2005)

- Simonovicová A., Gódyová M., Kunert J.: Biologia Bratislava 59, p.17-18 (2004)

- Sippel C., Koza M.M., Hansen T.C., Kuhs W.F.: Geophysical Research Abstracts 12, no.EGU2010-3614 (2010)

- Solomon W.R., Burge H.A., Muilenberg M.L.: Journal of Allergy and Clinical Immunology 72, p.443-447 (1983)

- Somero G.N., Osmond C.B., Bolis C.L.; Duman J., Wu D.W., Yeung K.L.: *Water and Life: Comparative Analysis of Water Relationships at the Organic, Cellular and Molecular Level*, ISBN[13] 9780387541129; Springer-Verlag TELOS, New York, USA (1992)

- Steinke I., Möhler O., Kiselev A., Niemand M., Saathoff H., Schnaiter M., Skrotzki J., Hoose C., Leisner T.: Atmospheric Chemistry and Physics 11, p.12945-12958 (2011)

- Stetzer O., Baschek B., Lüönd F., Lohmann U.: Aerosol Science and Technology 42, p.64-74 (2008)

- Sun J., Ariya P.A.: Atmospheric Environment 40, p.795-820 (2006)

- Swoboda I., Dang T.C.H., Heberle-Bors E., Vicente O.: Protoplasma 187, p.103-110 (1995)

- Takahashi T., Tanaka M., Brannan C.I., Jenkins N.A. Copeland N.G., Suda T., Nagata S.: Cell 76, p.969-976 (1994)

- Thompson A.M.: Science 256, p.1157-1165 (1992)

- Tsumuki H., Konno H.: Bioscience Biotechnology Biochemistry 58, p.578-579 (1994)

- Tsumuki H., Yanai H., Aoki T.: Annuals of Phytopathological Society of Japan 61, p.334-339 (1995)

- Turner M.A., Arellano F., Kozloff L.M.: Journal of Bacteriology 173, p.6515-6527 (1991)

- Vali G., Christensen M., Fresh R.W., Galyan E.L., Maki L.R., Schnell R.C.: Journal of Atmospheric Sciences 33, p.1565-1570 (1976)

- Vollhardt K.P.C., Schore N.E.: *Organic Chemistry – Structure and Function, 4th edn.*, ISBN[10] 0716743744; WH Freeman and Company, New York, USA (2003)

- von Blohn N., Mitra S.K., Diehl K., Borrmann S.: Atmospheric Research 78, p.182-189 (2005)

- Warren G., Wolber P.: Molecular Microbiology 5, p.239-243 (1991)

- Wolanczyk J.P., Storey K.B., Baust J.G.: Cryobiology 27, p.328-335 (1990)

- Wolber P.K., Deininger C.A., Southworth M.W., Vandekerckove J., van Montagu M., Warren G.J.: Proceedings of the National Academy of Sciences USA 83, p.7256-7260 (1986)

- Wolde P.R., Frenkel D.: Physical Chemistry Chemical Physics 1, p.2191-2196 (1999)

- Wösten H.A.B., Ruardy T.G., van der Mei H.C., Busscher H.J., Wessels J.G.H.: Colloids and Surfaces B: Biointerfaces 5, p.189-195 (1995)

- Xu H., Griffith H., Patten C.L., Glick B.R.: Canadian Journal of Microbiology 44, p.64-73 (1998)

- Yeh Y., Feeney R.E.: Chemical Reviews 96, p.601-618 (1996)

- Yttri K.E., Dye C., Kiss G.: Atmospheric Chemistry and Physics 7, p.4267-4279 (2007)

- Zachariassen K.E., Kristiansen E.: Cryobiology 41, p.257-279 (2000)

- Zimmermann F., Weinbruch S., Schütz L., Hofmann H., Ebert M., Kandler K., Worringen A.: Journal of Geophysical Research 113, D23204 (2008)

- Zimmermann B.: Applied Spectroscopy 64, p.1364-1373 (2010)

6.2.   Personal publication list

Pummer B.G.: "*Chemosensorik von Escherichia coli in realen Matrices*" (http://othes.univie.ac.at/3774/); Diploma Thesis, University of Vienna, supervised by F. L. Dickert, (2009).

Pummer B.G., Bauer H., Bernardi J., Bleicher S., Grothe H.: *Birch and conifer pollen are efficient atmospheric ice nuclei*; Atmospheric Chemistry and Physics Discussions 11, p.27219-27241 (2011)

Pummer B.G., Bauer H., Bernardi J., Bleicher S., Grothe H.: *Suspendable macromolecules are responsible for ice nucleation activity of birch and conifer pollen*; Atmospheric Chemistry and Physics 12, p.2541-2550 (2012)

Augustin S., Hartmann S., Pummer B.G., Grothe H., Niedermeier D., Clauss T., Voigtländer J., Tomsche L., Wex H., Stratmann F.: *Immersion freezing of birch pollen washing water*; Atmospheric Chemistry and Physics Discussions 12, p.32911-32943 (2012)

Pummer B.G., Bauer H., Bernardi J., Chazallon B., Facq S., Lendl B., Whitmore K., Grothe H.: *Chemistry and morphology of dried-up pollen suspension residues*; Journal of Raman Spectroscopy, **in review** (2013)

Pummer B.G., Atanasova L., Bauer H., Bernardi J., Druzhinina I.S., Grothe H.: *Spores of most common airborne fungi reveal no ice nucleation activity*; Biogeosciences Discussions, **in review** (2013)

Pummer B.G., Grothe H., Bauer H., Bernardi J., Bleicher S., Whitmore K.: *The ice nucleation activity of pollens and fungal spores* (Poster); Geophysical Research Abstracts 13, EGU2011-6041 (2011)

Pummer B.G., Bauer H., Bernardi J., Grothe H.: *The ice nucleation activity of pollens and fungal spores* (Poster); Bunsentagung 2011 – Book of Abstracts, p.300-301 (2011)

Pummer B.G., Bauer H., Bernardi J., Grothe H.: *The ice nucleation ability of pollens and fungal spores* (Oral); IUGG General Assembly 2011 – Book of Abstracts, no.961 (2011)

Pummer B.G., Bauer H., Bernardi J., Grothe H.: *The ice nucleation activity of pollen and fungal spores* (Oral); ICCPA – 10th International Conference on Carbonaceous Particles in the Atmosphere, p.29 (2011)

Pummer B.G., Bauer H., Bernardi J., Grothe H.: *Pollen surface components are responsible for ice nucleation* (Poster); 14. Österreichische Chemietage – Book of Abstracts, PO-160 (2011)

Pummer B.G., Bauer H., Bernardi J., Chazallon B., Facq S., Grothe H.: S*tudy on aqueous pollen suspensions* (Poster); Prix Amadée Award Ceremony of the Institut Francais de Vienne (2012)

Pummer B.G., Atanasova L., Bauer H., Bernardi J., Druzhinina I.S., Grothe H.: *Study on the ice nucleation activity of fungal spores (Ascomycota and Basidiomycota)* (Poster); Geophysical Research Abstracts 14, EGU2012-2402 (2012)

Pummer B.G., Atanasova L., Bauer H., Bernardi J., Druzhinina I.S., Grothe H.: *Search for biogenic ice nucleation activity (INA) – a study on Snomax, pollen, moulds and mushrooms* (Poster); 16th International Conference on Clouds and Precipitation, P.10.13 (2012)

Pummer B.G., Atanasova L., Bauer H., Bernardi J., Druzhinina I.S., Grothe H.: *Determining the ice nucleation of fungal spores in the oil immersion mode* (Oral, solicited); Workshop on Bioaerosol Effects on Clouds, Steamboat Springs (2012)

Pummer B.G., Bauer H., Bernardi J., Grothe H., Schmitt-Kopplin P.: *Progress on ince nucleation studies on pollen* (Oral, solicited); Workshop on Bioaerosol Effects on Clouds, Steamboat Springs (2012)

Hartmann S., Temkiv T., Pummer B.G., Augustin S., Clauss T., Niedermeier D., Wex H., Voigtländer J., Karlson U., Grothe H., Stratmann F.: *Immersion freezing of biological particles* (Oral); EAC2012 Granada – European Aerosol Conference Handbook, no.WG01S7O05, p.149 (2012)

Stratmann F., Wex H., Niedermeier D., Hartmann S., Augustin S., Clauss T., Voigtländer J., Pummer B.G., Grothe H.: *Ice nucleation rates of single protein complexes and single macromolecules* (Poster); 2012 Fall Meeting AGU, A13I-0297 (2012)

Pummer B.G., Atanasova L., Bauer H., Bernardi J., Druzhinina I.S., Müller C., Schmitt-Kopplin P., Whitmore K., Grothe H.: *Stress treatment of pollen and fungal spores – what are the impacts on IN activity?* (Oral, solicited); ESF-Workshop – Atmospheric Ice Nucleation, p.12 (2013)

Kaufmann L., Marcolli C., Pinti V., Pummer B.G., Kohn M., Welti A., Sierau B., Peter T.: *Comparison of ice nucleation between birch pollen and Hoggar mountain dust* (Oral); ESF-Workshop – Atmospheric Ice Nucleation, p.13 (2013)

Augustin S., Hartmann S., Pummer B.G., Grothe H., Niedermeier D., Clauss T., Voigtländer J., Tomsche L., Wex H., Stratmann F.: *Ice nucleation rates of single protein complexes and single macromolecules* (Oral, solicited); ESF-Workshop – Atmospheric Ice Nucleation, p.20-21 (2013)

Kohn M., Stetzer O., Sierau B., Welti A., Pummer B.G., Grothe H., Lohmann U.: *Immersion freezing of biological aerosol particles in the ZINC setup* (Oral); ESF-Workshop – Atmospheric Ice Nucleation, p.22 (2013)

Sierau B., Oehm C., Möhler O., Steinke I., Roth A., Freutel F., Schneider J., Pummer B.G., Grothe H., Abegglen M., Kohn M., Welti A., Stetzer O., Lohmann U.: *Towards the identification of individual biological particles as ice nuclei using single particle mass spectrometry* (Oral, solicited); ESF-Workshop – Atmospheric Ice Nucleation, p.35-36 (2013)

Grothe H., Pummer B.G., Bauer H., Bernardi J.: *The ice nucleationa ctivity of biological aerosols* (Oral, solicited); Geophysical Research Abstracts 14, p.5202 (2012)

Pummer B.G., Atanasova L., Bauer H., Bernardi J., Chazallon B., Druzhinina I.S., Grothe H.: *Ice nucleation of bioaerosols – a resumée* (Poster); Geophysical Research Abstracts 15, EGU2013-11962 (2013)

Augustin S., Hartmann S., Pummer B.G., Grothe H., Niedermeier D., Clauss T., Voigtländer J., Tomsche L., Wex H., Stratmann F.: *Immersion freezing of birch pollen washing water* (Poster); Geophysical Research Abstracts 15, EGU2013-4776 (2013)

Handle K., Loerting T., Bogdan A., Weiss F., Pummer B.G., Grothe H.: *Are water-in-oil emulsions suitable model systems for cloud glaciation?* (Poster); Geophysical Research Abstracts 15, EGU2013-14058 (2013)

Zolles T., Grothe H., Pummer B.G.: *Immersion freezing on mineral dust particles* (Poster); Geophysical Research Abstracts 15, EGU2013-4615 (2013)

Grothe H., Pummer B.G.: *Transnational Access Activity Report for EUROCHAMP-2*; report no.1, 6 pages (2010)

Pummer B.G.: *Scientific Report for MicroDICE, Short Visit*; report no.4989, 9 pages (2012)

Curriculum Vitae:

Name:	Bernhard Gerhard Pummer
Citizenship:	Austria
Status:	unmarried
Father:	Ernst Pummer
	*20.07.1953
Mother:	Elfriede Pummer (née Reigl)
	*22.12.1956

16.04.1985:	born in Vienna, Austria
1991-1995:	attending primary school in Trautmannsdorf/Leitha
1995-2003:	attending grammar school in Bruck/Leitha
04.06.2003:	graduation (pass with merit)
2003-2009:	chemistry diploma studies at University of Vienna (main subjects: food chemistry, environmental chemistry, theoretical chemistry)
2004-2005:	civilian service in Ignaz Semmelweis Hospital, Vienna
04.02.2009:	diploma examination (pass with distinction)
2010-2013:	PhD studies at Vienna University of Technology

Practicals:

Aug. 2006:	OFI (Austrian Res. Inst. f. Chem. and Technol.), Vienna

International research experience:

Sept.-Oct. 2010:	Bayreuth Center for Ecology and Environmental Research
Feb. 2011:	Université Lille 1
Feb. 2012:	Leibniz-Institute for Tropospheric Research Leipzig
Jan. 2013:	Swiss Federal Institute of Technology Zürich